

1 **Using observations and source specific model tracers to characterize**  
2 **pollutant transport during FRAPPÉ and DISCOVER-AQ**  
3  
4

5 **G. G. Pfister<sup>1</sup>, P. Reddy<sup>1,2</sup>, M.C. Barth<sup>1</sup>, F.F. Flocke<sup>1</sup>, A. Fried<sup>3</sup>, S.C. Herndon<sup>4</sup>, B.C. Sive<sup>5</sup>,**  
6 **J.T. Sullivan<sup>6</sup>, A.M. Thompson<sup>6</sup>, T.I. Yacovitch<sup>4</sup>, A.J. Weinheimer<sup>1</sup>, A. Wisthaler<sup>7</sup>**  
7

8 <sup>1</sup> Atmospheric Chemistry Observations and Modeling, National Center for Atmospheric  
9 Research, Boulder, Colorado, USA

10 <sup>2</sup> formerly Air Pollution Control Division, Colorado Department of Public Health and  
11 Environment, Boulder, Colorado, USA

12 <sup>3</sup> Institute of Arctic and Alpine Research, University of Colorado Boulder, Boulder, Colorado,  
13 USA

14 <sup>4</sup> Aerodyne Research Inc., Billerica, Massachusetts, USA.

15 <sup>5</sup> Air Resources Division, National Park Service, Denver, Colorado, USA

16 <sup>6</sup> Earth Sciences Division, NASA Goddard Space Flight Center, Greenbelt, Maryland, USA

17 <sup>7</sup> Department of Chemistry, University of Oslo, Oslo, Norway  
18

19 **Key Points:**

- 20 • Upslope flows are a frequent occurrence on high ozone days in the NFRMA thereby  
21 impacting remote mountain sites.
- 22 • Aircraft measurements and model tracers confirm transport of pollution to the mountains  
23 and spill-over into the valleys to the West of the Continental Divide
- 24 • The northern Foothills are frequently impacted by oil and gas sources, while the southern  
25 Foothills more frequently experience impact from urban sources.  
26

## 27 **Abstract**

28 Transport is a key parameter in air quality research and plays a dominant role in the Colorado  
29 Northern Front Range Metropolitan Area (NFRMA), where terrain induced flows and  
30 recirculation patterns can lead to vigorous mixing of different emission sources. To assess  
31 different transport processes and their connection to air quality in the NFRMA during the  
32 FRAPPÉ and DISCOVER-AQ campaigns in summer 2014, we use the Weather Research and  
33 Forecasting Model with inert tracers. Overall, the model represents well the measured winds and  
34 the inert tracers are in good agreement with observations of comparable trace gas concentrations.  
35 The model tracers support the analysis of surface wind and ozone measurements and allow for  
36 the analysis of transport patterns and interactions of emissions. A main focus of this study is on  
37 characterizing pollution transport from the NFRMA to the mountains by mountain-valley flows  
38 and the potential for recirculating pollution back into the NFRMA. One such event on 12 August  
39 2014 was well captured by the aircraft and is studied in more detail. The model represents the  
40 flow conditions and demonstrates that during upslope events, frequently there is a separation of  
41 air masses that are heavily influenced by oil and gas emissions to the North and dominated by  
42 urban emissions to the South. This case study provides evidence that NFRMA pollution not only  
43 can impact the nearby Foothills and mountain areas to the East of the Continental Divide, but  
44 that pollution can "spill over" into the valleys to the West of the Continental Divide.

## 45 **1. Introduction**

46 Two major field campaigns – the National Science Foundation (NSF)/National Center for  
47 Atmospheric Research (NCAR) and State of Colorado Front Range Air Pollution and  
48 Photochemistry Experiment (FRAPPÉ) and the 4<sup>th</sup> deployment of the National Aeronautics and  
49 Space Administration (NASA) Deriving Information on Surface conditions from Column and  
50 Vertically Resolved Observations Relevant to Air Quality (DISCOVER-AQ) – were conducted  
51 jointly in summer 2014 to study summertime ozone pollution in the Colorado Northern Front  
52 Range Metropolitan Area (NFRMA), an area that is in non-attainment of the current ozone  
53 standards. Characterizing and modeling air quality in the NFRMA poses large challenges due to  
54 the complex terrain and meteorology as well as the mix of diverse pollution sources including

55 urban sources, power plants, large industrial sources, agricultural activities, oil and gas  
56 exploration and natural sources like wildfires, biogenic VOCs or windblown dust.

57 The NFRMA is located at an elevation of roughly 1600-1800 m, on the plains just east of the  
58 Central Rocky Mountains. To the West of the NFRMA, the terrain becomes mountainous,  
59 mostly wooded, with scattered smaller communities up to elevations below 3000 m, and then  
60 transitions into the mostly uninhabited alpine region along the Continental Divide, reaching up to  
61 4300 m altitude. Several major river canyons extend from the high terrain down into the  
62 NFRMA, which in parts are less than 1 km wide, i.e. of sub-grid scale in most chemical transport  
63 models, adding to the complexity of the terrain and transport.

64 In the summer months, particularly during weak synoptic conditions, the local meteorology is  
65 mainly controlled by thermally driven, terrain-induced, diurnal flow patterns, often also referred  
66 to as upslope/downslope or mountain-valley winds (Johnson and Toth, 1982; Toth and Johnson,  
67 1985, Arritt et al., 1992; and references therein). This has unique consequences for the transport,  
68 mixing and photochemical processing of local emissions (Haagenson, 1978; Greenland, 1980;  
69 Doran, 1996; Baumann et al., 1997; Olson et al., 1997) including the potential of bringing  
70 NFRMA pollution into the pristine mountains (Parrish et al., 1986; Brodin et al., 2010; Brodin et  
71 al., 2011; Benedict et al., 2011; Darrouzet-Nardi et al. 2012). Conversely, stronger frontal  
72 passages can induce outflow of NFRMA pollution to the East, impacting downwind agricultural  
73 areas in the central Great Plains. Such export events, as well as thunderstorms, are the major  
74 mechanisms for cleaning out accumulated pollution in the NFRMA. The characteristics and  
75 variability of mountain-valley winds are the main focus of this paper, but we also assess the  
76 general distribution and mixing of different emission sources.

77 Transport is a key driver in air quality research and plays a dominant role in determining  
78 pollution levels, specifically in the Front Range, where terrain induced flow and recirculation  
79 patterns can lead to vigorous mixing of different emission sources. As a result, the analysis of  
80 wind roses does not necessarily provide sufficient information on the origin of air masses  
81 arriving at a certain location. A more appropriate method in this regard might be back-  
82 trajectories, but these do not provide information on the dilution and spatial distribution of  
83 different emissions unless methods such as a Lagrangian particle dispersion model (LPDM) is

84 used (e.g. Stohl et al., 2005; Angevine et al., 2013; Briode et al., 2013; Hegarty et al., 2013). In  
85 this work, to assess different transport processes and their connection to air quality in the  
86 NFRMA during the campaign period, we use a chemical transport model, the Weather Research  
87 and Forecasting Model (WRF) with inert tracers. During the campaign, we conducted a real-time  
88 WRF forecast which included tracers from different emission sectors and regions. This product  
89 showed high value as a planning tool during the campaign and is used in this study. The model  
90 tracers support the analysis of surface wind and ozone measurements and allow for the analysis  
91 of how emissions from different source types are transported and where and when we find  
92 efficient mixing of different emission sources. The analysis of the tracers can point towards  
93 conditions that should be investigated further using chemical measurements and modeling and is  
94 valuable in support of the field observations analysis.

95 Here, we provide an evaluation of the model and use the average spatial distribution of tracers to  
96 assess which regions are on average most impacted by which source sector and how these  
97 emissions typically are mixed. We use the WRF tracers to look in more detail at a day where the  
98 NCAR/NSF C-130 aircraft captured well an upslope event (12 August 2014) and compare this  
99 case study to other upslope events during the campaign period.

## 100 **2. Field Campaign Observations**

101 During summer 2014 two major field campaigns took place in the NFRMA with the objective to  
102 study the drivers of ozone pollution. The FRAPPÉ field experiment was carried out jointly with  
103 the 4<sup>th</sup> deployment of the NASA DISCOVER-AQ between 15 July – 20 August 2014 with most  
104 DISCOVER-AQ platforms ending on about 10 August. For simplicity, we refer to the joint  
105 campaigns as FRAPPÉ/DAQ.

106 Chemical and meteorological observations were conducted in total from five aircraft, multiple  
107 mobile vans, ozonesondes, lidars, tethered balloons, and numerous operational and additional  
108 surface sites. In this paper, we use measurements from two of the aircraft, the NASA P-3B and  
109 the NSF/NCAR C130. The NASA P-3 conducted flights on 16 days starting on 17 July and  
110 ending on 8 August 2014 following a repetitive pattern over the NFRMA. The flight pattern  
111 included spirals over 6 surface sites to assess the diurnal and small scale variability in pollutants.



112 For the NCAR/NSF C130, in contrast, flight patterns were designed to target specific objectives  
113 dictated by atmospheric conditions. The 15 flights from 26 July to 18 August 2014 were focused  
114 on emissions in the NFRMA, followed upslope transport of NFRMA pollution into the  
115 mountains, and measured Colorado Western slope emissions and outflow from the NFRMA. Our  
116 focus in this paper is on flights in the NFRMA and the nearby mountains. Aircraft data focused  
117 in here include NO<sub>x</sub>, ethane and ammonia data on the NCAR/NSF C-130 and NASA P-3. For  
118 more details on the data and measurement techniques the reader is referred to Weinheimer et al.,  
119 [1994] for NO<sub>x</sub> measurements, Yacovitch et al. [2014] for NASA P-3 ethane measurements, Sun  
120 et al. [2014] for NASA P-3 ammonia measurements, Richter et al. [2015] for NCAR/NSF C-130  
121 ethane measurements and Herndon et al. [2005] for NCAR/NSF C-130 ammonia measurements.

122 In Table 1 we list the surface sites that are included in this study with their location. The area  
123 topography is shown in Figure 1. In addition to sites in the NFRMA, we include four high  
124 altitude sites to the West of the NFRMA. The area of the NFRMA is rather small; the distance  
125 from Chatfield to Fort Collins is about 110 km and from RF North to Platteville about 70 km.  
126 Yet, as will be shown, the variability in emissions and dynamics is very high, posing significant  
127 challenges to characterizing the drivers behind high concentrations of air pollution.

### 128 **3. Model Description**

129 During the campaigns, the Weather Research and Forecasting Model (WRF) V3.3.1 was run in  
130 forecast mode to support flight design and forecasting. National Center for Environmental  
131 (NCEP) Global System Forecast (GSF) analysis fields at 0.5°x0.5° were used to initialize WRF  
132 at 00UTC and 12UTC and 48-hour forecasts were constrained by lateral boundary conditions  
133 from GFS forecasts. A 2-domain setup was used with a 15 km outer domain covering the  
134 Western U.S. (not shown) and an inner 3 km domain covering Colorado and parts of neighboring  
135 States. Only results of the inner domain are considered here. The vertical resolution was set to 36  
136 levels between the surface and 10 hPa. Other model configuration settings include the Yonsei  
137 University (YSU) boundary layer scheme [Hong et al., 2006; Hong 2010, Hu et al., 2013],  
138 Thompson microphysics [Thompson et al., 2008], the Rapid Radiative TransferModel for GCMs  
139 (RRTMG) radiation schemes [Iacono et al., 2008], the Kain-Fritsch cumulus scheme for the

140 outer domain [Kain, 2004], Noah land surface model [Tewari et al., 2004], and the Monin-  
141 Obukov surface layer scheme [Janjic, 1994]. Instantaneous model output is saved at each  
142 simulation hour. For comparison and integration with the observations, the hourly gridded model  
143 output has been interpolated to the time and location of the measurements.

144 We added a set of chemically inert tracers to WRF to track the transport of different source  
145 sectors. The tracers are only emitted from their respective sources and there are no other  
146 production mechanisms. These tracers are an addition to the scheme described by Barth et al.  
147 (2012). The tracers included in the current study are an oil and gas tracer ( $TR^{OG}$ ) representative  
148 of emissions from oil and natural gas (OG) activities in Colorado; an area tracer ( $TR^{Area}$ ) and a  
149 mobile tracer ( $TR^{Mobile}$ ) representative of Colorado area and mobile emissions, respectively; and  
150 an agricultural tracer ( $TR^{Agr}$ ) representative of agricultural emissions in Colorado. To define the  
151 tracer emissions, we chose surrogate chemical species that are characteristic for the specified  
152 emissions, but note that the tracers do not represent the chemical nature of the chemical  
153 surrogates. We use nitrogen oxide ( $NO_x$ ) for  $TR^{AREA}$  and  $TR^{Mobile}$ , ethane for  $TR^{OG}$  and ammonia  
154 ( $NH_3$ ) for  $TR^{Agr}$ .  $TR^{Area}$  and  $TR^{Mobile}$  are combined in our analysis ( $TR^{AreaMobile}$ ) and for  
155 simplicity also referred to as “urban”. Each tracer was given a 2-day lifetime, which allows to  
156 follow the transport but avoids that the tracers accumulate in the NFRMA.

157 Base emission inventories were chosen based on availability and representativeness for 2014  
158 sources. OG emissions are based on the Western Regional Air Partnership 2008 inventory.  
159 Comparison to more recent emission inventories now available to us (EPA NEI 2011 and an  
160 inventory based on 2014 activity data) shows that the 2008 inventory reasonably well represents  
161 the 2014 spatial distribution (not shown). Area and mobile sources are from a Colorado  
162 Department of Public Health and Environment inventory projected for 2018, and agricultural  
163 emissions are from the Environmental Pollution Agency (EPA) National Emission Inventory  
164 (NEI) 2011. An average diurnal cycle was superimposed on  $TR^{Area}$ ,  $TR^{Mobile}$  and  $TR^{Agr}$ . Other  
165 tracers not used in this analysis include a tracer from  $NO_x$  sources from neighboring states within  
166 the WRF inner domain, a lightning  $NO_x$  tracer, a stratospheric tracer, and a lateral boundary  
167 conditions tracer.

168 In Figure S1 we plot maps of the model emission tracers together with the same sites shown in  
169 Figure 1. In Figure S2 we show the diurnal cycle in  $TR^{Area}$  and  $TR^{Mobile}$ . The majority of the  
170 tracer emissions are within the NFRMA and there are no major emission sources for 100 km and  
171 more to the West. To create a continuous time series from the individual forecast cycles we  
172 extracted forecast hours 6-18 from each 00 and 12 UTC cycle, i.e. we allow for a 6 hour spinup.  
173 Only when specifically noted, we use the results from a single forecast cycle only. We do note  
174 that model simulations might vary substantially between different forecast cycles, however, this  
175 study is not about evaluating the performance of individual forecast lead times.

#### 176 **4. Model Evaluation – Meteorology**

177 We provide an evaluation of the modeled meteorology and transport during the FRAPPÉ/DAQ  
178 period. We focus on the performance of model winds given that the focus of this study is on  
179 NFRMA transport patterns, and assess the general model performance over the period of the  
180 campaign. Individual case studies are presented later in the paper. We select only surface sites  
181 for which both ozone and wind observations are available.

182 We begin with an evaluation of modeled 10 m winds to surface observations taken at selected  
183 sites in the NFRMA. In Figure 2, we compare the vector average wind direction and average  
184 wind speed at six locations, which are used later in the analysis. Statistics are shown over the  
185 FRAPPÉ time period (15 July – 20 August). These include two sites in the NFRMA near the  
186 Foothills (RF North and the NASA P-3 spiral location NREL Golden), and two locations in the  
187 Colorado Eastern plains (WC Tower and Aurora East). In addition, we include two high  
188 elevation sites, Longs Peak and Trail Ridge Road, for which wind and ozone measurements are  
189 available. The Longs Peak station is located just to the West of the Peak to Peak Highway, and  
190 Trail Ridge Road is situated just below the Continental Divide on the east side near Trail Ridge  
191 Road. Evaluations for additional surface sites are shown in Figure S3 and include the remaining  
192 NASA P-3 spiral locations. Except for Trail Ridge Road, where hourly averages are provided,  
193 observations are available as 1-minute averages. For direct comparison to the surface sites, the  
194 observations are hourly averaged and then compared to the instantaneous hourly model output.  
195 We expect that most of the surface sites are impacted by local effects that likely will not get

196 resolved by the model despite a 3 km grid resolution. We also note that the definition of a  
197 “vector averaged” wind direction can be misleading given the high variability, but nevertheless  
198 allows insight into general flow regimes.

199 For NFRMA sites, the model represents well the average wind speed at 10 m above ground level  
200 (agl) with the exception of Fort Collins CSU (Figure S3), where the model is biased high. Both  
201 observations and model show a tendency for highest wind speeds in the afternoon. The model  
202 captures the average wind direction at most sites with a dominance of easterly (upslope) winds in  
203 the morning/early afternoon. Winds take on a more westerly component (downslope) in the late  
204 afternoon and during nighttime, but the wind direction varies more strongly amongst the sites as  
205 local topography and large scale flow patterns influence the buildup of the downsloping winds.  
206 Sites in the Northern NFRMA (Fort Collins CSU and WC Tower) show a dominance of winds  
207 from the NW at night. Both Fort Collins CSU and the Weld County Tower site are in the Cache  
208 la Poudre drainage, which might explain the northwesterly flow at night. The WC Tower site  
209 might also be under the influence of northwesterly flow coming from the western corner of the  
210 Cheyenne Ridge which has a steeper slope than the Platte Valley to the South. Sites from Denver  
211 up to Greeley (e.g. La Casa, BAO, Platteville), however, show winds mostly from the SW,  
212 representing the drainage flows along the Platte River Valley, the region stretching from Denver  
213 to about Greeley (Toth et al., 1995)

214 The two sites near the Foothills (NREL Golden and RF North) show westerly downsloping  
215 winds taking over late afternoon/early evening and while the model performs well during the  
216 periods of pronounced slope winds, it has slight difficulty representing the switch from upslope  
217 to downslope winds. These two sites specifically are impacted by sub-grid local topographic  
218 features as they are nestled near the Foothills at or near the mouth of canyons. The model with a  
219 3 km resolution has difficulties fully representing these conditions. The winds during this  
220 transition period are also more variable compared to periods of established slope winds adding,  
221 additional challenge.

222 Even though we can identify general flow patterns across the NFRMA region, there are notable  
223 differences amongst the different sites representing complex mixing and circulation patterns.  
224 Wind direction can vary across even neighboring sites such as Platteville and WC Tower, which

225 are both located in the Colorado Eastern plains and only 22 km apart. While at WC Tower winds  
226 after midnight are mostly from the North, Platteville (Figure S3) shows drainage flows from the  
227 South-West during nighttime. The drainage flows are not very prominent in the observations,  
228 because the site is situated in a shallow topographical depression which leads to localized  
229 disturbances in the wind fields. The model does not resolve the small scale topographical  
230 influence and more clearly shows the drainage flows. Drainage flows are also evident at the  
231 nearby BAO site and at the downtown Denver La Casa site. Upslope flows dominate at both sites  
232 during the day but are more variable at Platteville compared to WC Tower. This demonstrates  
233 that wind direction alone, albeit helpful, cannot necessarily be used to identify the origin of  
234 plumes measured at any of the surface sites. This is important to keep in mind in the analysis of  
235 the data and warrants the integration of different data sets and models to assess transport flows  
236 and source impacts.

237 The two high altitude sites Longs Peak and Trail Ridge Road, which are considered as being  
238 representative of remote conditions and strongly influenced by the higher-level Westerlies, show  
239 an overall dominance of winds from the NW in the measurements. The model, in contrast,  
240 simulates at both sites winds more strongly from the W as is typical for free-tropospheric winds  
241 in the northern mid-latitudes. The Longs Peak site is located in the valley of Cub Creek, which  
242 has a NW to SE orientation and likely channels the local winds. The model cannot resolve this  
243 and the model elevation interpolated to this site is higher compared to the actual elevation (2854  
244 m versus 2743 m). A similar influence of topography might cause the NW wind direction at Trail  
245 Ridge Road. Winds show a higher deviation from the north-westerly (westerly in the model)  
246 direction in the afternoon indicating that occasional upslope flows interrupt the typical Westerly  
247 flow. This is true specifically at Longs Peak, which is closer to the NFRMA. The model  
248 overestimates the wind speed at both sites which is likely related to the model not simulating the  
249 influence of small scale topography and unresolved surface roughness.

250 To provide further evaluation of the model performance regarding the vertical structure of key  
251 meteorological parameters, we compare wind observations taken by ozone sondes launched at  
252 Platteville and Fort Collins West (Figures 3 a and b). At Platteville, where data from 40 ozone  
253 sonde launches are available (13 July – 10 Aug, daytime only) the model represents well the

254 average profiles of wind speed, relative humidity and temperature throughout the atmosphere.  
255 Note that what appears like a shallow inversion layer in temperature is due to only four data  
256 points at the lowermost altitude bin and cannot be regarded as representative for the entire time  
257 period. The model picks up the overall profile shape in wind direction, except at the lowermost  
258 altitude bins, where the model simulates easterly winds while the average wind direction in the  
259 observations is from the S. This is in line with the surface data. As can be seen from windroses  
260 (Figure 3 c) and from Figure S3, the average wind direction at the surface is dominated by  
261 Easterlies in the model throughout the day, while the measurements are much more variable in  
262 the morning and from mostly the ESE sector in the afternoon indicating that the model presents  
263 more the regional flow and has difficulties picking up the local variability.

264 The model shows a good agreement in wind direction for Fort Collins-West, where data from 12  
265 launches are available (20 July-6 August). WRF simulates the mean SSE winds near the surface,  
266 but transitions faster to Westerlies above compared to the observations. Wind speed, which  
267 compared well at Platteville, is overestimated at the lowermost altitude bin, which is in  
268 agreement with the comparison of wind speed data at the nearby Fort Collins CSU site. The  
269 modeled relative humidity and temperature profiles agree well with the observations.

270 Finally, we also provide a brief evaluation of the modeled boundary layer height (PBLH) for  
271 selected time periods. Figure 4 compares the model to the PBLH derived from Micropulse Lidar  
272 (MPL) data at FC West, Platteville and NREL Golden. This is not a true direct comparison given  
273 the different definitions of the modeled and retrieved PBLH, but shown here to give an  
274 indication of the model's ability to represent the typical PBLH and day-to-day variability. The  
275 YSU PBL scheme used in the model is a first-order nonlocal scheme, with a countergradient  
276 term and an explicit entrainment term in the turbulence flux equation for heat or momentum [Hu  
277 et al., 2013]. In YSU, the PBLH is defined as the level in which minimum flux exists at the  
278 inversion level. The MPL retrieved PBLH, in contrast, have been obtained from gradients or  
279 variance in the backscatter profile, wavelet covariance, and fits to idealized profiles [Compton et  
280 al., 2013].

281 Despite the noise in the data, some unreasonable looking MPL retrievals (e.g. the first four days  
282 at Platteville) and the different definitions of PBLH, we can see that the model overall represents

283 the PBLH and the day-to-day variability fairly well, specifically for NREL Golden and FC West  
284 whereas the model underestimates more often the PBLH at Platteville. This is in line with the  
285 model also showing higher uncertainty in representing the wind direction at Platteville, thus  
286 performing less well for this site than for some others. Comparing PBLH amongst the three sites  
287 it is interesting to note that the PBLH can vary notably reflecting the local nature of sites and, in  
288 general, the variability in meteorological and dynamical conditions across the NFRMA.

## 289 **5. Relationship between model tracers and chemical tracers**

290 The modeled tracers are not directly comparable to any specific chemical measurements, but  
291 indirectly can be evaluated by assessing the correlation with their respective surrogate chemical  
292 tracer, i.e. the chemical species used to define the inert emission tracers. Such an analysis also  
293 gives insight to what degree the inert tracers can assist in the analysis of chemical measurements.  
294 We assess the average tracer distribution and provide a statistical analysis to determine how well  
295 the model tracers relate to one-minute averaged measurements of  $\text{NO}_x$ ,  $\text{C}_2\text{H}_6$  and  $\text{NH}_3$ , i.e. the  
296 species the tracer emissions were scaled to, on both aircraft (NASA P-3 and NCAR/NSF C-130).  
297 Similar to before, hourly output of the model tracers was interpolated to the time, location and  
298 altitude of the aircraft. The interpolation from hourly output is expected to lead to errors in  
299 representing the observed variability, but these errors are partly smoothed by investigating larger  
300 spatial and temporal averages.

301 In Figure 5 we show NCAR/NSF C-130 measurements of  $\text{NO}_x$  and  $\text{C}_2\text{H}_6$  mixing ratios together  
302 with mixing ratios of  $\text{TR}^{\text{AreaMobile}}$  and  $\text{TR}^{\text{OG}}$  (Results for  $\text{TR}^{\text{Agr}}$  and  $\text{NH}_3$  are shown in Figure S4).  
303 Only flight data within the NFRMA and below 3 km agl have been selected. Similar plots for the  
304 NASA P-3 aircraft data are shown in Figure 6 and Figure S5. For these graphs, the aircraft  
305 measurements have been averaged on a 0.1 degree x 0.1 degree grid for the NCAR/NSF C-130  
306 flights and on a 0.05 degree x 0.05 degree grid for the NASA P-3 flights to ensure a reasonable  
307 number of points feeding into the analysis. The NCAR/NSF C-130 flight patterns are more  
308 variable and less repetitive; hence a larger averaging grid is used compared to NASA P-3, which  
309 used a repetitive flight pattern. For the NCAR/NSF C-130 analysis we also select a slightly  
310 larger region compared to the NASA P-3, including flight legs over the Foothills. However, the

311 general conclusions remain the same independent of grid size or region. The spatial correlation  
312 coefficient R is listed in the graphs as well as in Table 2 and has been calculated when applying  
313 different filtering in altitude. Grid averages are only calculated for grids where at least 3 data  
314 points are available

315 We find that the spatial pattern of the tracers is overall representative of the spatial pattern  
316 derived for the measured chemical tracers. We do not expect a perfect agreement between the  
317 tracers and their surrogate chemical species given that our inert tracers have a different lifetime  
318 than their chemical surrogates and that we are comparing hourly instantaneous model output to  
319 1-minute average aircraft measurements. Uncertainties in modeled winds, PBLH and vertical  
320 mixing or the underlying emissions also impact the comparison. In line with the source regions  
321 (Figure S1), highest  $\text{NO}_x$  and  $\text{TR}^{\text{AreaMobile}}$  concentrations are found near the Denver urban area. In  
322 contrast,  $\text{C}_2\text{H}_6$  and  $\text{TR}^{\text{OG}}$ , and  $\text{NH}_3$  and  $\text{TR}^{\text{Agr}}$  are highest NE of the urban area, but elevated  
323 values extend all the way into the northern part of the Denver urban area. Spatial correlations are  
324 in the range ~0.7-0.9 between the inert tracers and their respective surrogates. However, given  
325 that OG and agricultural sources both originate from similar regions, higher R values are also  
326 calculated for  $\text{TR}^{\text{Agr}}$  with  $\text{C}_2\text{H}_6$  and for  $\text{TR}^{\text{OG}}$  with  $\text{NH}_3$ .

327 Filtering for lower altitudes, in general, reduces slightly the correlations given that the number of  
328 available data points is reduced and that near-surface concentrations are expected to be more  
329 impacted by small scale variability and local effects. Significant R values, however, are also  
330 calculated when a more stringent filtering for altitudes below 1 km agl is applied. In the case of  
331 the NCAR/NSF C-130, where flights in the selected NFRMA region were focused on measuring  
332 emissions and mostly conducted at low altitudes, 98% of the selected NFRMA data are below 3  
333 km ag, and 63% are below 1 km agl. For the NASA P-3, the corresponding values are 77% and  
334 48%, respectively.

335 In Figure 7 we look at the spatial correlations of the model tracers  $\text{TR}^{\text{AreaMobile}}$  and  $\text{TR}^{\text{OG}}$  with  
336 different chemical tracers. For the analysis, gridded averages of all model and observational data  
337 are derived and these are used to calculate the spatial correlation. We show the correlations when  
338 all flights are considered as well as correlations for individual flights so as to represent the  
339 variability encountered on individual days. This analysis helps to identify which chemical tracers



340 are suited for fingerprinting air masses and, in turn, can be used for evaluating the model tracer  
341 sources and transport. A larger number of VOC species was measured on the NCAR/NSF C-130  
342 compared to the NASA P-3, but for those chemical tracers that were measured on both aircraft  
343 the findings are similar. The correlations can be highly variable between flights and reflect  
344 variations in the model performance and also the species lifetime. The fresher the emissions that  
345 were sampled and the simpler the chemistry for a chemical species, the better we expect the  
346 model tracers to represent the chemical observations.

347  $\text{NO}_x$ , Ethanol and Toluene as well as Ethylbenzene and o-Xylene, the latter two only measured  
348 on the NCAR/NSF C-130, show a high correlation with  $\text{TR}^{\text{AreaMobile}}$  and a rather low correlation  
349 with  $\text{TR}^{\text{OG}}$  indicating these to be valuable tracers for urban emissions. In turn, ethane, propane  
350 and methane show a consistently good correlation with  $\text{TR}^{\text{OG}}$  and low correlation with  
351  $\text{TR}^{\text{AreaMobile}}$  and can be considered as indicators for emissions from OG sources. High  
352 correlations with  $\text{TR}^{\text{OG}}$  are found for  $\text{NH}_3$  due to the collocation of agricultural and OG sources.  
353 Benzene is emitted by both urban and OG sources and the mean correlation is high with both  
354 model tracers on the NCAR/NSF C-130, while on the NASA P-3 it has good correlation with  
355  $\text{TR}^{\text{OG}}$  but low R with  $\text{TR}^{\text{AreaMobile}}$ . In part, this might be attributed to the NASA P-3 flight pattern  
356 where high benzene values during spirals over Platteville in the OG source region (Halliday et  
357 al., 2016) dominate the signal. Both aircraft, however, show a large spread in R values across the  
358 individual flights pointing out the dependence of the derived correlation on the flight patterns  
359 and specific meteorological conditions on any given flight day.

360 Correlations of  $\text{TR}^{\text{AreaMobile}}$  with CO are high for the NASA P-3 but much lower (~0.5) for the  
361 NCAR/NSF C-130. This is due to a much smaller number of data points available for the  
362 NCAR/NSF C-130. The CO instrument on this aircraft experienced problems during the first part  
363 of the campaign and data are only available for August flights. On either aircraft, CO does not  
364 show any correlation with the OG source tracer, yet CO commonly is used to normalize  
365 emissions and measured concentrations for a variety of airmasses. This analysis, however,  
366 suggests that it is more appropriate to identify source specific tracers when analyzing emission  
367 ratios, conduct inverse modeling studies or look at species ratios to account for dilution effects,  
368 specifically in regions of diverse sources.

## 369 **6. Average Tracer Distributions**

370 The comparison with observations shows that the model captures the general flow regimes and  
371 source regions well. Here we now use just the model tracers to visualize the transport and  
372 distribution of different source types. Note that we only focus on surface data and do not have  
373 information on entrainment from higher altitudes from the measurements. In Figure 8, we plot  
374 the average spatial distribution of  $TR^{\text{AreaMobile}}$  and  $TR^{\text{OG}}$  for different times of the day to  
375 demonstrate where, on average, the strongest impact from the different emission sectors is found.  
376 We calculate the average mixing ratio within the planetary boundary layer (PBL) to reduce the  
377 influence of diurnal changes in vertical mixing and dilution. As noted by Zhang et al. [2016] and  
378 Kaser et al. [2017] and as was also observed during the campaign from measurements of  $\text{NO}_x$   
379 that were taken during the P-3 spirals, concentrations are not necessarily well mixed within the  
380 PBL. However, we believe that the PBL average tracer concentrations are a more suited quantity  
381 to analyze and the general findings and conclusions do not change if instead surface  
382 concentrations were considered. In addition to showing the average spatial tracer distribution, we  
383 denote the average surface ozone concentrations at all locations, where during FRAPPÉ/DAQ  
384 surface ozone monitors were placed. This also includes sites not listed in Table 1. In support of  
385 the analysis we further show in Figure S6 the average daytime ventilation index for the same  
386 times shown in Figure 8. The Ventilation Index is the mathematical product of the mixing height  
387 and the average horizontal transport wind throughout the depth of the PBL and provides an  
388 estimate of how high and how far pollutants will disperse.

389 During nighttime (0-6LT), when the urban emissions are at their diurnal minimum, the  
390 distribution of  $TR^{\text{AreaMobile}}$  reveals a pooling of emissions from the Denver Metro area into the  
391 Platte River Valley, i.e. towards the region with strongest OG sources. Lowest ozone mixing  
392 ratios are found in the Denver Metro area, WC Tower (located in Greeley) and Fort Collins  
393 (FTC) CSU, where high  $\text{NO}_x$  from urban sources (Figure S1) causes ozone titration, and at  
394 Platteville, likely due to transport of high  $\text{NO}_x$  and low ozone from the Denver area.

395 In the morning (6-12 LT) flow reversal transports aged emissions back into the NFRMA mixing  
396 with fresh emissions from the OG source region and fresh emissions from the Metro Area. The  
397 ventilation index indicates that during morning there is limited venting in the NFRMA with

398 lowest values for the north-eastern NFRMA. In the afternoon (12-18 LT), the source regions are  
399 more strongly separated and the ventilation index shows that efficient venting out of the PBL is  
400 possible. Similar to what is seen for the morning, the lowest ventilation index is simulated for the  
401 north-eastern NFRMA (marginal-good). Transport of NFRMA tracers into the Foothills becomes  
402 evident. The highest surface ozone is seen for BAO, which interestingly coincides with the  
403 region where strong mixing of  $TR^{OG}$  and  $TR^{AreaMobile}$  is estimated. One explanation is the mix of  
404 airmasses, another possible explanation for this could also be that, independent of the flow  
405 regime, the daytime upslope flow towards the foothills is more likely to pass BAO compared to  
406 other sites. In the evening (18-24LT), when the PBL faded away limiting the degree of mixing  
407 (not shown), the  $TR^{AreaMobile}$  and  $TR^{OG}$  source regions are more clearly separated and the tracers  
408 remain close to their sources. Even though  $TR^{AreaMobile}$  and  $TR^{OG}$  have sources throughout  
409 Colorado, that could potentially impact the NFRMA, we did not find, on average, a significant  
410 transport of emissions from any other source regions in Colorado, at least not in the 2-day  
411 lifetime the inert tracers represent.

412 The mixing of aged urban pollution and fresh emissions from OG sources in the morning has  
413 interesting implications for chemistry. The early morning buildup of ozone in these mixed air  
414 masses warrants further detailed photochemistry studies as it will influence the magnitude of the  
415 afternoon ozone maximum. Similarly, follow-up chemical studies are needed to validate whether  
416 the most efficient ozone production is happening in air masses with the strongest mixing from  
417 the different emission sectors such as suggested by the tracer analysis. Mixing of hydrocarbon-  
418 rich air from the oil and gas area around Greeley with  $NO_x$  rich air from the Denver urban area  
419 could possibly result in more efficient ozone production than in either of the contributing air  
420 masses by themselves.

421 In Figure 9 we calculate statistics for the model tracers for surface sites in Colorado for which  
422 ozone measurements during FRAPPÉ/DAQ are available, to provide insight into the range of  
423 different regimes that were covered by the surface sampling. As before, we show statistics for  
424 the PBL averaged tracer concentrations to omit the impact of diurnal changes in boundary layer  
425 height and limit the data to daytime (10-17 LT) to emphasize the influence during the

426 photochemically most active period of the day. During nighttime (not shown) the statistics are  
427 more strongly dominated by the nearby sources due to the shallow PBL.

428  $TR^{\text{AreaMobile}}$  is largest at monitoring sites in and near the Denver metro area the highest being La  
429 Casa, CAMP and I-25. This can be expected as this is the region with the largest industrial  
430 sources and most transportation. Looking at  $TR^{\text{Area}}$  and  $TR^{\text{Mobile}}$  separately (not shown) we find a  
431 much broader coverage across sites in the NFRMA for the latter reflecting the wide-spread  
432 impact of emissions from transportation ranging from sites close to the Foothills to East of  
433 Denver.  $TR^{\text{Area}}$  has higher values compared to  $TR^{\text{Mobile}}$  due to the high emission strength of  
434 individual point sources (Figure S1), which dominate the spatial pattern.

435 Maximum mean  $TR^{\text{OG}}$  impact is experienced at surface sites in the north-eastern NFRMA (WC  
436 Tower and Platteville), which have an overall minor impact from  $TR^{\text{AreaMobile}}$ , and also other sites  
437 located nearby OG sources such as BAO (Erie) and Longmont. The  $TR^{\text{OG}}$  influence is decreasing  
438 towards the South, but elevated concentrations are found throughout all NFRMA sites. At high  
439 elevation sites West of the NFRMA, the concentrations for both  $TR^{\text{AreaMobile}}$  and  $TR^{\text{OG}}$  show a  
440 general decline with increasing distance from the NFRMA, yet sites like Longs Peak, Squaw  
441 Mountain or Niwot Ridge do also show elevated tracers indicating transport from the NFRMA as  
442 will be discussed later. It should be noted that pollution from upslope events typically reaches  
443 these sites later in the afternoon/evening, which is not fully covered by the chosen time window.

444 While the average  $TR^{\text{AreaMobile}}$  and  $TR^{\text{OG}}$  concentrations overall agree well with the emission  
445 source regions, this analysis reveals a large variability likely due to efficient mixing and  
446 transport in the NFRMA and hints at the existence of a variety of changing chemical regimes. To  
447 show how conditions change over the course of a day, we include in Figures 10 and 11 statistics  
448 of the diurnal cycle for tracer and ozone concentrations for the same surface sites that are  
449 highlighted in Figure 9. Note that for these graphs, we show the diurnal cycle from 6am to 6am  
450 LT, similar to Figure 2. The tracers indicate transport of emissions to the surface sites but given  
451 they are only emitted and have no chemical production associated, are not a representation for  
452 ozone concentrations.

453 The selected sites later are used to discuss upslope events and also represent different source  
454 regions: The two easternmost NFRMA sites include WC Tower located in the OG and  
455 agricultural source region and Aurora East located east of the Denver area. The two other  
456 NFRMA sites are located near the Foothills and include RF North at the interface of urban and  
457 OG source regions and Golden, West of Denver (Figure 1). It has to be kept in mind that  
458  $TR^{\text{AreaMobile}}$  has a diurnal cycle with largest emissions during the day (Figure S2), which biases  
459 the diurnal cycle in concentrations towards higher daytime values. The OG emissions have no  
460 diurnal cycle attached. The average wind direction and speed for these sites have been discussed  
461 above (also see Figure 2) except for Mines Peak and Squaw Mountain for which no wind  
462 measurements are available.

463 In line with the overall tracer distribution discussed in Figure 8, WC Tower, located within the  
464 region of strong OG and agricultural activities, has the highest OG tracer concentrations of the  
465 selected sites. WC Tower is located in Greeley, a town of about 100,000 people and ~20 km east  
466 of a major S-N oriented Highway (I-25). Greeley also is surrounded by oil and gas facilities.  
467 Hence, we do expect that tracer concentrations are impacted by nearby sources and might reach  
468 the site independent of wind direction. While Greeley is in the region of drainage flows from the  
469 Denver Area, nighttime winds, on average, are from a Northerly direction. This suggests that  
470 mostly sources in the Greeley area contribute to elevated tracer concentrations, but given the  
471 localized representativeness of the wind data at surface sites, it is likely that emission transport  
472 from the Denver region through the more regional flow, as suggested in Figure 8, adds to  
473 elevated tracer levels.

474 At RF North and NREL Golden, where the average wind directions are similar, both tracers peak  
475 around late morning/noon as easterly upslope flows transport emissions from the NFRMA  
476 region to these sites. Enhanced ventilation and a higher PBLH also allow for more efficient  
477 mixing and distribution of emissions within the NFRMA as the day progresses. The magnitude  
478 of  $TR^{\text{OG}}$  decreases with distance from the OG source region, i.e. is higher at RF North compared  
479 to NREL Golden, while  $TR^{\text{AreaMobile}}$  is higher at NREL Golden due to the proximity of urban  
480 sources. From the four sites considered, Aurora-East shows the lowest tracer concentrations as  
481 the dominant flow patterns in the south-eastern NFRMA tend to carry pollutants away from this

482 site. The enhancement in the tracers in the morning is in line with winds from the Denver area  
483 (N-NW). Ozone concentrations, also shown in the graphs, peak generally earlier at the eastern  
484 Sites compared to sites closer to the Foothills (around noon versus early afternoon). The average  
485 daytime concentrations are in the order of ~60 ppb for all sites, but the rate of the morning  
486 buildup and the width of the daytime maximum varies across the sites, indicating that different  
487 processes are contributing to the ozone production.

488 Model tracer concentrations and ozone at mountain sites are shown in Figure 11. From the four  
489 sites considered, Mines Peak is the furthest West of the NFRMA (Figure 1). Tracer  
490 concentrations are smaller compared to NFRMA sites because there are no nearby sources and  
491 the tracers get diluted during the transport from the NFRMA. Ozone, in contrast, which is not  
492 emitted and only chemically produced in the atmosphere, can reach higher concentrations at the  
493 mountains sites compared to sites in the NFRMA. On average,  $TR^{OG}$  is higher at the Northern  
494 Sites (Longs Peak and Trail Ridge Road), while  $TR^{AreaMobile}$  is higher at the southern sites  
495 (Squaw Mountain and Mines Peak). This is, because the urban and OG emissions are often  
496 separated during upslope transport with Denver metro area air masses staying further South and  
497 OG influenced air masses staying further North. This is indicated in Figure 8 and will be  
498 discussed in more detail in the next Section.

499 The peaks in  $TR^{AreaMobile}$  and  $TR^{OG}$  occur in the late afternoon/evening; the closer a site to the  
500 NFRMA (i.e. the further east) the earlier the peak. The distance between Trail Ridge Road to  
501 WC Tower is 95 km, between Longs Peak and Platteville 67 km, between Squaw Mountain and  
502 downtown Denver 45 km, and 65 km between Mines Peak and downtown Denver. On average,  
503 there is a ~2-3 hours delay between Mines Peak and Squaw Mountain and between Longs Peak  
504 and Trail Ridge Road. Trail Ridge and Mines Peak are the furthest from the NFRMA and as a  
505 result reach their peak the latest. The peak in the model tracers coincides roughly with an  
506 increase in ozone or an increase in the variability in ozone. Mean hourly maximum ozone  
507 concentrations are highest for Trail Ridge (58 ppb) and about 54-55ppb for the other sites.

508 Many of the features shown in the average spatial and temporal patterns of the model tracers and  
509 also in wind direction can be explained by mountain-valley winds suggesting this was a

510 dominant transport pattern during FRAPPÉ/DAQ. General mountain-valley flows and selected  
511 cases for these flow patterns will be discussed in greater detail in the following Section.

## 512 **7. Mountain-Valley Transport**

513 Mountain-Valley winds or upslope-downslope winds are a common occurrence in the Colorado  
514 Front Range, developing under clear sky conditions and weak synoptic-scale winds. The  
515 development of mountain-valley winds is a complex interaction between thermally driven and  
516 ambient flow. For more detail the reader is referred to previous studies (e.g., Arritt et al., 1992,  
517 Bauman et al., 1997 or Reddy and Pfister, 2016) and to the recent study by Sullivan et al. (2016),  
518 who provide a discussion on mountain-valley flows in the NFRMA during FRAPPÉ/DAQ. A  
519 brief overview is given here. In the morning, daytime solar heating of higher terrain and sun-  
520 facing slopes causes a pressure gradient and generates localized slope winds, which draw air  
521 from the valley floor. This results in winds blowing up-valley (from the SE, E and NE in the  
522 NFRMA) that are more regional in scale than the slope winds. For the scales we look at here, we  
523 will define both flow patterns as “upslope”. Given the limited resolution of the model it will not  
524 be able to fully resolve the narrow canyons and related slope winds, which will introduce  
525 uncertainties in the simulated development of mountain-valley flows as well as localized wind  
526 directions due to channeling effects. The air masses, when reaching the mountain tops during the  
527 afternoon, get lifted vertically and mix into the prevailing westerlies. Vertical mixing and re-  
528 entrainment into the boundary layer potentially close the loop and might bring part of the  
529 pollution back into the Front Range.

530 How much of the pollution transported to the East in the free troposphere is mixing back down to  
531 the surface is poorly understood. The study by Kaser et al. (2017) uses the FRAPPÉ/DAQ data to  
532 quantify the effect of ozone entrainment, yet the field measurements do not allow a complete  
533 separation of the contribution of recirculation from that of regional and long-range pollution.  
534 Efficient recirculation with a high potential of impacting surface concentrations occurs when the  
535 winds within the PBL change from easterly at the surface to westerly at the top of the PBL.  
536 Subsidence on the east end of the solenoid could introduce re-circulated and free-tropospheric  
537 material into the top of the PBL. Understanding the re-circulation patterns and associated

538 pollution build-up and how well models are able to represent them are important factors in air  
539 pollution studies. Here, we use the model tracers together with observations made from different  
540 platforms during FRAPPÉ/DAQ to visualize and characterize mountain-valley winds  
541 encountered during the campaign.

542 The implications of mountain-valley transport in regard to air quality are the transport of  
543 pollution into the mountains and its impact on pristine regions, the impact of possible  
544 recirculation of Front Range pollution, the buildup of ozone and the mixing of pollution into the  
545 free troposphere. To establish the frequency and timing of general upslope flows we show in  
546 Figure 12 the frequency of upsloping and downsloping winds during FRAPPÉ/DAQ at selected  
547 surface sites. The upslope direction has been chosen based on visual analysis of windroses and is  
548 defined as a 90 degree wide swath surrounding the most prominent upslope angle for each site.  
549 This definition is somewhat arbitrary but necessary because the direction of upslope flows can be  
550 highly variable due to the influence of topography and large-scale weather systems. However,  
551 the general conclusions hold regardless of the definitions applied.

552 The analysis shows a dominant upslope flow during daytime at all sites. Upslope flows develop  
553 the earliest at the sites closest to the Foothills (RF-North and Golden) and then spread to the East  
554 and into the mountains. Daytime upslope winds are also dominant at the sites east of the  
555 NFRMA, but these do not show a well-established downslope (or drainage) flow in line with the  
556 average wind direction in Figure 2. The model represents the observed patterns well at NFRMA  
557 sites as well as mountain sites but predicts daytime upslope flows too frequently at the NFRMA  
558 sites as well as at Longs Peak. Note that the timing of upslope flow based on the wind analysis is  
559 in line with the diurnal cycle of the tracers shown in Figure 11. For the mountain sites, the model  
560 suggests a more pronounced downslope pattern which is due to our definition of downslope as  
561 winds from within  $270\pm 45$  degree and the fact that the model winds are predominantly from the  
562 West, while measured winds at Trail Ridge Road and Longs Peak are mostly from the NW and  
563 variable across the W-N, respectively (Figure 2).

564 To assess how important mountain-valley winds are on high ozone days, we show in Figure 13  
565 concentration wind roses for ozone and  $TR^{OG}$  for Longs Peak and Trail Ridge Road. The data are



566 separated into high and low ozone days, which has been defined as the average ozone  
567 concentration at RF-North for 12-18LT being > 70 ppb (high) or < 60 ppb (low). The results are  
568 similar if other nearby Front Range Foothills sites are used or if we choose a different threshold  
569 for high ozone such as 75 ppb. Note that there are more data points for low ozone days compared  
570 to high ozone days, which is due to the FRAPPÉ/DAQ time period overall being characterized  
571 by few high pollution episodes.

572 High ozone at the Foothills sites, in general, results in high ozone at the mountain sites. On high  
573 ozone days, the measurements show a strong component of upslope flows with elevated ozone  
574 concentrations (> 60 ppb) during the afternoon, whereas for low ozone days the dominant wind  
575 direction is from the West and North West with ozone concentrations mostly below 60 ppb. This  
576 is in line with findings by Reddy and Pfister (2016) who state that high ozone days occur mostly  
577 on days with upper level high pressure ridges. In addition to bringing warmer temperatures and  
578 fewer clouds, upper level ridges in this region reduce synoptic winds and thus allow cyclic  
579 terrain-driven circulations.

580 The model simulates the measured wind statistics well and on high ozone days suggests  
581 significantly enhanced TR<sup>OG</sup> from the SE sector, which confirms that the high ozone is related to  
582 transport of pollution from the NFRMA. Longs Peak shows a higher variability of the measured  
583 wind directions compared to Trail Ridge Road. This is explained by the Longs Peak sites being  
584 more strongly affected by local influences whereas the site of Trail Ridge Road is more exposed  
585 and somewhat better captures the regional flow. Similar conclusions as for Longs Peak and Trail  
586 Ridge Road are drawn for Squaw Mountain and Mines Peak if model winds are used to  
587 substitute the missing wind measurements (not shown).

## 588 **7.1 Thermally driven upslope and transport over the Divide**

589 On 12 August 2014, the NCAR/NSF C-130 conducted a flight designed to measure the upslope  
590 of Front Range pollution into the mountains that was forecast by various model products  
591 including the WRF Tracer model. The flight consisted of two parts. The first part was targeted at  
592 characterizing daytime pollution and emissions in the Front Range, and the second part (22:41-  
593 2:26 UTC or 16:41-20:26 LT) included a set of S-N legs over the city and the Foothills, followed

594 by two legs over the Continental Divide and a missed approach into Granby Airport (40.09N, -  
595 105.94W, 2500 m) located in the Fraser Valley West of the Divide. Upslope transport was  
596 evident to the Divide and spillover of high ozone air into the Fraser Valley over Berthoud Pass  
597 (where Mines Peak is located) was observed. We use the aircraft data together with the model  
598 tracers and surface measurements to investigate in detail the upslope flow and the pollution  
599 “spill-over” across the Continental Divide. Here, as well as throughout the rest of the paper when  
600 we focus on individual days, we restrict the analysis to a single model cycle to avoid  
601 inconsistencies in the model data over the course of a day. We select the 12 UTC (6 LT) forecast  
602 cycles as this allows for the shortest forecast lead and the most constrained of the forecast with  
603 analysis fields; i.e. for 12 August we select the model forecast cycle 20140812 12UTC.

604 Figure 14 shows measured ethane and NO<sub>x</sub> concentrations together with the modeled TR<sup>OG</sup> and  
605 TR<sup>AreaMobile</sup> concentrations. The measured and modeled wind data are added to each of the  
606 graphs. The model data are interpolated to the time and location of the 1-minute merged  
607 observations and all data sets are then averaged over a 0.1 degree x 0.1 degree grid. Only the  
608 second part of the NCAR/NSF C-130 flight, which focused on the upslope event, is considered  
609 and only data below 2 km agl are used to emphasize the impact on near-surface pollution levels.  
610 The 2 km agl upper limit does not guarantee that all the data were within the PBL, but is used  
611 here to have sufficient number of data points to demonstrate the spatial variability. Specifically,  
612 over the Foothills and the continental Divide, the aircraft often was not able to get close enough  
613 to the ground due to the flight restrictions and sampling was done in parts above the PBL in  
614 prevailing westerlies more strongly influenced by background tracer concentrations.

615 The aircraft data demonstrate a strong push of Front Range pollution into the mountains and a  
616 clear distinction between airmasses dominated by urban emissions and those dominated by oil  
617 and gas sources with the former mostly impacting the southern Foothills, and the latter impacting  
618 the Northern Foothills. The highest NO<sub>x</sub> concentrations, used here as a tracer for urban  
619 emissions, are seen in the southern legs of the aircraft track and it is evident from the data that  
620 this pollution has been transported to the Continental Divide and actually also descended into the  
621 valleys to the West, which was measured by the aircraft during the missed approach into Granby  
622 airport. The highest ethane concentrations are seen in the northernmost legs of the aircraft track.

623  $TR^{\text{AreaMobile}}$  and  $TR^{\text{OG}}$  give a good representation of the features found in the aircraft data and  
624 the model also simulates well the wind field with mostly easterly and south-easterly winds over  
625 the region at the lowermost altitudes during the upslope event. The model data interpolated to the  
626 flight track do not show the enhanced ethane concentrations measured during the time of the  
627 aircraft descent into Granby but, as will be shown later, the model simulates the “spill over” of  
628  $TR^{\text{OG}}$ .

629 A closer look at the high elevation surface sites is provided in Figure 15. In this graph, the  
630 diurnal cycles for ozone,  $TR^{\text{OG}}$  and  $TR^{\text{AreaMobile}}$  are shown for 12 August. We also include, for  
631 reference, their respective average diurnal cycle. Upslope is more pronounced at the northern  
632 mountain sites, but all four mountain sites experience above average influence from  $TR^{\text{AreaMobile}}$ ,  
633 with Longs Peak and Trail Ridge Road also impacted by transport of enhanced  $TR^{\text{OG}}$ . On this  
634 day, the ozone reported at Longs Peak and Trail Ridge Road was amongst the highest of all the  
635 sites considered, which can be attributed to the nature of the upslope flow and the highest  
636 afternoon surface ozone concentrations being reported at the northern NFRMA sites. Ozone  
637 concentrations and model tracers increase starting after noon, when stable upslope winds had  
638 established (Figure S7). At Trail Ridge Road, a pronounced second peak in the tracers is  
639 modeled at around 22 LT roughly coinciding with a slight increase or leveling-off in ozone and a  
640 switch in winds from E to W. Looking at model longitudinal cross sections (not shown here) this  
641 likely is related to return flow of NFRMA transported tracers. Similar return flow is also seen at  
642 Longs Peak albeit less pronounced for the model tracers.

643 Ozone concentrations and model tracers at Squaw Mountain and Mines Peak reach their maxima  
644 later in the day compared to Longs Peak and Trail Ridge Road with maximum concentrations of  
645 ~65-70 ppb.  $TR^{\text{AreaMobile}}$  is enhanced while  $TR^{\text{OG}}$  remains fairly low, which is in agreement with  
646 the air mass separation discussed earlier. We attempt to establish the start of the upslope flow for  
647 northern and southern parts of the Front Range using wind data for WC Tower and Aurora East,  
648 respectively (Figure S7). Both observations and model show that upslope winds in the northern  
649 part of the Front Range (WC Tower) developed earlier in the morning compared to southern sites  
650 (Aurora East), which adds to the difference in the timing of the air masses arriving at the

651 mountain sites. Different transport pathways will also add to the different timing at the mountain  
652 sites.

653 Figure 16 provides a different view of the transport across the divide by showing a longitude –  
654 altitude cross section along 40.09N for TR<sup>OG</sup>. We use TR<sup>OG</sup> because it has no sources near the  
655 Granby area and demonstrates the transport from NFRMA better than TR<sup>AreaMobile</sup>, which has  
656 some local sources in the Granby area. As mentioned above, upslope flows developed around  
657 mid-morning at the Foothills site and by 22 UTC (16 LT) upslope winds in the PBL covered the  
658 entire region from the Plains up to the Continental Divide. On the Western side of the Divide  
659 upslope winds (Westerlies) are present. Accordingly, TR<sup>OG</sup> is enhanced all the way from the  
660 Front Range up to the Divide and low on the Western side of the Divide. The model estimates  
661 the PBLH at ~2 km agl. We can also see a weak solenoid flow with updraft over the Divide,  
662 winds switching to westerlies near the top of the PBL and an area of downdraft over the eastern  
663 NFRMA. As stated earlier, such a flow pattern has the potential of recirculating Front Range  
664 pollution back to the Front Range and bringing it back to the surface efficiently. A radiosonde  
665 launched at the BAO Tower in Erie (Table 1) indicates a switch in the winds from south-  
666 easterlies to West at about 3 km, which agrees well with the model for the same time (not  
667 shown).

668 At 2 UTC on 13 August 2014 (20 LT on 12 August 2014), which is around the time of the  
669 missed approach of the NCAR/NSF C-130 into Granby airport, upslope flow on the eastern side  
670 of the Divide continues, but on the Western side we now see downsloping winds prevailing  
671 carrying the air masses from the Front Range down into the Fraser Valley. The model PBL has  
672 shrunk to about 500 m, but upsloping winds on the eastern side in the Divide and downsloping  
673 winds on the Western side of the Divide also persist above the PBL. Tracer concentrations  
674 remain elevated above the PBL in the NFRMA. There are no PBL measurements in the NFRMA  
675 for evaluation available for this day and time, but the NCAR/NSF C-130 temperature and water  
676 vapor measurements during the descent into Granby indicate that there have been two different  
677 mixing regimes with one layer up to about 500 m agl, which is in line with the model PBLH, and  
678 another layer up to about 1000 m agl (not shown). Wind measurements at most surface sites as  
679 well as model results show a shift to westerly winds at the eastern side of the Divide after ~20

680 LT accompanied with an increase in ozone concentrations and model tracers (not shown). Until  
681 FRAPPÉ/DAQ there was uncertainty whether NFRMA pollution can potentially impact the  
682 valleys to the West of the Continental Divide. The aircraft measurements together with the  
683 model tracers confirm a “spill-over” of pollution and provide a well-documented case for such an  
684 event.

## 685 **7.2 Discussion**

686 The case study for 12 August demonstrates a general separation of OG and urban dominated air  
687 masses during upslope events. This leads to the question if air masses are always separated  
688 during upslope events given that such dominance would have different implications for air  
689 quality impacts on remote mountain areas than if the pollutants were more mixed. A tendency  
690 towards a separation of airmasses is indicated by the model showing a dominance of TR<sup>OG</sup> at  
691 Longs Peak and Trail Ridge Road and a dominance of TR<sup>AreaMobile</sup> at Squaw Mountain and Mines  
692 Peak over the entire FRAPPÉ/DAQ period (Figure 11). To demonstrate the variability in upslope  
693 events, we show in Figure 17 the spatial distribution of TR<sup>OG</sup> and TR<sup>AreaMobile</sup> for different days  
694 when upslope was modeled together with the average surface ozone concentrations for all sites  
695 where measurements are available. We focus on 14-20 LT as this covers the time period when  
696 upslope generally reaches the high mountain sites. In addition to the average over the  
697 FRAPPÉ/DAQ period and the 12 August case study discussed above and where air mass  
698 separation was observed, we also show results for 22 July, and 2, 4 and 8 August. All these days  
699 demonstrate transport of NFRMA pollution to the mountains, but the spatial patterns and  
700 strength of the upslope vary considerably. In addition to the graphs, we list in Table 3 for the  
701 cases shown the maximum hourly ozone concentrations together with the respective local hour  
702 for selected mountain and NFRMA sites.

703 First, we look at the general tracer distribution on 12 August and compare to the average over the  
704 campaign period. On this day, TR<sup>OG</sup> showed a more widespread distribution compared to the  
705 average distribution, but elevated TR<sup>OG</sup> concentrations stayed mostly North and shows only a  
706 small influence on the Denver area. With the onset of upslope around mid-morning (see Figure  
707 S6 for wind direction plots for WC-Tower and Aurora East) the flow patterns change and SE  
708 flows push the NFRMA tracers into the Foothills at the same time keeping TR<sup>OG</sup> away from the

709 Denver Area. As the day progresses, the strong upslope flow continues transporting the tracers  
710 all the way to the Continental Divide similar to what was seen from the aircraft data. The high  
711 elevation surface ozone monitors report elevated ozone up to ~80 ppb at Longs Peak and Trail  
712 Ridge Road at 14 LT and 15 LT and also the Niwot Ridge monitors report hourly ozone  
713 concentrations above 70 ppb. In line with this, the highest surface ozone in the NFRMA on this  
714 day has been recorded at sites close to the Foothills in the Northern part of the NFRMA, yet none  
715 of these sites reach hourly ozone maxima as high as the mountain sites (Table 3). It is interesting  
716 to note that the surface ozone monitors along the E-W transect into the mountains report elevated  
717 ozone, yet surface ozone in the Denver area, where the air is coming from, is low. This suggests  
718 that (1) the airmasses from the Denver area had a great potential for forming ozone and (2) the  
719  $\text{NO}_x$  and VOC mix in the Denver area has a high ozone forming potential also without  
720 significant contributions from OG. The amount of ozone produced during upslope transport is  
721 clearly a topic that should be explored further using chemistry observations and modeling.

722 The highest ozone day experienced during the campaign was on 22 July 2014. Compared to the  
723 average conditions and the patterns seen on 12 August,  $\text{TR}^{\text{OG}}$  extended further South in the  
724 afternoon mixing with areas of high  $\text{TR}^{\text{AreaMobile}}$ , whereas  $\text{TR}^{\text{AreaMobile}}$  had only a small impact on  
725 the north-eastern NFRMA. Widespread high ozone comes along with the widespread emission  
726 tracers. Clear skies, a lower and slow growing PBLH (Figure 4; evident for NREL Golden) and  
727 reduced ventilation (not shown) resulted in less dilution with increased tracer concentrations,  
728 which contributed to the high ozone concentrations. During the transport into the Foothills,  $\text{TR}^{\text{OG}}$   
729 and  $\text{TR}^{\text{AreaMobile}}$  stay mostly separate, yet the distribution of both tracers is shifted to the South  
730 compared to 12 August. The model also indicates transport across the Divide reaching the  
731 Granby area ~ 20 LT on 23 July (not shown).

732 Hourly ozone concentrations reached 80 ppb and higher on 22 July at most NFRMA sites. Ozone  
733 concentrations remained elevated into the late afternoon/evening in and near the Foothills but  
734 decreased at surface sites in the southern and eastern NFRMA. This might be explained in that,  
735 similar to 12 August, recirculation of NFRMA pollution lead to ozone buildup and the onset of  
736 downsloping winds ~18LT at sites near the Foothills likely contributed to keeping ozone values  
737 elevated. A potential solenoid flow has been discussed by Sullivan et al. (2016) for the northern

738 NFRMA on 22 July around 2 UTC (20 LT) when ozone concentrations at Fort Collins West and  
739 RF North experienced a small second peak. Similar to what was shown for 12 August, we do see  
740 recirculation flows and subsidence over the NFRMA but mostly these are simulated during the  
741 day whereas at 2 UTC (20 LT) the model simulations show the establishment of surface  
742 downsloping winds. However, we note that the wind and PBL fields for 22 July change notably  
743 between the different forecast cycles pointing towards a larger uncertainty in the model transport  
744 for this event.

745 Strongly elevated ozone concentrations are also detected at the mountain sites on 22 July. Hourly  
746 ozone concentrations greater than 80 ppb occur at Squaw Mountain and Mines Peak around  
747 16LT and 17LT, respectively, where enhanced  $TR^{AreaMobile}$  and slightly enhanced  $TR^{OG}$  is  
748 modeled. The ozone concentrations at the mountain sites are higher than would be suggested by  
749 the tracers, but this is because the tracers are purely emission tracers and have no chemical  
750 production, whereas ozone was produced efficiently during the transport to the mountains.  $TR^{OG}$   
751 is enhanced at Longs Peak and Trail Ridge Road, but  $TR^{AreaMobile}$  remains low in line with the  
752 reduced influence of  $TR^{AreaMobile}$  in the north-eastern NFRMA on this day. Still, Longs Peak and  
753 Trail Ridge Road experience peaks in ozone concentrations of 76 ppb and 82 ppb, respectively,  
754 demonstrating the ozone formation potential of air masses originating from the OG area and  
755 transported over the northern part of the Front Range urban areas.

756 On 2 August, upslope is very pronounced in the South with  $TR^{AreaMobile}$  being transported well  
757 beyond the Continental Divide. Similar to the two cases discussed before, the two tracers are  
758 mostly separated during transport into the mountains yet transport of  $TR^{OG}$  appears to be weaker.  
759 This might have contributed to the lower ozone concentrations at Longs Peak and Trail Ridge  
760 Road (72 ppb and 71 ppb, respectively), whereas higher maximum ozone was detected at Squaw  
761 Mountain and Mines Peak (77 ppb).

762 On 3 August, we see that fairly strong upslope transports the tracers to the West but, similar to  
763 the day before, is most established at the southern part of the NFRMA with high levels of  
764  $TR^{AreaMobile}$  reaching to and beyond the Continental Divide. The model tracers agree well with  
765 the emission data measured by the NCAR/NSF C-130 on this day (not shown here), when a  
766 similar flight pattern was carried out as on 12 August. Numerous sites in the NFRMA reach

767 hourly ozone maxima beyond 80 ppb including the northern Foothills sites, yet Longs Peak and  
768 Trail Ridge Road hourly ozone concentrations remain in the moderate range. Similar to the day  
769 before, Mines Peak and Squaw Mountain reach the highest ozone concentrations of 84 ppb at 19  
770 LT and 79 ppb at 21 LT, respectively.

771 Our last example is 8 August, when upslope was weakest of the days considered. We chose this  
772 day because it reflects elevated ozone along the W-E transect of ozone monitors and where  $TR^{OG}$   
773 and  $TR^{AreaMobile}$  intersect. The NFRMA monitors near the start of this transect close to the  
774 Foothills (RF North and SBCreek) reach > 80 ppb at 16 LT and the two Niwot Ridge sites at the  
775 end of this transect reach 78 ppb at 17 LT. From the four main mountain sites, only Longs Peak  
776 and Squaw Mountain show enhanced ozone with the former reaching a narrow peak of 75 ppb at  
777 18 LT and the latter a much broader peak of up to 78 ppb at 17 LT, respectively. It is also  
778 interesting to note that  $TR^{OG}$  shows enhanced concentrations West of the Divide on this day.  
779 This is not related to transport from the NFRMA but to eastward transport of OG emissions from  
780 the Western Slopes.

781 The considered cases show that upslope flow conditions can be quite variable. While OG sources  
782 are the main contributor to tracer concentrations in the northern mountains and urban sources  
783 represent the major contribution to tracer concentrations in the southern mountains, one cannot  
784 exclude that either emissions sources can impact any of the remote area. Whether or not air  
785 masses remain separated during upslope flows depends on the degree of mixing in the NFRMA  
786 and on the direction of the upslope. The tracer analysis also points towards efficient ozone  
787 production under conditions when airmasses originating from OG source regions mix with  
788 airmasses originating from urban and mobile source sectors. In addition, we find a tendency for  
789 highest hourly ozone concentrations occurring at NFRMA sites closest to the Foothills.

790 The inert model tracers are valuable in the analysis of upslope flows as they do not depend on  
791 conditions being conducive to ozone production. Not all upslope days necessarily are also high  
792 ozone days and even on low ozone days, other pollutants (e.g. ammonia) still might be  
793 transported to the mountain regions affecting the ecosystems when deposited (e.g. Benedict et  
794 al., 2011; Benedict et al., 2013; Thompson et al., 2015)



## 795 **8. Conclusions**

796 We have introduced a set of inert emission tracers in the regional Weather Research and  
797 Forecasting Model (WRF) to assist in flight planning during the FRAPPÉ and DISCOVER-AQ  
798 campaigns in summer 2014 in the Colorado Northern Front Range Metropolitan Area (NFRMA).  
799 The tracers represent the emissions from oil and gas activities and from urban sources in  
800 Colorado and have shown high value for forecasting during the campaigns and for the analysis of  
801 the comprehensive measurement data set. The tracers help to visualize the flow patterns and  
802 support chemical analysis with information about mixing of air masses from different emission  
803 sources. This paper also serves to provide an overall evaluation of the tracers as they have been  
804 used in other studies (Vu et al., 2016).

805 The NFRMA is a very challenging region to model because of the complex topography but  
806 comparison to wind observations from surface sites and ozone sonde launches shows that the  
807 model overall simulates well the general wind patterns, which are dominated by mountain-valley  
808 flows. However, the model does not necessarily resolve the very localized nature of the surface  
809 wind measurements. Statistical analysis of chemical trace gases measured from aircraft with the  
810 respective model tracers reveals a high degree of correlation and provides confidence in using  
811 the model to support the analysis of transport patterns in the NFRMA.

812 The tracers provide a means of analyzing the general distribution and mixing of different  
813 emission sources. During nighttime, the urban tracer reveals a pooling of emissions from the  
814 Denver Metro Area to the NE towards the region of strong oil and gas sources. Flow reversal in  
815 the morning transports aged urban emissions together with fresh oil and gas emissions towards  
816 the Metro area with important implications for chemistry. Around mid-morning upslope flows  
817 frequently develop starting at near-Foothills sites and then spreading to the East and West. These  
818 have the potential of carrying NFRMA pollution to the remote mountain areas. During the  
819 campaigns, numerous cases of upslope flows have been encountered and these form the focus of  
820 this study.

821 The analysis of model tracers and surface ozone observations together with wind data at  
822 NFRMA and mountain sites demonstrates that on days with high ozone values at NFRMA

823 Foothills sites there is also a high likelihood of strong upslope flows and as a result the mountain  
824 sites experience high ozone and high tracer concentrations. On 12 August 2014, the NCAR/NSF  
825 C-130 well captured a strong upslope event, which was forecast by the tracer model. The aircraft  
826 followed transport of NFRMA pollution towards the Continental Divide and also captured spill-  
827 over into the Frasier Valley on the West side of the Continental Divide. Measured chemical  
828 tracers and modeled emission tracers both indicate a separation of airmasses from the northern  
829 and southern parts of the NFRMA with the former mostly influenced by oil and gas emissions  
830 and the latter by urban emissions. While there seems to be a tendency for oil and gas and urban  
831 influenced airmasses to be separated during upslope events, this is not necessarily true for all  
832 events and the exact nature of the impact of NFRMA pollution on remote mountain areas  
833 depends on the degree of mixing in the NFRMA and the general direction of upslope flows  
834 which can vary from NE to E or SE.

835 The presented analysis demonstrates that oil and gas pollutants from sources to the North and  
836 Northeast of Denver frequently remain unmixed with Denver-based pollutants as they are both  
837 transported to the mountains in upslope flow and potentially spill over the Continental Divide  
838 into the valleys to the West. Some of the transported pollution gets lofted and recirculated back  
839 to the NFRMA. This implies that mountain sites are not necessarily representative of  
840 inflow/background conditions. Even if winds are from the West, the air masses still can carry  
841 some influence from sources in the NFRMA given that NFRMA pollution can be transported  
842 across the Divide and then brought back via return flows. For this reason, it is important to look  
843 at the air mass history and not just actual wind data. The study also demonstrates how complex  
844 the flow patterns in the NFRMA can be and their high variability on small scales (in time and  
845 space) highlights how crucial it is for models to provide a reasonably accurate simulation of  
846 transport when assessing air quality. The NFRMA contains a range of different emission sources  
847 with very different chemical signatures and the photochemistry is strongly dependent on their  
848 degree of mixing and interaction. The FRAPPÉ and DISCOVER-AQ provide highly valuable  
849 data on flow patterns frequently occurring in the Front Range and provide an excellent testbed  
850 for evaluating model performance.

851

852 **Acknowledgements**

853 The data for this paper are publicly available at the FRAPPÉ/DISCOVER-AQ data archive  
854 (<http://www-air.larc.nasa.gov/missions/discover-aq/discover-aq.html>) including model output  
855 along the aircraft flight tracks. Forecast graphics from the WRF tracer simulation are available  
856 from the FRAPPÉ Field Catalog (<http://catalog.eol.ucar.edu/frappe>). The authors would like to  
857 thank the State of Colorado/Colorado Department of Public Health and Environment and the  
858 National Science Foundation (NSF) for funding of FRAPPÉ and NASA for funding of  
859 DISCOVER-AQ. The authors acknowledge the use of WRF-Chem version 3.3.1  
860 ([http://www2.mmm.ucar.edu/wrf/users/download/get\\_source.html](http://www2.mmm.ucar.edu/wrf/users/download/get_source.html)) and Stu McKeen at NOAA  
861 for providing the NEI 2011 emissions inventory  
862 ([ftp://aftp.fsl.noaa.gov/divisions/taq/emissions\\_data\\_2011/](ftp://aftp.fsl.noaa.gov/divisions/taq/emissions_data_2011/)). We further acknowledge Alpine  
863 Geophysics, Ramboll/Environ and the Western Regional Air Partnership (WRAP) for help with  
864 sector based emission inventories. We thank Richard Clark (Millersville University), Raymond  
865 Hoff (U. Maryland) and Timothy Berkoff (University of Maryland) for providing PBLH data.  
866 The Niwot Ridge surface ozone measurements were prepared by Audra McClure (NOAA) and  
867 Russel Long (US EPA) provided surface data for NREL Golden. NASA P-3 CO data were  
868 carried out by Glen Diskin (NASA Langley), NCAR-C130 CO measurements were carried out  
869 by Teresa Campos (NCAR/ACOM) and NCAR TOGA VOC data were carried out by Eric Apel  
870 (NCAR/ACOM). Aircraft VOC WAS samples have been collected and analyzed by Don Blake  
871 (UC Irvine). Ethane on the NASA P-3 was measured by the Aerodyne Research, Inc. mini-  
872 TILDAS and we acknowledge Joseph R. Roscioli and John Nowak for collecting NH<sub>3</sub> data using  
873 the Aerodyne Research, Inc. dual-TILDAS spectrometer. Dirk Richter, Peter Weibring and  
874 James Walega (INSTAAR) contributed to collecting ethane measurements on the NCAR/NSF C-  
875 130. PTR-ToF-MS measurements on the NASA P-3 were carried out by P. Eichler, T. Mikoviny,  
876 and M. Müller, and were supported by the Austrian Federal Ministry for Transport, Innovation  
877 and Technology (bmvit) through the Austrian Space Applications Programme (ASAP) of the  
878 Austrian Research Promotion Agency (FFG). We acknowledge the help of Arthur Mizzi  
879 (NCAR/ACOM) and NCAR/MMM with conducting the model simulations. G. Pfister's work has

880 in parts been supported by the NASA AQUEST project (grant NNX11AI51G). The National  
881 Center for Atmospheric Research is sponsored by the National Science Foundation.

882

883 **References**

884 Angevine, W. M., et al. (2013), Pollutant transport among California regions, *J. Geophys. Res.*  
885 *Atmos.*, 118, 6750–6763, doi:10.1002/jgrd.50490.

886 Arritt, R.W., J.M. Wilczak, G.S. Young (1992), Observations and Numerical Modeling of an  
887 Elevated Mixed Layer, *Monthly Weather Review*, Volume 20, 2869-2880.

888 Barth, M. C., Lee, J., Hodzic, A., Pfister, G., Skamarock, W. C., Worden, J., Wong, J., and  
889 Noone, D.: Thunderstorms and upper troposphere chemistry during the early stages of the  
890 2006 North American Monsoon, *Atmos. Chem. Phys.*, 12, 11003-11026, doi:10.5194/acp-  
891 12-11003-2012, 2012.

892 Baumann, K., E. J. Williams, J. A. Olson, J. W. Harder, and F. C.  
893 Fehsenfeld (1997), Meteorological characteristics and spatial extent of upslope events during  
894 the 1993 Tropospheric OH Photochemistry Experiment, *J. Geophys. Res.*, 102(D5), 6199–  
895 6213, doi:10.1029/96JD03251.

896 Benedict, K. B., J. L. Collett, C. M. Carrico, S. Raja, F. M. Schwandner, M. Schurman, E. Levin,  
897 D. Day, S. M. Kreidenweis, W. C. Malm, and B. A. Schichtel (2011), Transport and  
898 deposition of reactive nitrogen in the Rocky Mountain region. *Abstr. Pap. Amer. Chem. Soc.*,  
899 242, Meeting Abstract: 303-ENVR, Aug. 28, 2011.

900 Benedict, K. B., Carrico, C. M., Kreidenweis, S. M., Schichtel, B., Malm, W. C. and Collett, J.  
901 L. (2013), A seasonal nitrogen deposition budget for Rocky Mountain National Park.  
902 *Ecological Applications*, 23: 1156–1169. doi:10.1890/12-1624.1

903 Brioude, J., Arnold, D., Stohl, A., Cassiani, M., Morton, D., Seibert, P., Angevine, W., Evan, S.,  
904 Dingwell, A., Fast, J. D., Easter, R. C., Pisso, I., Burkhardt, J., and Wotawa, G.: The  
905 Lagrangian particle dispersion model FLEXPART-WRF version 3.1, *Geosci. Model Dev.*, 6,  
906 1889-1904, <https://doi.org/10.5194/gmd-6-1889-2013>, 2013.

907 Brodin, M., D. Helmig, S. Oltmans (2010), Seasonal ozone behavior along an elevation gradient  
908 in the Colorado Front Range Mountains. *Atmospheric Environment* 44 :5305-5315

909 Brodin, M., D. Helmig, B. Johnson, and S. Oltmans (2011), Comparison of ozone concentrations  
910 on a surface elevation gradient with balloon-borne ozonesonde measurements. *Atmos.*  
911 *Environ.*, 45, 5431- 5439.

912 Compton, J.C., R. Delgado, T.A. Berkoff, and R.M. Hoff (2013): Determination of Planetary  
913 Boundary Layer Height on Short Spatial and Temporal Scales: A Demonstration of the  
914 Covariance Wavelet Transform in Ground-Based Wind Profiler and Lidar Measurements. *J.*  
915 *Atmos. Oceanic Technol.*, 30, 1566–1575, <https://doi.org/10.1175/JTECH-D-12-00116.1>

916 Darrouzet-Nardi, A., J. Erbland, W. D. Bowman, J. Savarino, and M. W. Williams (2012),  
917 Landscapelevel nitrogen import and export in an ecosystem with complex terrain, Colorado  
918 Front Range. *Biogeochemistry*, 109, 271-285.

919 Doran, J.C. (1996), The influence of Canyon Winds on flow fields near Colorado's Front Range,  
920 *J. Appl. Meteorology*, Volume 35, 587-600.

921 Greenland, D. (1980), The Climate of Niwot Ridge, Front Range, Colorado, U.S.A., *Arctic and*  
922 *Alpine Research*, vol. 21, no. 4, 1989, pp. 380–391., [www.jstor.org/stable/1551647](http://www.jstor.org/stable/1551647).

923 Haagensohn, P. L., (1979), Meteorological and climatological factors affecting Denver air  
924 quality, *Atmos. Environ.*, 13, 79–85.

925 Halliday, H. S., A. M. Thompson, A. Wisthaler, D. Blake, R. S. Hornbrook, T. Mikoviny, M.  
926 Müller, P. Eichler, E. C. Apel, and A. J. Hills, Atmospheric benzene observations from oil  
927 and gas production in the Denver Julesburg basin in July and August 2014, *J. Geophys. Res.*  
928 *Atmos.*, 121, doi:10.1002/2016JD025327, 2016.

929 Hegarty, J., R. R. Draxler, A. F. Stein, J. Brioude, M. Mountain, J. Eluszkiewicz, T. Nehr Korn, F.  
930 Ngan, and A. Andrews (2013), Evaluation of Lagrangian particle dispersion models with  
931 measurements from controlled tracer releases, *J. Appl. Meteorol. Climatol.*, 52, 2623–2637.

932 Herndon, S.C., et al., Characterization of urban pollutant emission fluxes and ambient  
933 concentration distributions using a mobile laboratory with rapid response instrumentation,

934 Faraday Discuss. 2005, 130, 327-329. Jimenez, R., et al., In Atmospheric trace gas  
935 measurements using a dual quantum-cascade laser mid-infrared absorption spectrometer,  
936 Proc. of SPIE, 2005; Mermelstein, C.; Bour, D., Eds. 2005. McManus, J.B., et al.,  
937 Application of quantum cascade lasers to high-precision atmospheric trace gas  
938 measurements., Opt. Eng., 2010, 39, (11), 111124-111124-11.

939 Hong, S. Y. Noh, and J. Dudhia, 2006: A new vertical diffusion package with an explicit  
940 treatment of entrainment processes. Mon. Wea. Rev., 134, 2318–2341,  
941 doi:10.1175/MWR3199.1

942 Hong, S. Y. (2010), A new stable boundary layer mixing scheme and its impact on the simulated  
943 East Asian summer monsoon, Quart. J. Roy. Meteor. Soc., 136(651), 1481–1496,  
944 doi:10.1002/Qj.665.

945 Hu, X.-M., P. M. Klein, and M. Xue (2013), Evaluation of the updated YSU planetary boundary  
946 layer scheme within WRF for wind resource and air quality assessments, J. Geophys. Res.  
947 Atmos., 118, 10,490–10,505, doi:10.1002/jgrd.50823.

948 Iacono, M. J., J. S. Delamere, E. J. Mlawer, M. W. Shephard, S. A. Clough, and W. D. Collins,  
949 2008: Radiative forcing by long-lived greenhouse gases: Calculations with the AER  
950 radiative transfer models. *J. Geophys. Res.*, 113, D13103.

951 Johnson, R.H. and J.J. Toth (1982), Topographic effects and weather forecasting in the Colorado  
952 PROFS mesonetwork area, Preprint Volume: 9th Conference on Weather Forecasting and  
953 Analysis, June 28 - July 1, 1982; Seattle, WA, 440-445.

954 Kaser, L., E. G. Patton, G. G. Pfister, A. J. Weinheimer, D. D. Montzka, F. Flocke, A. M.  
955 Thompson, R. M. Stauffer, and H. S. Halliday (2017), The effect of entrainment through  
956 atmospheric boundary layer growth on observed and modeled surface ozone in the Colorado  
957 Front Range, J. Geophys. Res. Atmos., 122, 6075–6093, doi:10.1002/2016JD026245.

958 Kain, John S., 2004: The Kain–Fritsch convective parameterization: An update. *J. Appl. Meteor.*,  
959 43, 170–181.

960 Janjic, Z. I., 1994: The step-mountain Eta coordinate model: further developments of the  
961 convection, viscous sublayer and turbulence closure schemes. *Mon. Wea. Rev.*, 122, 927–  
962 945.

963 Olson, J. A., K. Baumann, C. J. Volpe, J. W. Harder, E. J. Williams, and G. H.  
964 Mount (1997), Meteorological overview of the 1993 OH Photochemistry Experiment, *J.*  
965 *Geophys. Res.*, 102(D5), 6187–6197, doi:10.1029/96JD00402.

966 Parrish, D.D., D.W. Fahey, E.J. Williams, S.C. Liu, M. Trainer, P.C. Murphy, D. L. Albritton,  
967 F.C. Fehsenfeld, F.C., (1986) Background ozone and anthropogenic ozone enhancement at  
968 Niwot Ridge, Colorado. *Journal of Atmospheric Chemistry* 4 :63-80

969 Reddy, P. J., and G. G. Pfister (2016), Meteorological factors contributing to the interannual  
970 variability of midsummer surface ozone in Colorado, Utah, and other western U.S. states, *J.*  
971 *Geophys. Res. Atmos.*, 121, 2434–2456, doi:10.1002/2015JD023840.

972 Richter, D., P. Weibring, J. Walega, A. Fried, S.M. Spuler, M.S. Taubman (2015), Compact  
973 highly sensitive multi-species airborne mid-IR spectrometer. *Applied Physics B: Lasers and*  
974 *Optics*, 119(1 SI): 119-131. DOI: 10.1007/s00340-015-6038-8-9071

975 Stohl, A., Forster, C., Frank, A., Seibert, P., and Wotawa, G.: Technical note: The Lagrangian  
976 particle dispersion model FLEXPART version 6.2, *Atmos. Chem. Phys.*, 5, 2461-2474,  
977 <https://doi.org/10.5194/acp-5-2461-2005>, 2005.

978 Sullivan, J. T., et al. (2016), Quantifying the contribution of thermally driven recirculation to a  
979 high-ozone event along the Colorado Front Range using lidar, *J. Geophys. Res. Atmos.*,  
980 121,10,377–10,390, doi:10.1002 /2016JD025229.

981 Sun, K., K. Cady-Pereira, D.J. Miller, L. Tao, M.A. Zondlo, J.B. Nowak, J.A. Neuman, T.  
982 Mikoviny, M. Müller, A. Wisthaler, A.J. Scarino, C.A. Hostetler (2014), Validation of TES  
983 ammonia observations at the single pixel scale in the San Joaquin Valley during  
984 DISCOVER-AQ, *J. Geophys. Res. Atmos.*, 120 (10) (2015), pp. 5140–5154,  
985 <http://dx.doi.org/10.1002/2014JD022846>

986 Tewari, M., F. Chen, W. Wang, J. Dudhia, M. A. LeMone, K. Mitchell, M. Ek, G. Gayno, J.  
987 Wegiel, and R. H. Cuenca, 2004: Implementation and verification of the unified NOAA land  
988 surface model in the WRF model. 20th conference on weather analysis and forecasting/16th  
989 conference on numerical weather prediction, pp. 11–15.

990 Thompson, Gregory, Paul R. Field, Roy M. Rasmussen, William D. Hall, 2008: Explicit  
991 Forecasts of Winter Precipitation Using an Improved Bulk Microphysics Scheme. Part II:  
992 Implementation of a New Snow Parameterization. *Mon. Wea. Rev.*, **136**, 5095–5115.

993 Thompson, T. M., M. A. Rodriguez, M. G. Barna, K. A. Gebhart, J. L. Hand, D. E. Day, W. C.  
994 Malm, K. B. Benedict, J. L. Collett Jr., and B. A. Schichtel (2015), Rocky Mountain National  
995 Park reduced nitrogen source apportionment, *J. Geophys. Res. Atmos.*, 120, 4370–4384.  
996 *doi:10.1002/2014JD022675*.

997 Toth, J. J., and R. H. Johnson (1985), Summer surface flow characteristics over northeast  
998 Colorado, *Mon. Weather Rev.*, 113(9), 1458–1469.

999 Vu, K. T., Dingle, J. H., Bahreini, R., Reddy, P. J., Campos, T. L., Diskin, G. S., Fried, A.,  
1000 Herndon, S. C., Hornbrook, R. S., Huey, G., Kaser, L., Montzka, D. D., Nowak, J. B.,  
1001 Richter, D., Roscioli, J. R., Shertz, S., Stell, M., Tanner, D., Tyndall, G., Walega, J.,  
1002 Weibring, P., Weinheimer, A. J., Pfister, G., and Flocke, F.: Impacts of the Denver Cyclone  
1003 on Regional Air Quality and Aerosol Formation in the Colorado Front Range during  
1004 FRAPPÉ 2014, *Atmos. Chem. Phys.*, 16, 12039–12058, *doi:10.5194/acp-16-12039-2016*,  
1005 2016.

1006 Weinheimer, A.J., J.G. Walega, B.A. Ridley, B.L. Gary, D.R. Blake, N.J. Blake, F.S. Rowland,  
1007 G.W. Sachse, B.E. Anderson, J.E. Collins, Meridional distributions of NO<sub>x</sub>, NO<sub>y</sub>, and other  
1008 species in the lower stratosphere and upper troposphere during AASE II, *Geophys. Res. Lett.*,  
1009 *21*, 2583–2586, 1994.

1010 Yacovitch TI, Herndon SC, Roscioli JR, Floerchinger C, McGovern RM, et al. (2014),  
1011 Demonstration of an Ethane Spectrometer for Methane Source Identification. *Environ Sci*  
1012 *Technol* 48(14): 8028–8034. *doi:10.1021/es501475q*.



1013 Zhang, Y., Wang, Y., Chen, G., Smeltzer, C., Crawford, J., Olson, J., Szykman, J., Weinheimer,  
1014 A., Knapp, D., Montzka, D. D., Wisthaler, A., Mikoviny, T., Fried, A., and G. Diskin (2016),  
1015 Large vertical gradient of reactive nitrogen oxides in the boundary layer: Modeling analysis  
1016 of DISCOVER-AQ 2011 observations, *J. Geophys. Res. Atmos.*, 121, 1922-1934,  
1017 doi:10.1002/2015JD024203.

1018

1019

1020 Table 1: Location information for surface sites mentioned in this study ordered by longitude.  
1021 Sites focused at in the analysis are indicated by “A”, NASA P-3 spiraling sites by “S”, non-spiral  
1022 Front Range sites by “F” and mountain sites by “M”. The Continental Divide stretches along the  
1023 highest elevation points.

1024

1025 Table 2: Spatial correlations of aircraft measurements of  $\text{NO}_x$ ,  $\text{C}_2\text{H}_6$  and  $\text{NH}_3$  with model tracers  
1026 for (top row) 0-3km and (second row) 0-2km, 0-1km and all altitudes. See text for details on the  
1027 calculation of spatial correlation. R values larger than 0.7 are marked in bold characters.

1028

1029 Table 3: Maximum hourly surface ozone concentrations and hour of occurrence for the five days  
1030 shown in Figure 17. Only monitoring sites as part of the CDPHE network are included together  
1031 with the four mountain sites used before and two additional high altitude sites at Niwot Ridge.  
1032 Sites are ordered from West to East and only values equal or larger than 70 ppb are shown for  
1033 NFRMA sites. Values above 75 ppb are highlighted in bold. The start time of the hourly  
1034 averaging period is listed. NA indicate days with missing observations. Sites close to the  
1035 Foothills on the western edge of the NFRMA are shown in *Italic*.

1036

1037 Figure 1: Topography of the study region. Light grey dots indicate the four mountain sites used  
1038 in this study, dark grey dots the 4 sites in the NFRMA used in the analysis of upslope events.  
1039 White dots indicate other NFRMA spiral sites for the NASA P-3. Site characteristics are listed in  
1040 Table 1. Additional sites used later in the analysis are indicated by triangles. County lines are  
1041 shown as solid lines.

1042

1043 Figure 2: Measured (black) and modeled (red) diurnal cycle for 6am – 6am LT in wind direction  
1044 (vector average for wind speed > 0.3 m/s ; left) and wind speed (right) for selected surface sites.  
1045 Shown are mean, median, standard deviation and, for wind speed only, minimum and maximum  
1046 over the FRAPPÉ time period (15 July – 20 August).

1047 Figure 3: Measured (black) and modeled (red) average wind direction, wind speed, relative  
1048 humidity and temperature for sonde launches in (a) Platteville (40 sonde launches) and (b) Fort  
1049 Collins West (40.59N and -105.14W; 12 sonde launches) and (c) windroses for Platteville from  
1050 surface measurements for 8-12LT and 14-20LT. For averaging the sonde wind direction data  
1051 only observations with wind speed > 0.3 m/s were considered.

1052

1053 Figure 4: Observed and modeled PBL height for (from top to bottom): Fort Collins West,  
1054 Platteville and Golden for 19 July – 11 August.

1055

1056 Figure 5: Observed NCAR/NSF C-130 NO<sub>x</sub> and ethane concentrations and model tracers  
1057 TR<sup>AreaMobile</sup> and TR<sup>OG</sup> averaged over 0.1 deg x 0.1 deg for altitudes < 3km agl. Averages of  
1058 observed and model tracer concentrations are calculated for grids with at least 3 data points. The  
1059 spatial correlation is listed here, as well as in Table 2. Areas above 2500m a.s.l. are shaded in  
1060 grey.

1061

1062 Figure 6: Observed NASA P-3 NO<sub>x</sub> and ethane concentrations and model tracers averaged over  
1063 0.05 deg x 0.05 deg for altitudes < 3km agl. Averages of observed and model tracer  
1064 concentrations are calculated for grids with at least 3 data points. The spatial correlation is listed  
1065 here, as well as in Table 2. Areas above 2500m a.s.l. are shaded in grey.

1066

1067 Figure 7: Spatial correlations between measured species and ratios and model tracers for the  
1068 area/mobile (blue) and OG (red) sources. Big circles represent the average over all flights, small  
1069 circles represent results for individual flights. Top: NCAR/NSF C130 flights (same spatial  
1070 coverage as Figure 5); Bottom: NASA P-3 flights. Statistics are derived for data points below  
1071 3 km a.g.l. See text for details on the calculation of spatial correlation.

1072

1073 Figure 8: Average spatial tracer distribution (average concentrations within the PBL) for 0-6LT,  
1074 6-12LT, 12-18LT and 18-24 LT for the FRAPPÉ time period (14 July to 21 August). Contour  
1075 lines show the PBL average for  $TR^{AreaMobile}$ , filled contours show the PBL average  $TR^{OG}$   
1076 concentrations. Colored points denote the mean ozone measured at surface sites. The tracers are  
1077 scaled by a common factor and then by their mean ratio ( $TR^{AreaMobile} = 60 \bullet TR^{OG}$ ) to appear on  
1078 the same scale.

1079

1080 Figure 9: Tracer Statistics for surface sites employed during FRAPPÉ/DAQ for  $TR^{AreaMobile}$  (top)  
1081 and  $TR^{OG}$  (bottom). Sites are arranged from West to East and averaged over 10-17 LT (though  
1082 an average over all times would not look vastly different). Sites focused on in the analysis of  
1083 upslope events are colored in red. Shown are mean (dot), median (triangle), standard deviation  
1084 (horizontal bars), 10<sup>th</sup> and 90<sup>th</sup> percentiles (thick line), minima and maxima (thin lines). In  
1085 addition to sites shown in Figure 1 we also added sites in the Global Ozone (GO3) project (Black  
1086 Hawk, Lyons, East Boulder and Longmont) as well as additional sites from the CDPHE network  
1087 (I-25 Denver, CAMP).

1088

1089 Figure 10: Average diurnal observed surface ozone (black) and PBLH average  $TR^{OG}$  (red) and  
1090  $TR^{AreaMobile}$  (blue) for selected surface sites in the Front Range for 6am – 6am LT. Shown are  
1091 mean, median, standard deviation, minimum and maximum. A line is drawn through the mean  
1092 values.

1093

1094 Figure 11: As Figure 10 but for selected surface sites in the mountains. Note the y-scale is  
1095 reduced to half of the one used in Figure 10.

1096

1097 Figure 12: Upslope (red) and Downslope (black) statistics from observations (solid lines) and  
1098 WRF (dotted lined). Flow is defined when winds are from within a defined wind sector at least  
1099 2/3<sup>rd</sup> of the time within a given hour (Note that wind data for Trail Ridge Road are available

1100 hourly only and that model data are also only available on an hourly basis). Upslope: Upslope  
1101 Angle  $\pm 45$ deg; Downslope:  $270 \pm 45$ deg; only data with wind speeds  $> 0.3$  m/s (i.e. data that are  
1102 not defined calm based on Beaufort scale). The upslope angle has been defined based on  
1103 windrose analysis. The frequency is given as percentage of upslope or downslope of all valid  
1104 measurements.

1105

1106 Figure 13: Ozone and Tracer roses for (a) Longs Peak (1-minute data) and (b) Trail Ridge road  
1107 (hourly data) on days when RF North 12-18LT average ozone was  $> 70$  ppb (“RF North HIGH”)  
1108 or  $< 60$  ppb (“RF North LOW”). Only data for 12-20LT are shown.

1109

1110 Figure 14: NCAR/NSF C-130 measured ethane and NO<sub>x</sub> (top row) and modeled TR<sup>OG</sup> and  
1111 TR<sup>AreaMobile</sup> (bottom row) for the the upslope part of the 12 August flight (after refueling). All  
1112 data averaged over 0-2km ag and a 0.1 deg x 01 deg grid. The vector averaged measured and  
1113 modeled winds for each grid point are shown by the windbarbs and the monitoring sites RF  
1114 North, NREL Golden, WC Tower, Aurora East and Golden are indicated by diamond symbols.  
1115 Areas above 2500m a.s.l. are shaded in grey.

1116

1117 Figure 15: as Figure 10 but for 12 August 2014 and for mountain sites only. Lines show the  
1118 average diurnal cycle from Figure 11.

1119

1120 Figure 16: Longitude-Altitude Cross Section of TR<sup>OG</sup> at 40.09N (single grid box in latitude) for  
1121 12 August 22 UTC (16 LT, top) and 13 August 2 UTC (12 August 20 LT, bottom); The location  
1122 of the Granby airport is indicated by the black dot. Horizontal winds are indicated by black  
1123 arrows, vertical winds are shown as white arrows. For clarity, only vertical winds  $> 0.2$ m/s are  
1124 included. The height of the PBLH is plotted as a black line.

1125

1126 Figure 17: as Figure 8 but for 14-20 LT. Top row: average over FRAPPÉ period and 12 August;  
1127 middle row: 22 July and 2 August; bottom row: 3 and 8 August.  
1128

1129 Table 1: Location information for surface sites mentioned in this study ordered by longitude.  
 1130 Sites focused at in the analysis are indicated by “A”, NASA P-3 spiraling sites by “S”, non-spiral  
 1131 Front Range sites by “F” and mountain sites by “M”.

1132

Site	Latitude (N)	Longitude (W)	Elevation (m asl)	Type
Aurora East (AUREAST)	39.639	-104.569	1552	AF
Platteville	40.182	-104.727	1516	S
Weld County (WC) Tower	40.386	-104.737	1484	AF
LaCasa	39.779	-105.005	1602	S
BAO	40.043	-105.006	1579	S
Chatfield Park (CHATPARK)	39.534	-105.070	1676	S
Fort Collins (FTC) CSU	40.571	-105.080	1524	S
NREL Golden	39.744	-105.178	1832	AFS
RF North	39.913	-105.189	1802	AF
Squaw Mountain	39.681	-105.496	3420	AM
Longs Peak	40.278	-105.545	2743	AM
Trail Ridge Road	40.39	-105.686	3498	AM
Mines Peak	39.794	-105.764	3805	AM

1133

1134

1135 Table 2: Spatial correlations of aircraft measurements of NO<sub>x</sub>, C<sub>2</sub>H<sub>6</sub> and NH<sub>3</sub> with model tracers  
 1136 for (top row) 0-3km and (second row) 0-2km, 0-1km and all altitudes. See text for details on the  
 1137 calculation of spatial correlation. R values larger than 0.7 are marked in bold characters.

	<i>TR</i> <sup>AreaMobile</sup>		<i>TR</i> <sup>OG</sup>		<i>TR</i> <sup>Agr</sup>	
	<i>C-130</i>	<i>P-3</i>	<i>C-130</i>	<i>P-3</i>	<i>C-130</i>	<i>P-3</i>
<i>NO<sub>x</sub></i>	<b>0.82</b>	<b>0.72</b>	0.23	0.20	0.21	0.12
	<b>0.81,0.79,0.82</b>	0.69,0.67, <b>0.79</b>	0.18,0.07,0.23	0.10,-0.04,0.37	0.16,0.02,0.21	0.06,-0.05,0.26
<i>C<sub>2</sub>H<sub>6</sub></i>	0.38	-0.02	<b>0.80</b>	<b>0.86</b>	<b>0.76</b>	<b>0.80</b>
	0.35,0.20,0.39	-0.14,-0.27,0.25	<b>0.79,0.76,0.80</b>	<b>0.85,0.84,0.90</b>	<b>0.75,0.70,0.76</b>	<b>0.80,0.78,0.84</b>
<i>NH<sub>3</sub></i>	0.06	-0.03	<b>0.73</b>	<b>0.73</b>	<b>0.70</b>	<b>0.81</b>
	0.04,-0.07,0.08	-0.14,-0.36,0.11	<b>0.73,0.68,0.74</b>	<b>0.70,0.65,0.77</b>	0.69,0.66, <b>0.70</b>	<b>0.81,0.79,0.82</b>

1138

1139

1140

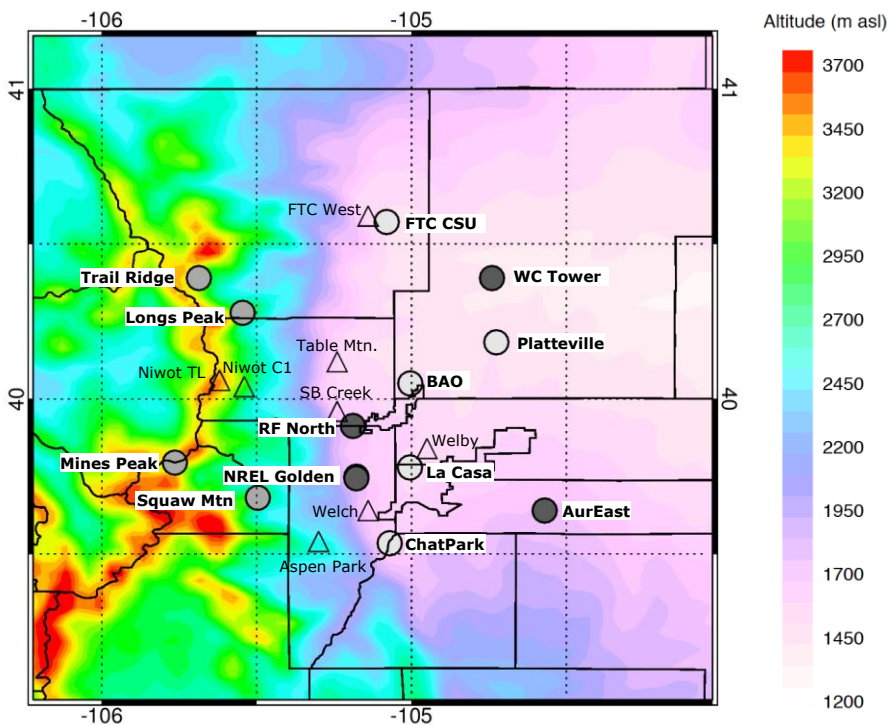
1141 Table 3: Maximum hourly surface ozone concentrations and hour of occurrence for the five days  
 1142 shown in Figure 17. Only monitoring sites as part of the CDPHE network are included together  
 1143 with the four mountain sites used before and two additional high altitude sites at Niwot Ridge.  
 1144 Sites are ordered from West to East and only values equal or larger than 70 ppb are shown for  
 1145 NFRMA sites. Values above 75 ppb are highlighted in bold. The start time of the hourly  
 1146 averaging period is listed. NA indicate days with missing observations. Sites close to the  
 1147 Foothills on the western edge of the NFRMA are shown in *Italic*.

	12 Aug	22 July	2 Aug	3 Aug	8 Aug
Mines Peak	71 ppb (19 LT)	<b>88 ppb (17 LT)</b>	<b>77 ppb (20LT)</b>	<b>79 ppb (21 LT)</b>	54 ppb (5 LT)
Trail Ridge	<b>80 ppb (17 LT)</b>	<b>82 ppb (21 LT)</b>	71 ppb (21 LT)	69 ppb (24 LT)	59 ppb (20 LT)
Longs Peak	<b>78 ppb (16 LT)</b>	<b>76 ppb (20 LT)</b>	72 ppb (18 LT)	62 ppb (13 LT)	<b>75 ppb (18 LT)</b>
Squaw Mtn.	66 ppb (18 LT)	<b>86 ppb (16 LT)</b>	<b>77 ppb (20 LT)</b>	<b>84 ppb (19 LT)</b>	<b>78 ppb (17 LT)</b>
Niwot C1	73 ppb (16LT)	<b>80 ppb(18LT)</b>	65 ppb (17LT)	65 ppb (18 LT)	<b>78 ppb (17 LT)</b>
Niwot TL	<b>77 ppb (17 LT)</b>	NA	68 ppb (21 LT)	72 ppb (21 LT)	<b>78 ppb (17 LT)</b>
Aspen Park		<b>85 ppb (15 LT)</b>			72 ppb (19 LT)
<i>SBCreek</i>		<b>89 ppb (18 LT)</b>	<i>73 ppb (16 LT)</i>	<b>75 ppb (15 IT)</b>	<b>83 ppb (16 LT)</b>
<i>Table Mtn</i>		<b>92 ppb (16 LT)</b>	<b>77 ppb (17 LT)</b>	<b>85 ppb (15 LT)</b>	<b>78 ppb (15 LT)</b>
Welch		<b>87 ppb (15 LT)</b>		<b>76 ppb (14 LT)</b>	
<i>RF North</i>	<i>72 ppb (16LT)</i>	<b>94 ppb (17 LT)</b>	<b>77 ppb (16 LT)</b>	<b>83 ppb (14 LT)</b>	<b>86 ppb (16 LT)</b>
<i>FTC West</i>	<b>75 ppb (16LT)</b>	<b>88 ppb (18 LT)</b>	<b>77 ppb (16LT)</b>	<b>81 ppb (15 LT)</b>	
FTC CSU	70 ppb (13LT)	<b>86 ppb (16 LT)</b>	<b>77 ppb (15 LT)</b>	<b>83 ppb (16 LT)</b>	
<i>Chatfield</i>		<b>92 ppb (14 LT)</b>		<b>80 ppb (14 LT)</b>	
LaCasa		74 ppb (15 LT)	70 ppb (16 LT)	<b>80 ppb (14 LT)</b>	
CAMP		71 ppb (14 LT)		74 ppb (14 LT)	
Welby		<b>76 ppb (15 LT)</b>		72 ppb (14 LT)	
WC Tower			71 ppb (12 LT)	<b>84 ppb (14 LT)</b>	71 ppb (13 LT)
AurEast					

1149 Location information for sites not included in Table 1: Niwot C1 40.04N and -105.54W; Niwot  
 1150 TL 40.06N and -105.62W; Aspen Park 39.54N and -105.3W; South Boulder Creek (SBCreek)  
 1151 39.96N and -105.24W; Table Mtn 40.12N and -105.24W; Welch 39.64N and -105.14W; FTC  
 1152 West 40.59N and -105.14W; Welby 39.84N and -104.95W

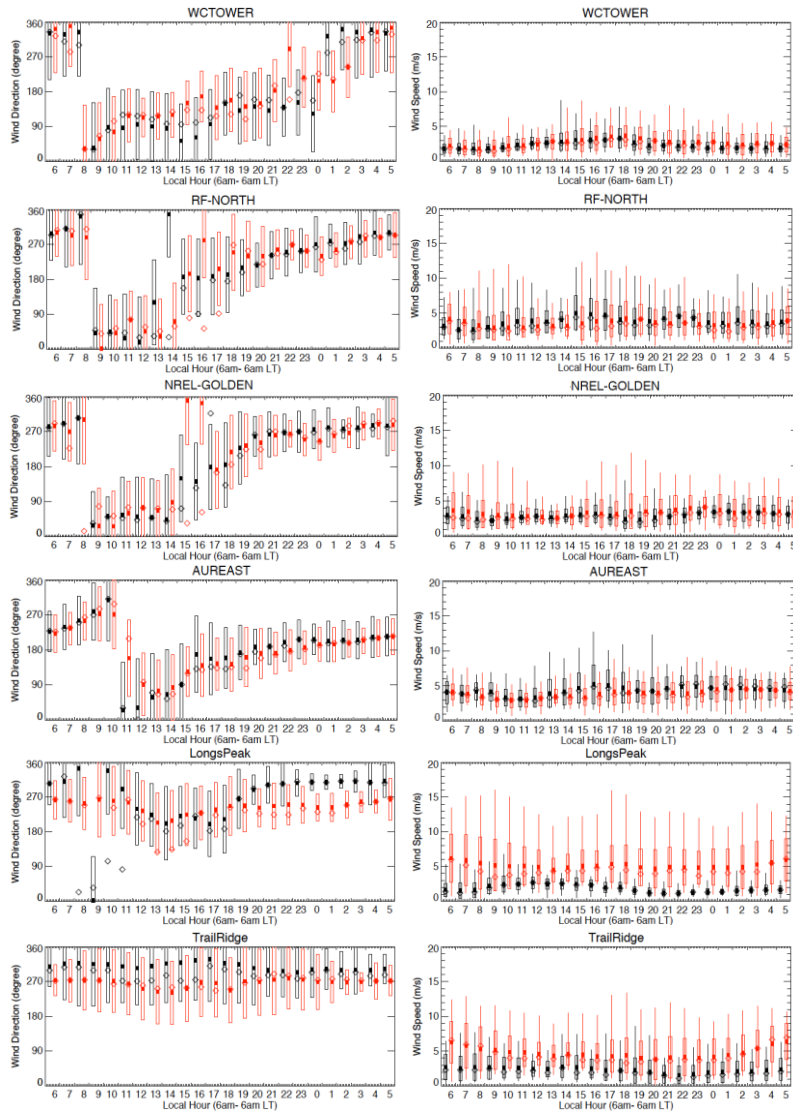


1154 Figure 1: Topography of the study region. Light grey dots indicate the four mountain sites used  
 1155 in this study, dark grey dots the 4 sites in the NFRMA used in the analysis of upslope events.  
 1156 White dots indicate other NFRMA spiral sites for the NASA P-3. Site characteristics are listed in  
 1157 Table 1. Additional sites used later in the analysis are indicated by triangles. County lines are  
 1158 shown as solid lines. The Continental Divide stretches along the highest elevation points.



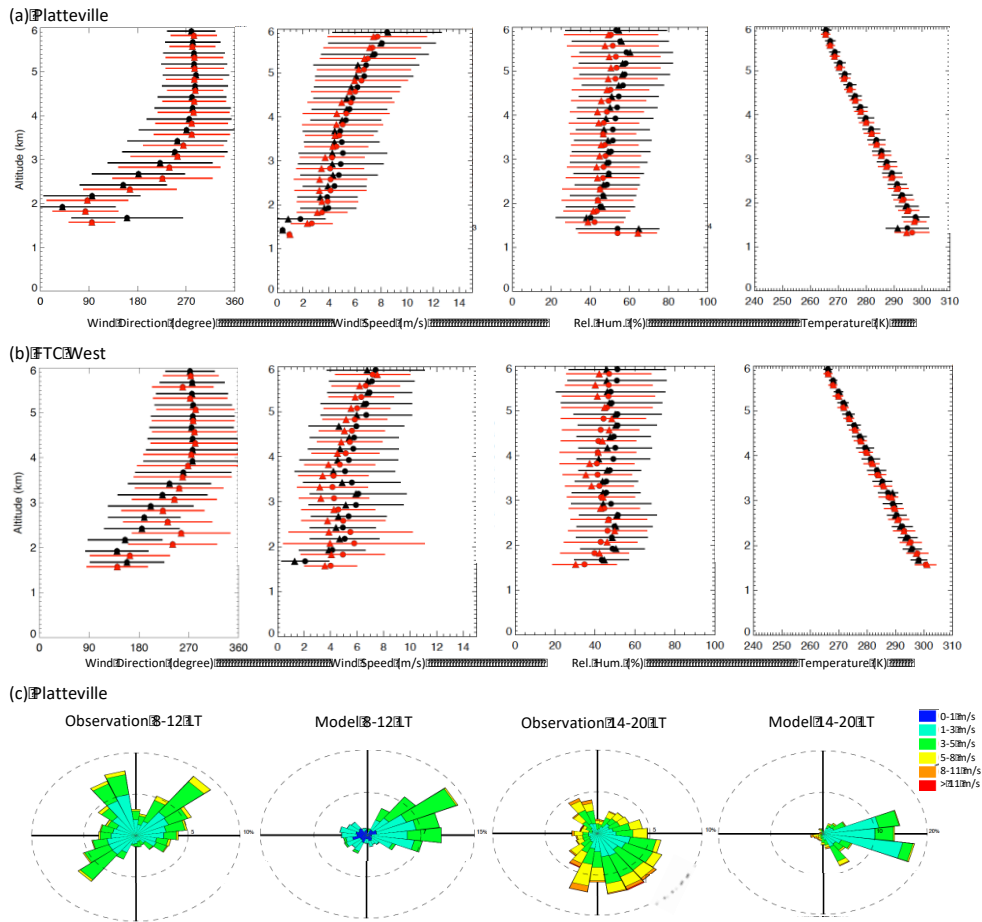
1159  
 1160

1161 Figure 2: Measured (black) and modeled (red) diurnal cycle for 6am – 6am LT in wind direction  
 1162 (vector average for wind speed > 0.3 m/s ; left) and wind speed (right) for selected surface sites.  
 1163 Shown are mean, median, standard deviation and, for wind speed only, minimum and maximum  
 1164 over the FRAPPÉ time period (15 July – 20 August).



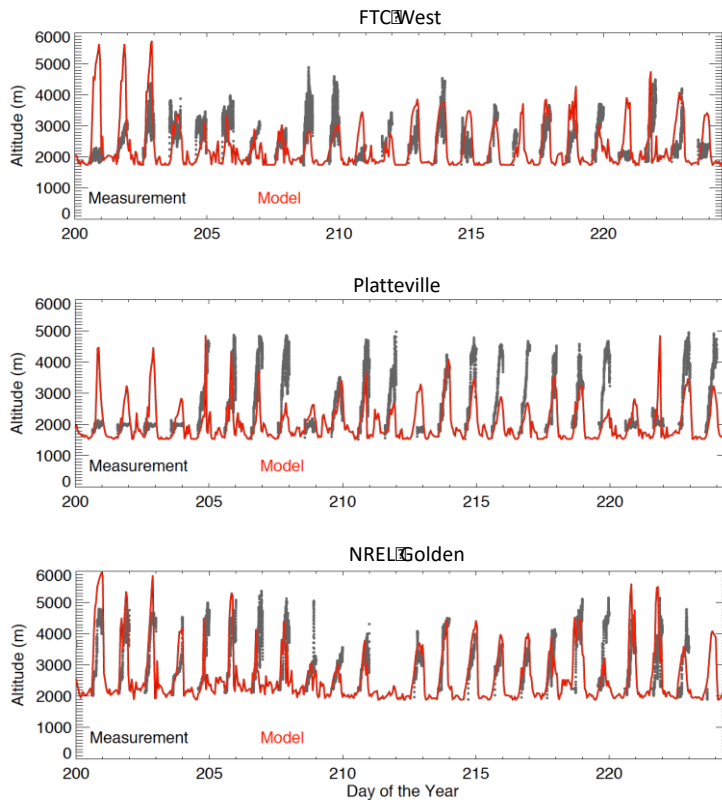
1165

1166 Figure 3: Measured (black) and modeled (red) average wind direction, wind speed, relative  
 1167 humidity and temperature for sonde launches in (a) Platteville (40 sonde launches) and (b) Fort  
 1168 Collins West (40.59N and -105.14W; 12 sonde launches) and (c) windroses for Platteville from  
 1169 surface measurements for 8-12LT and 14-20LT. For averaging the sonde wind direction data  
 1170 only observations with wind speed > 0.3 m/s were considered.



1171  
 1172

1173 Figure 4: Observed and modeled PBL height for (from top to bottom): Fort Collins West,  
1174 Platteville and Golden for 19 July – 11 August.

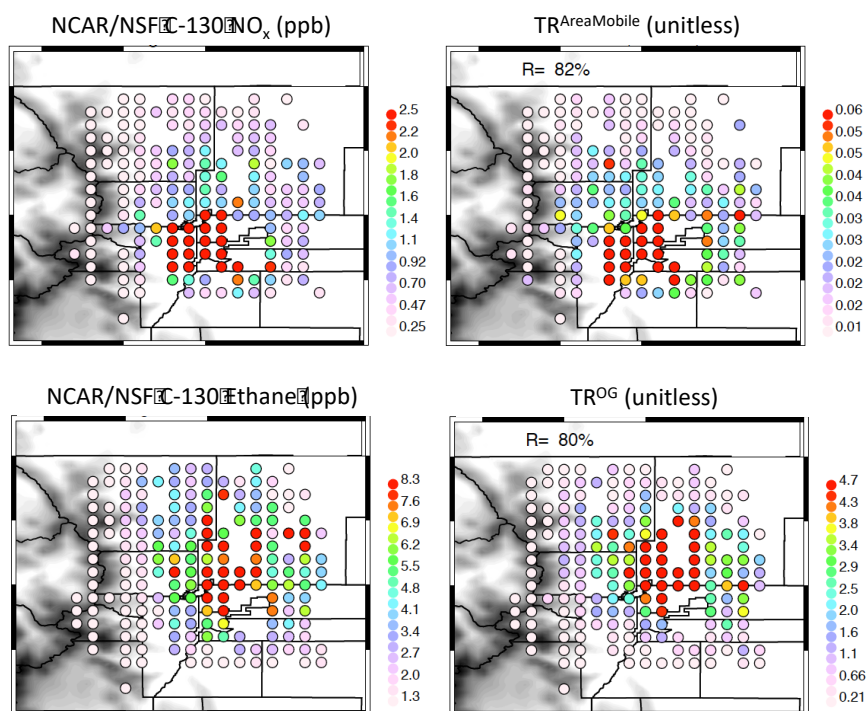


Formatted: Font: Times, 12 pt, Font color: Red

1175  
1176

1177 Figure 5: Observed NCAR/NSF C-130 NO<sub>x</sub> and ethane concentrations and model tracers  
 1178 TR<sup>AreaMobile</sup> and TR<sup>OG</sup> averaged over 0.1 deg x 0.1 deg for altitudes < 3 km agl. Averages of  
 1179 observed and model tracer concentrations are calculated for grids with at least 3 data points. The  
 1180 spatial correlation is listed here, as well as in Table 2. Areas above 2500m a.s.l. are shaded in  
 1181 grey.

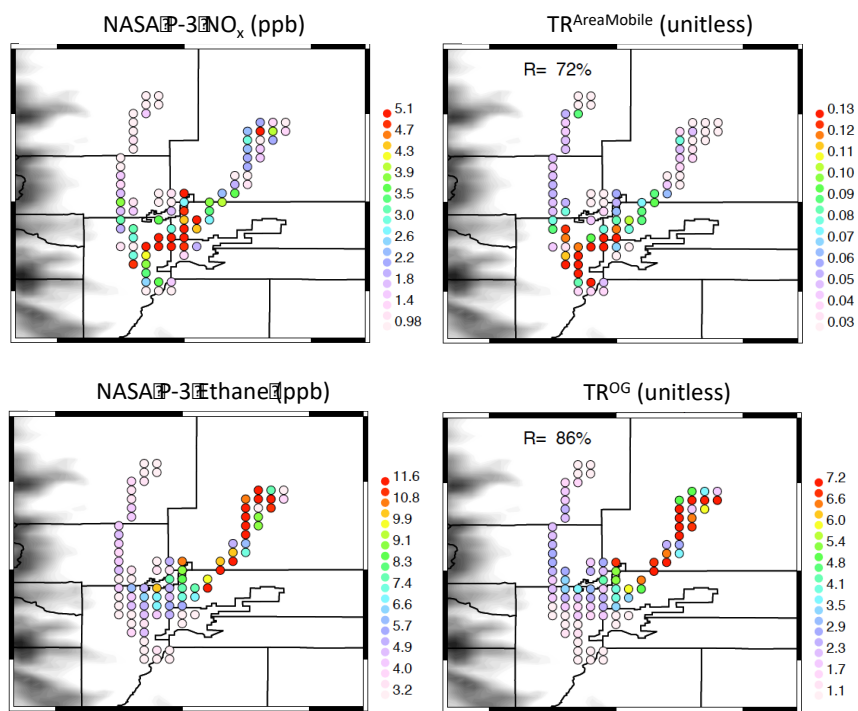
1182  
 1183



1184  
 1185

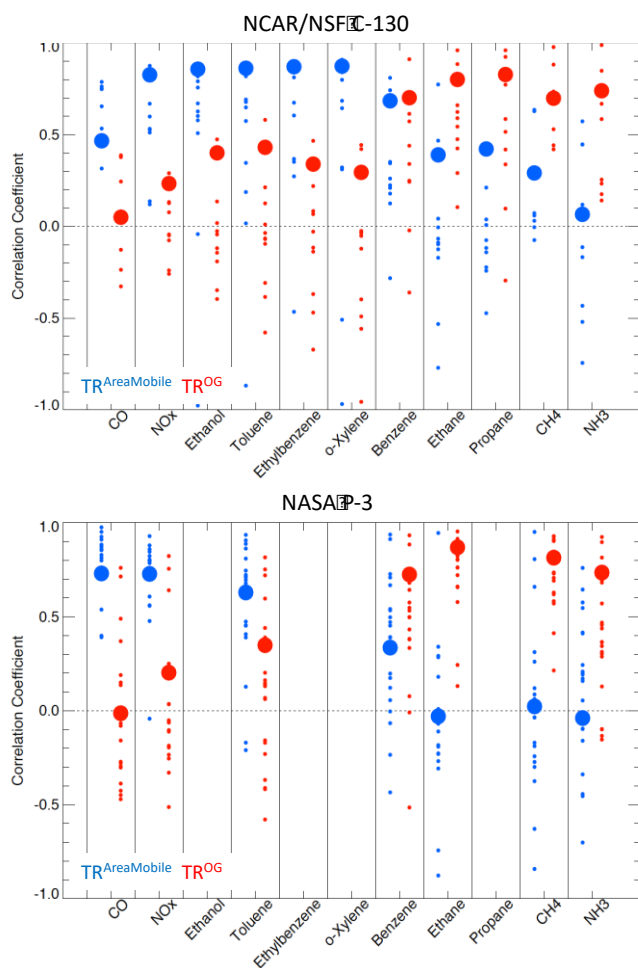
1186 Figure 6: Observed NASA P-3 NO<sub>x</sub> and ethane concentrations and model tracers averaged over  
1187 0.05 deg x 0.05 deg for altitudes < 3 km agl. Averages of observed and model tracer  
1188 concentrations are calculated for grids with at least 3 data points. The spatial correlation is listed  
1189 here, as well as in Table 2. Areas above 2500m a.s.l. are shaded in grey.

1190  
1191

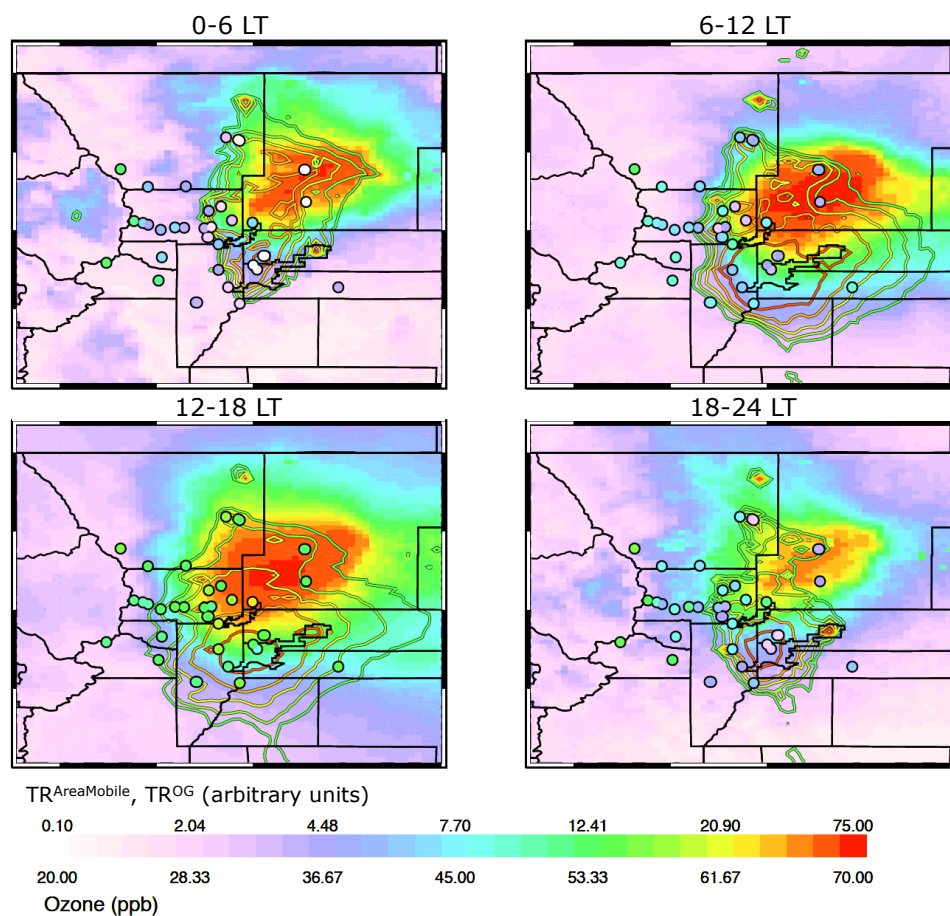


1192  
1193

1194 Figure 7: Spatial correlations between measured species and ratios and model tracers for the  
 1195 area/mobile (blue) and OG (red) sources. Big circles represent the average over all flights, small  
 1196 circles represent results for individual flights. Top: NCAR/NSF C130 flights (same spatial  
 1197 coverage as Figure 5); Bottom: NASA P-3 flights. Statistics are derived for data points below  
 1198 3 km a.g.l. See text for details on the calculation of spatial correlation.



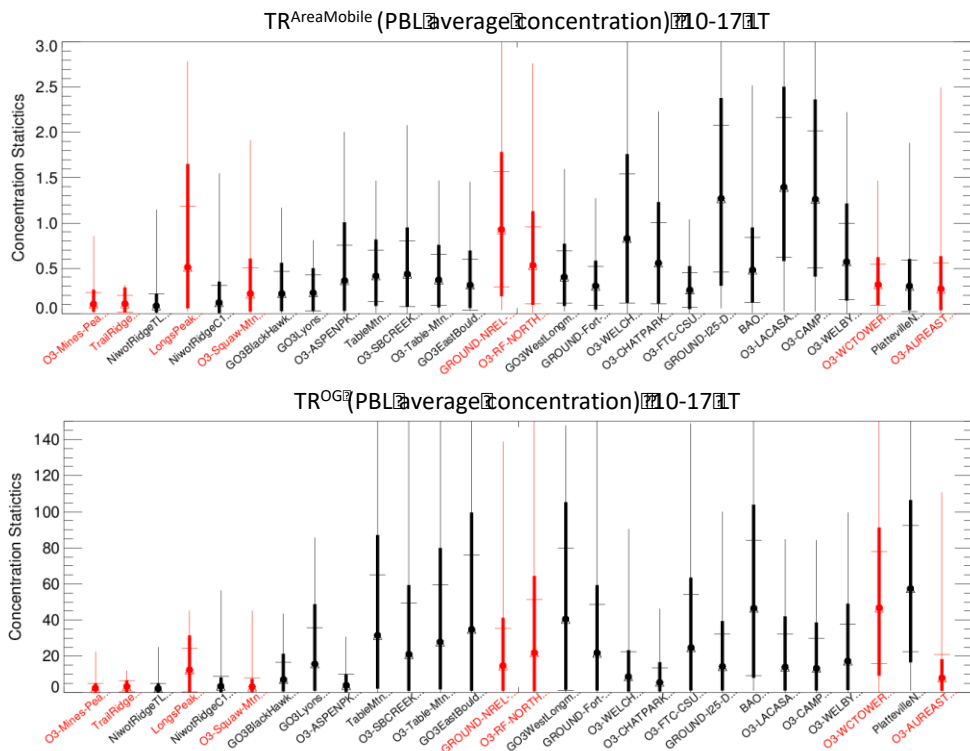
1199 Figure 8: Average spatial tracer distribution (average concentrations within the PBL) for 0-6LT,  
 1200 6-12LT, 12-18LT and 18-24 LT for the FRAPPÉ time period (14 July to 21 August). Contour  
 1201 lines show the PBL average for  $TR^{AreaMobile}$ , filled contours show the PBL average  $TR^{OG}$   
 1202 concentrations. Colored points denote the mean ozone measured at surface sites. The tracers are  
 1203 scaled by a common factor and then by their mean ratio ( $TR^{AreaMobile} = 60 \cdot TR^{OG}$ ) to appear on  
 1204 the same scale.



1205  
 1206  
 1207

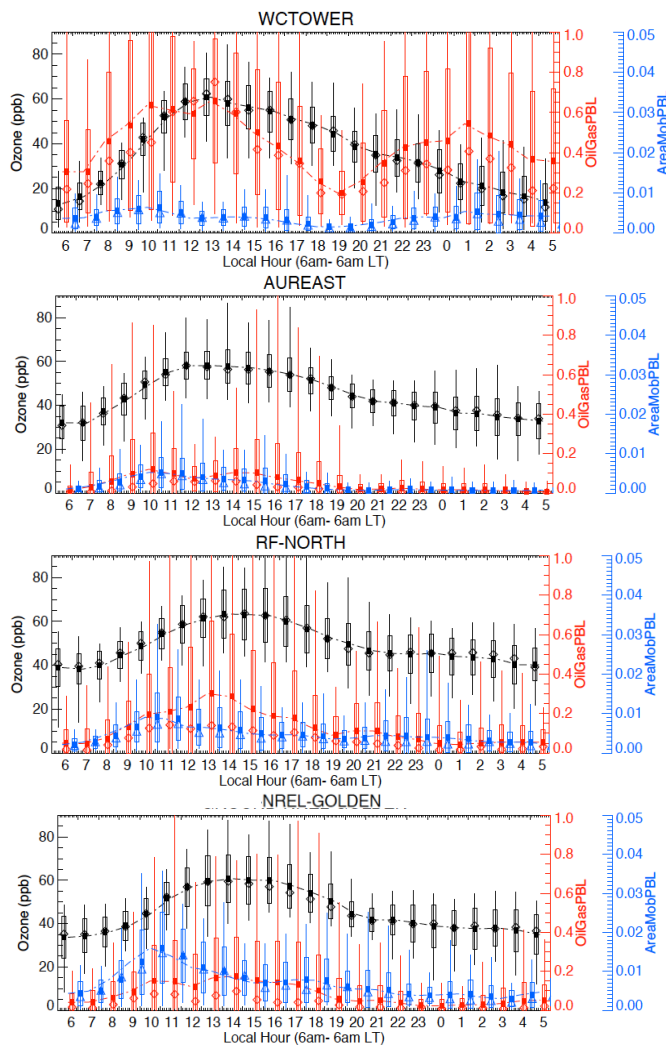


1208 Figure 9: Tracer Statistics for surface sites employed during FRAPPÉ/DAQ for TR<sup>AreaMobile</sup> (top)  
 1209 and TR<sup>OG</sup> (bottom). Sites are arranged from West to East and averaged over 10-17 LT (though  
 1210 an average over all times would not look vastly different). Sites focused on in the analysis of  
 1211 upslope events are colored in red. Shown are mean (dot), median (triangle), standard deviation  
 1212 (horizontal bars), 10<sup>th</sup> and 90<sup>th</sup> percentiles (thick line), minima and maxima (thin lines). In  
 1213 addition to sites shown in Figure 1 we also added sites in the Global Ozone (GO3) project (Black  
 1214 Hawk, Lyons, East Boulder and Longmont) as well as additional sites from the CDPHE network  
 1215 (I-25 Denver, CAMP).



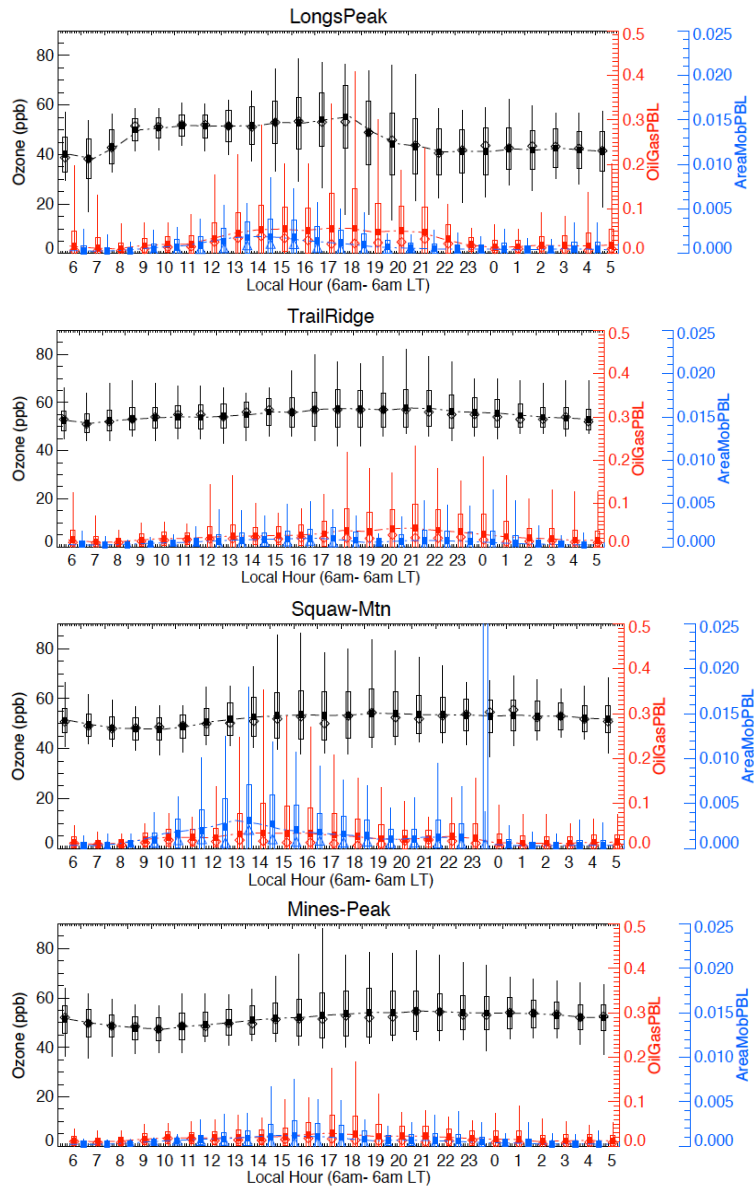
1216  
 1217  
 1218

1219 Figure 10: Average diurnal observed surface ozone (black) and PBLH average TR<sup>OG</sup> (red) and  
 1220 TR<sup>AreaMobile</sup> (blue) for selected surface sites in the Front Range for 6am – 6am LT. Shown are  
 1221 mean, median, standard deviation, minimum and maximum. A line is drawn through the mean  
 1222 values.



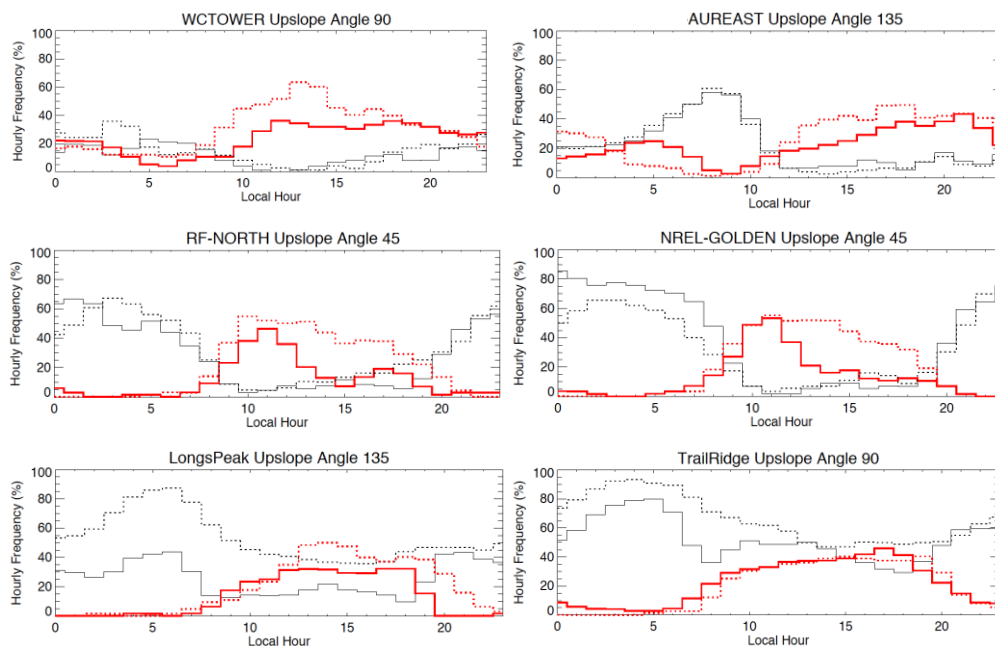
1223  
 1224

1225 Figure 11: As Figure 10 but for selected surface sites in the mountains. Note the y-scale is  
1226 reduced to half of the one used in Figure 10.



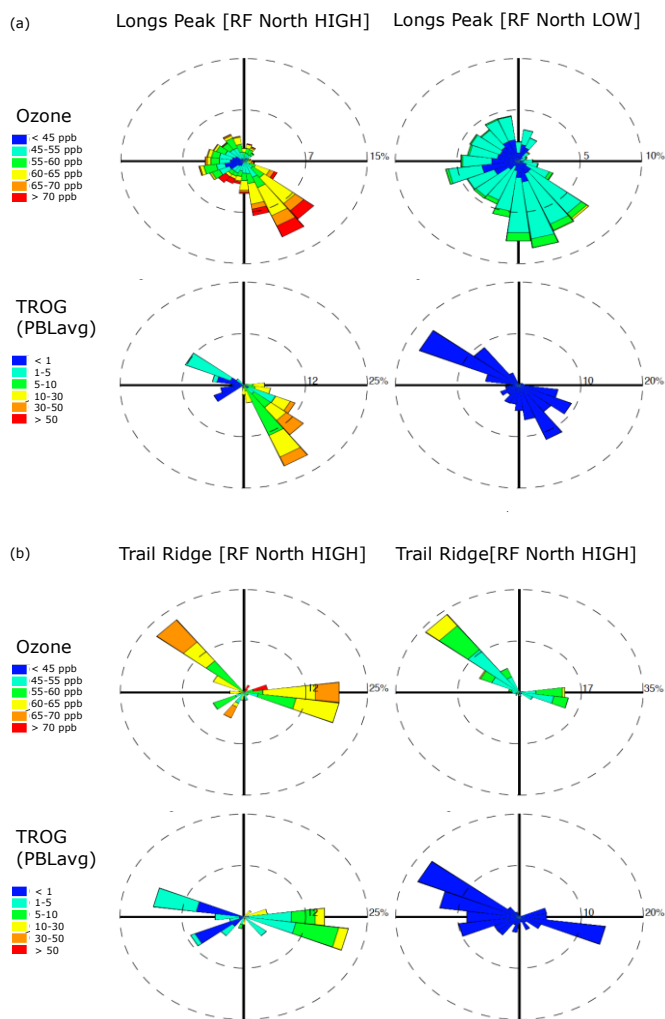
1227

1228 Figure 12: Upslope (red) and Downslope (black) statistics from observations (solid lines) and  
 1229 WRF (dotted lined). Flow is defined when winds are from within a defined wind sector at least  
 1230  $2/3^{\text{rd}}$  of the time within a given hour (Note that wind data for Trail Ridge Road are available  
 1231 hourly only and that model data are also only available on an hourly basis). Upslope: Upslope  
 1232 Angle  $\pm 45\text{deg}$ ; Downslope:  $270\pm 45\text{deg}$ ; only data with wind speeds  $> 0.3 \text{ m/s}$  (i.e. data that are  
 1233 not defined calm based on Beaufort scale). The upslope angle has been defined based on  
 1234 windrose analysis. The frequency is given as percentage of upslope or downslope of all valid  
 1235 measurements.



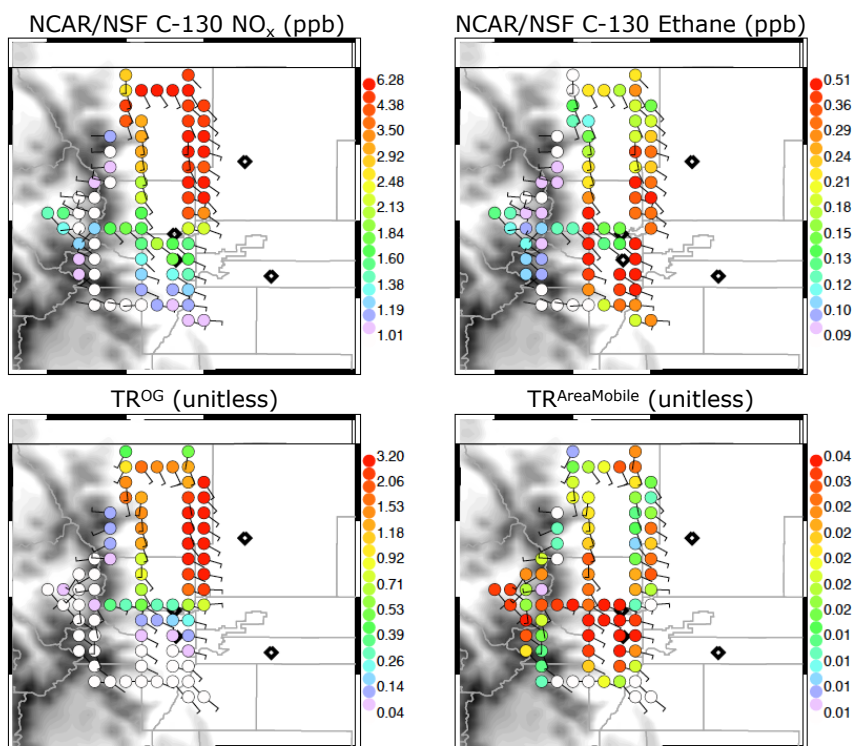
1236  
 1237

1238 Figure 13: Ozone and Tracer roses for (a) Longs Peak (1-minute data) and (b) Trail Ridge road  
 1239 (hourly data) on days when RF North 12-18LT average ozone was > 70 ppb (“RF North HIGH”)  
 1240 or < 60 ppb (“RF North LOW”). Only data for 12-20LT are shown.



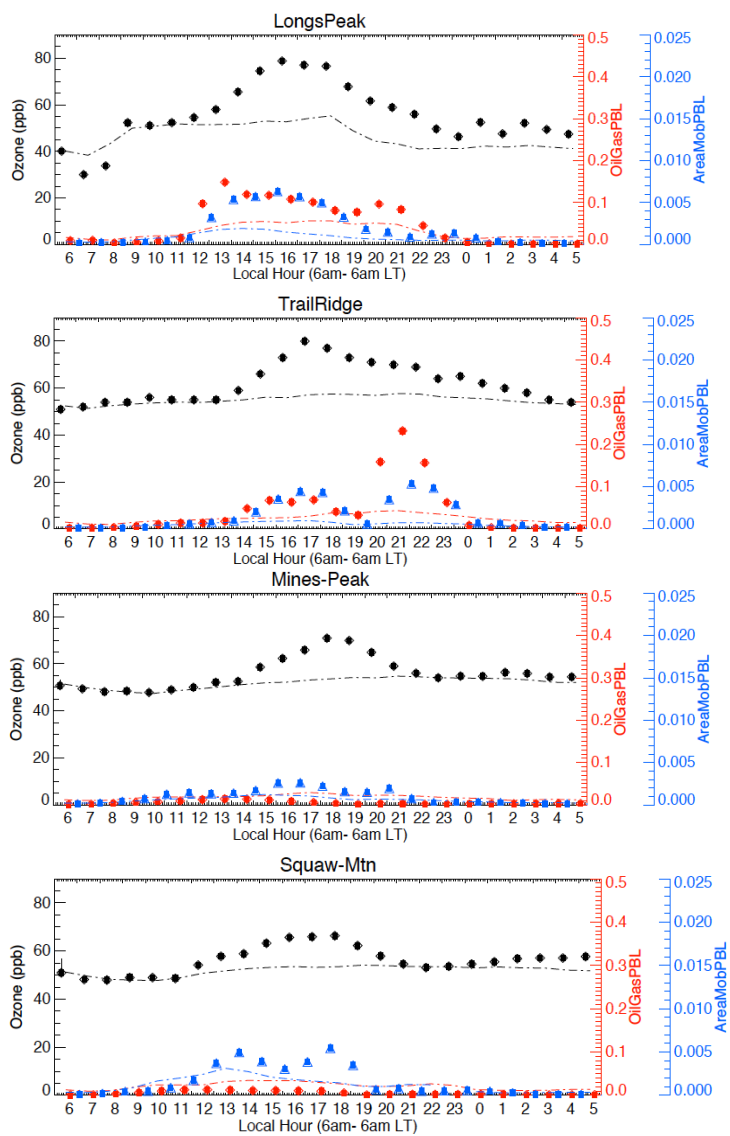
1241  
 1242

1243 Figure 14: NCAR/NSF C-130 measured ethane and NO<sub>x</sub> (top row) and modeled TROG and  
 1244 TRAreaMobile (bottom row) for the the upslope part of the 12 August flight (after refueling). All  
 1245 data averaged over 0-2km ag and a 0.1 deg x 01 deg grid. The vector averaged measured and  
 1246 modeled winds for each grid point are shown by the windbarbs and the monitoring sites RF  
 1247 North, NREL Golden, WC Tower, Aurora East and Golden are indicated by diamond symbols.  
 1248 Areas above 2500m a.s.l. are shaded in grey.



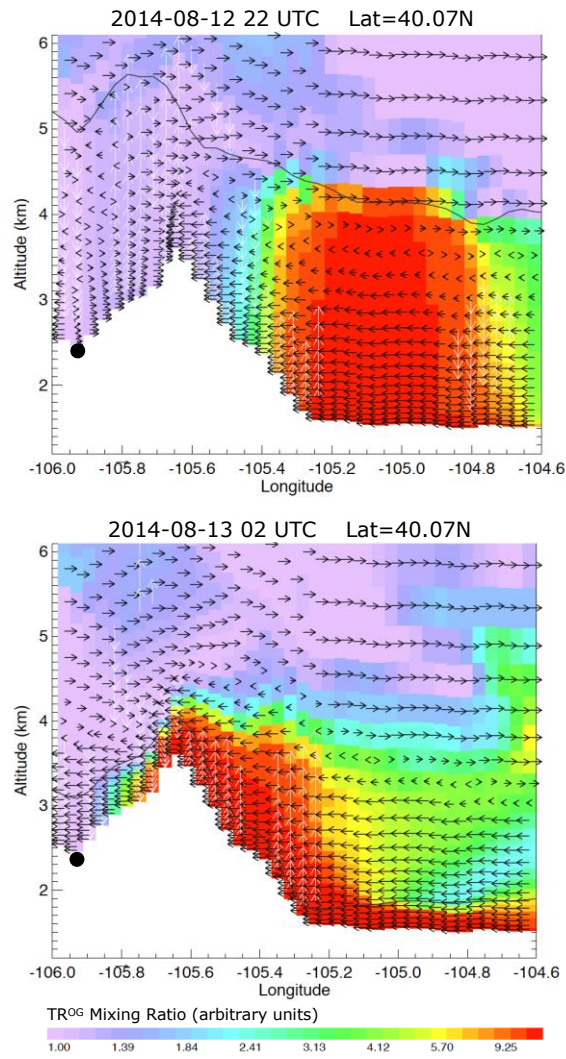
1249  
 1250

1251 Figure 15: as Figure 10 but for 12 August 2014 and for mountain sites only. Lines show the  
1252 average diurnal cycle from Figure 11.



1253  
1254

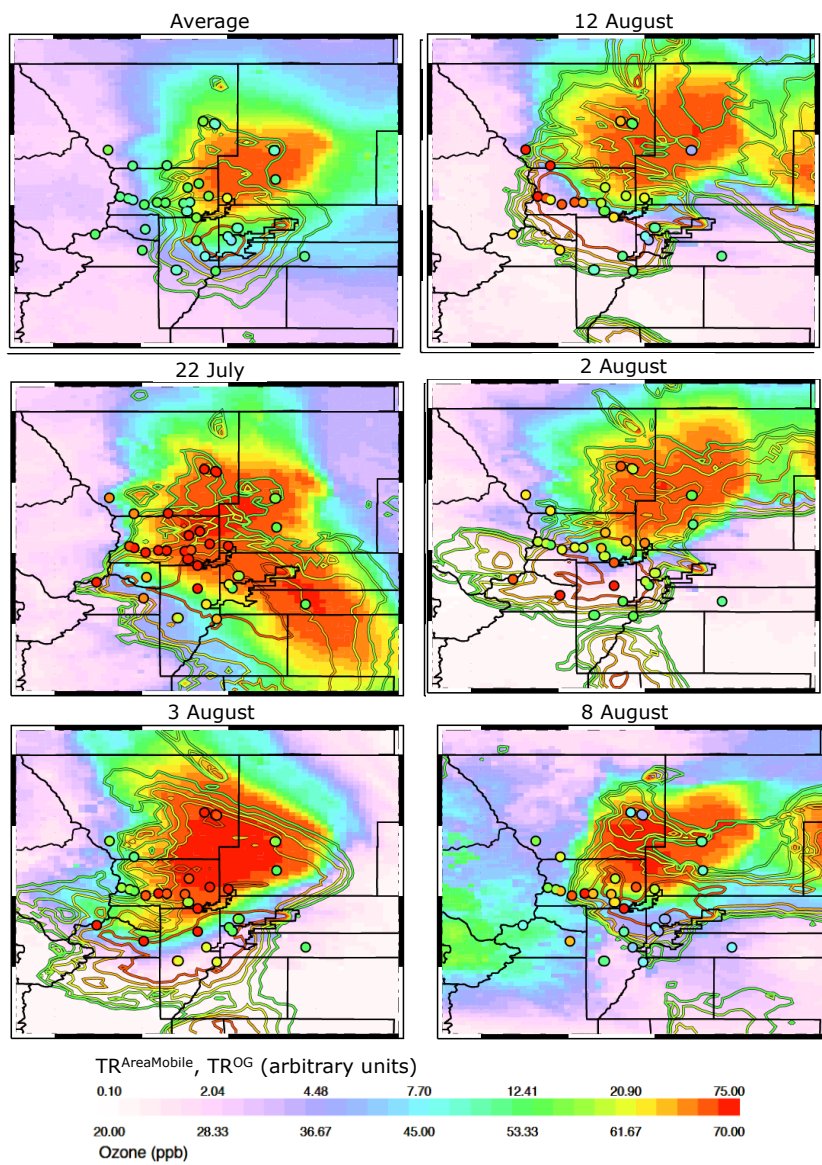
1255 Figure 16: Longitude-Altitude Cross Section of TR<sup>OG</sup> at 40.09N (single grid box in latitude) for  
 1256 12 August 22 UTC (16 LT, top) and 13 August 2 UTC (12 August 20 LT, bottom); The location  
 1257 of the Granby airport is indicated by the black dot. Horizontal winds are indicated by black  
 1258 arrows, vertical winds are shown as white arrows. For clarity, only vertical winds > 0.2m/s are  
 1259 included. The height of the PBLH is plotted as a black line.



1260



1261 Figure 17: as Figure 8 but for 14-20 LT. Top row: average over FRAPPÉ period and 12 August;  
1262 middle row: 22 July and 2 August; bottom row: 3 and 8 August.



1263

Figure 1.

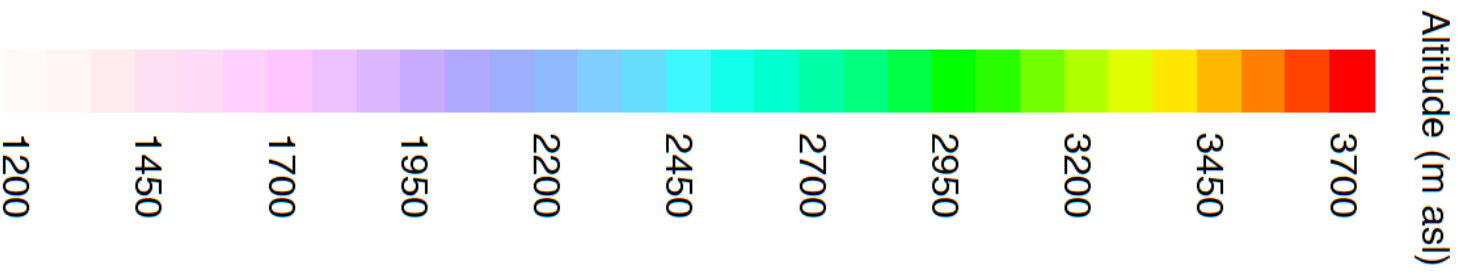
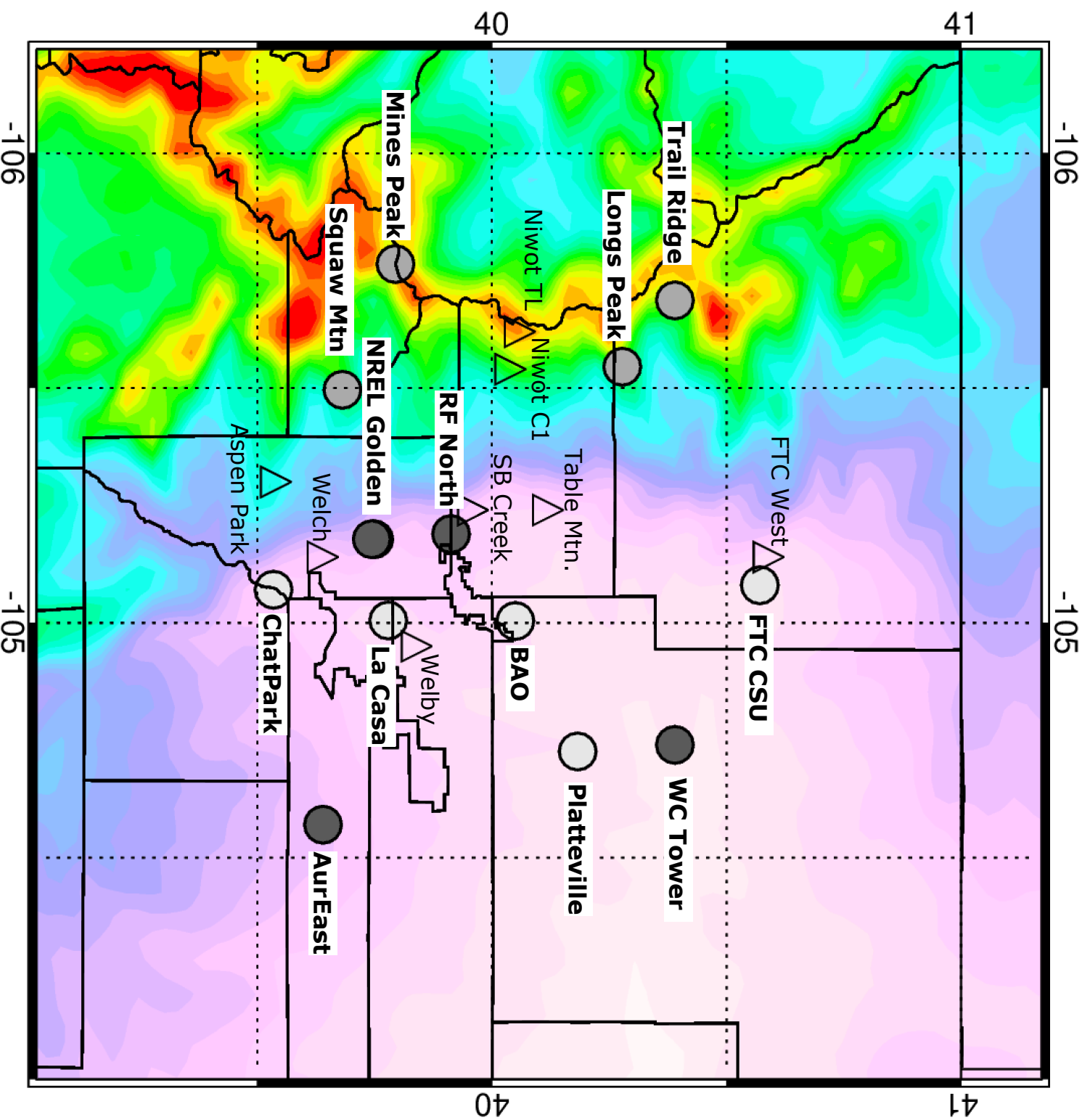


Figure 2.

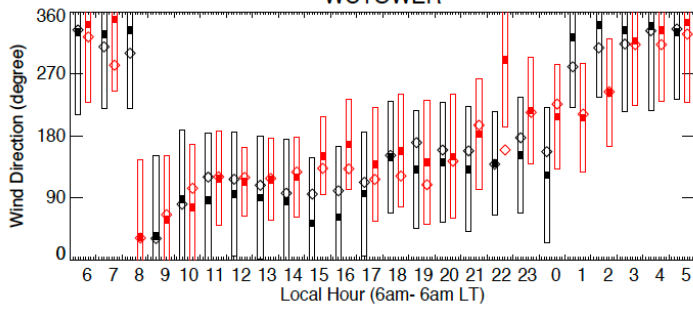
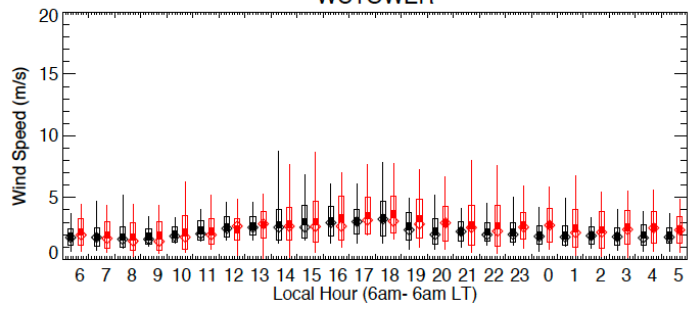
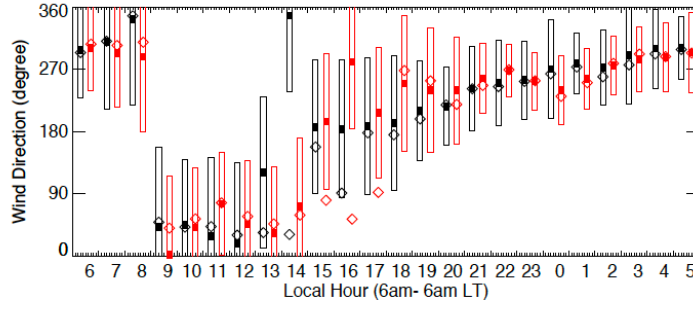
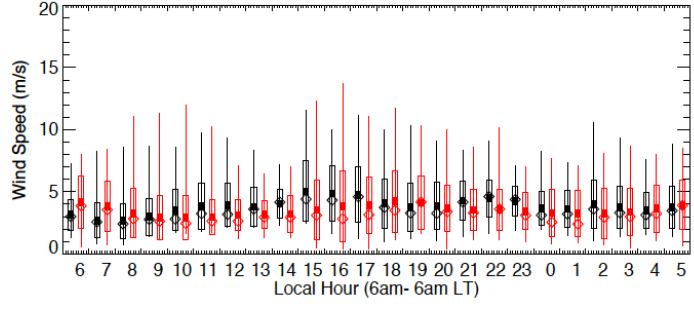
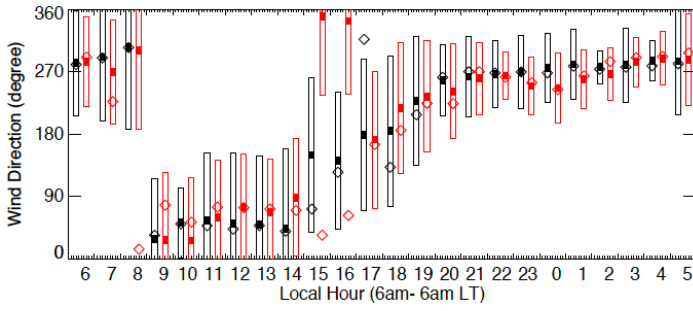
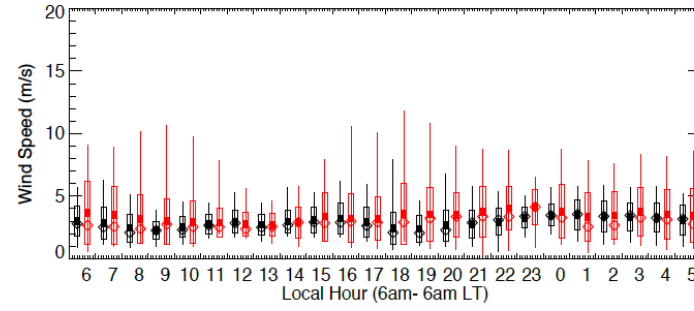
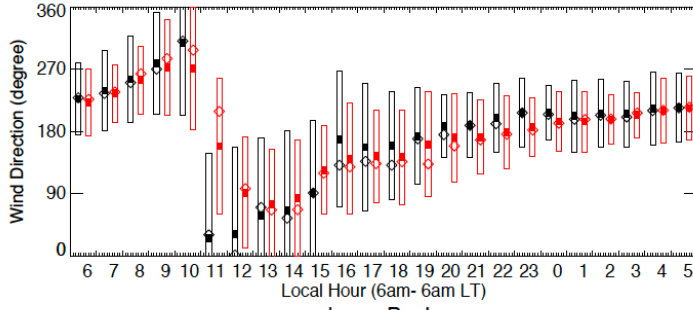
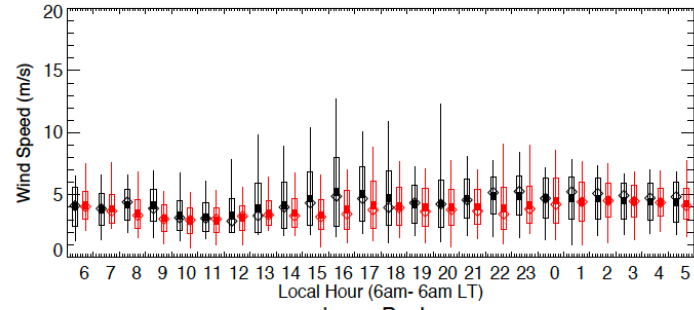
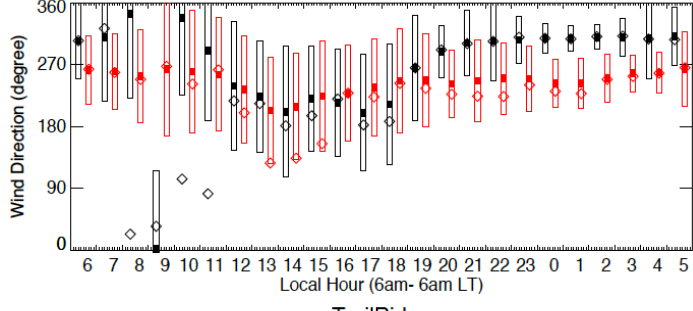
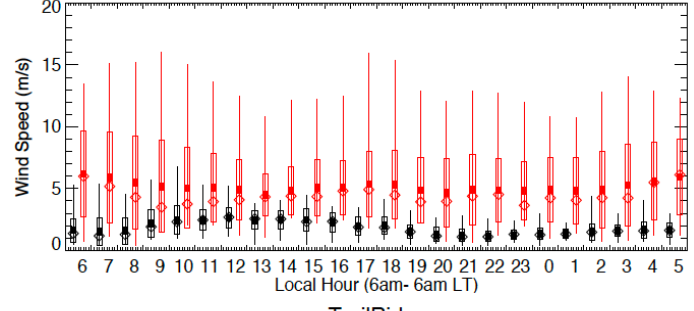
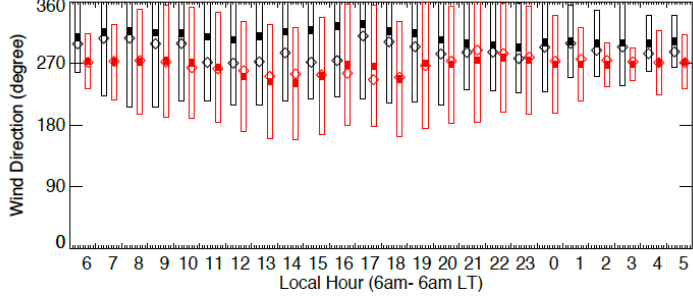
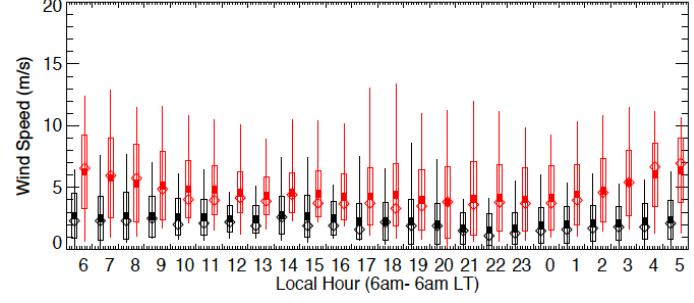
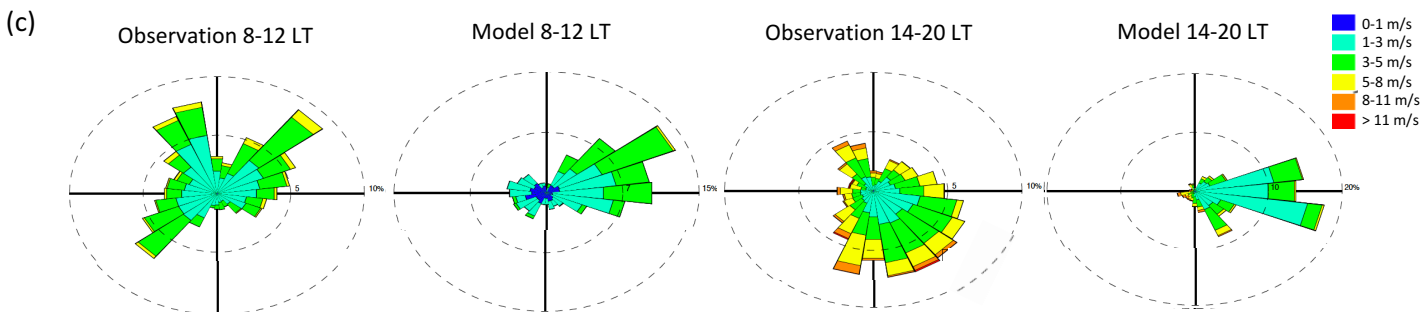
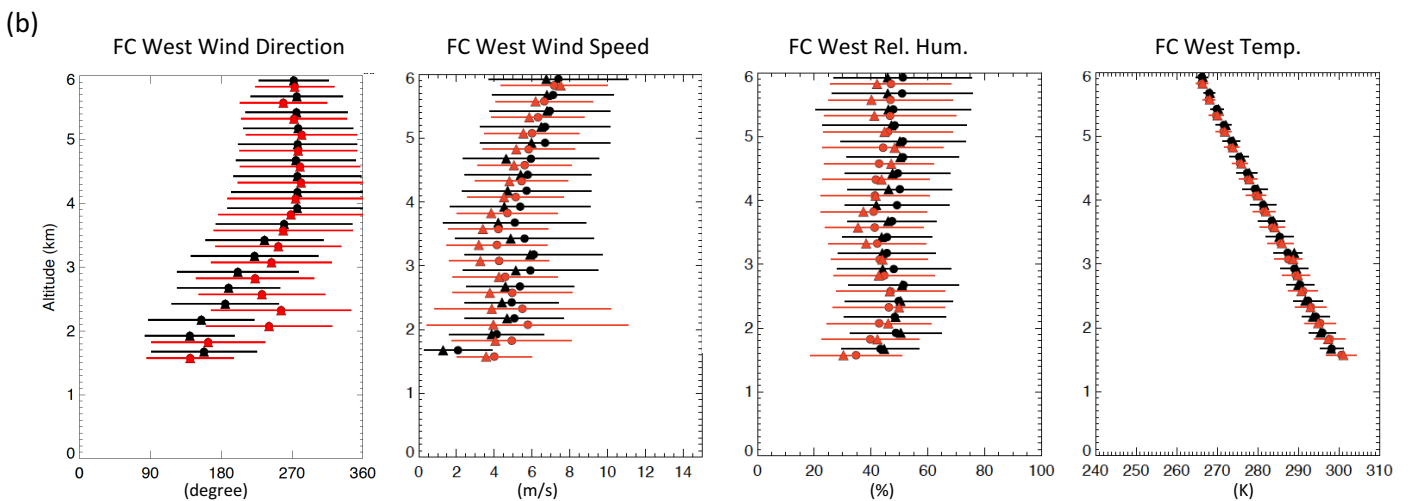
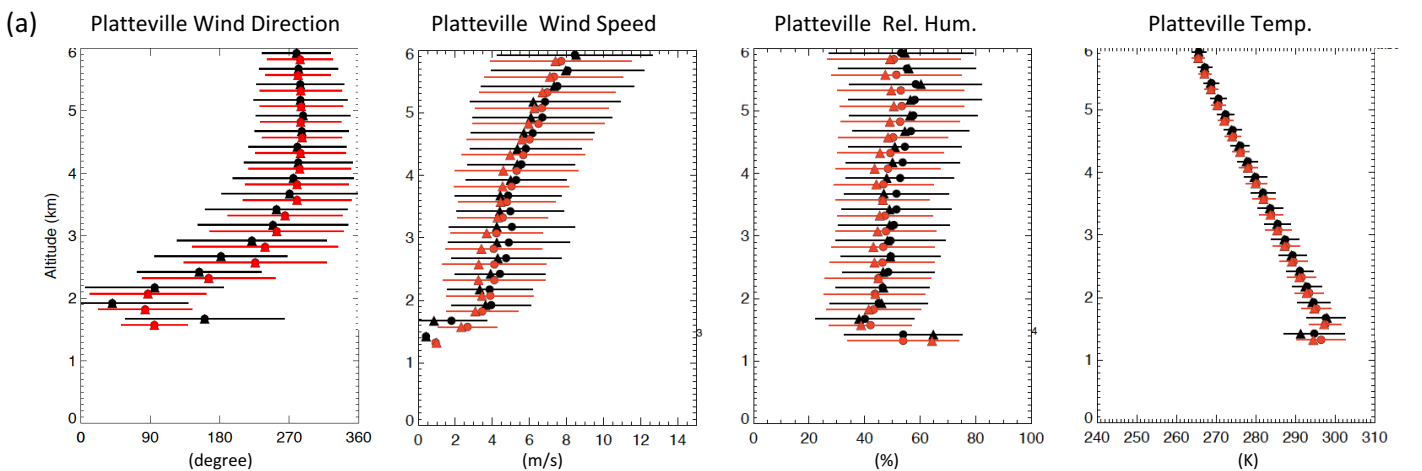
**WCTOWER****WCTOWER****RF-NORTH****RF-NORTH****NREL-GOLDEN****NREL-GOLDEN****AUREAST****AUREAST****LongsPeak****LongsPeak****TrailRidge****TrailRidge**

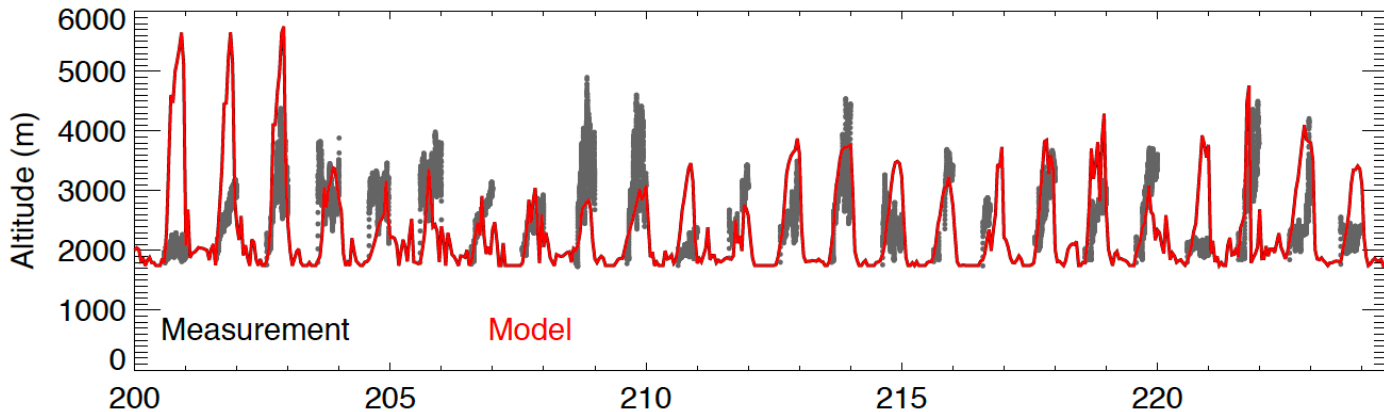
Figure 3.



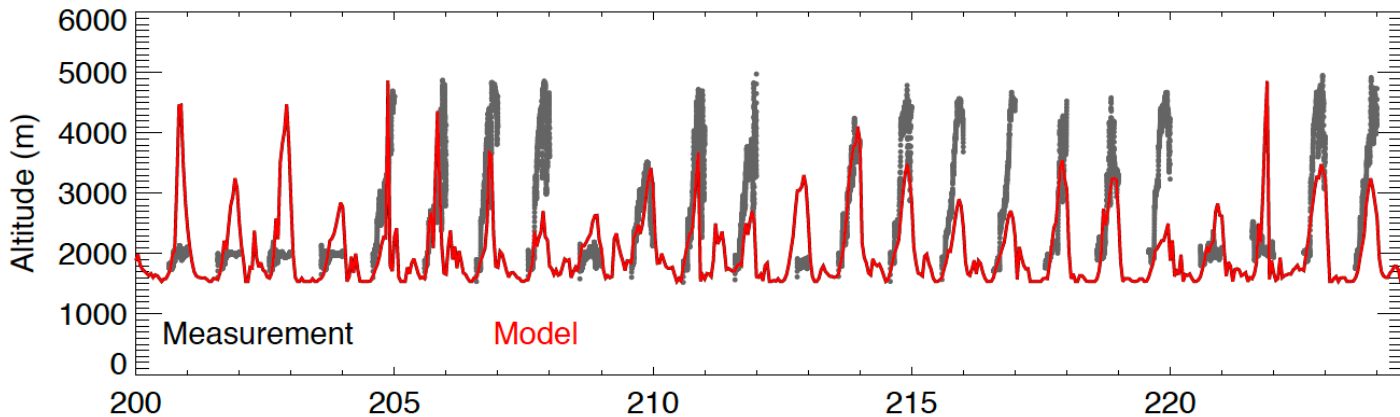
**Figure 4.**



### FTC West



### Platteville



### NREL Golden

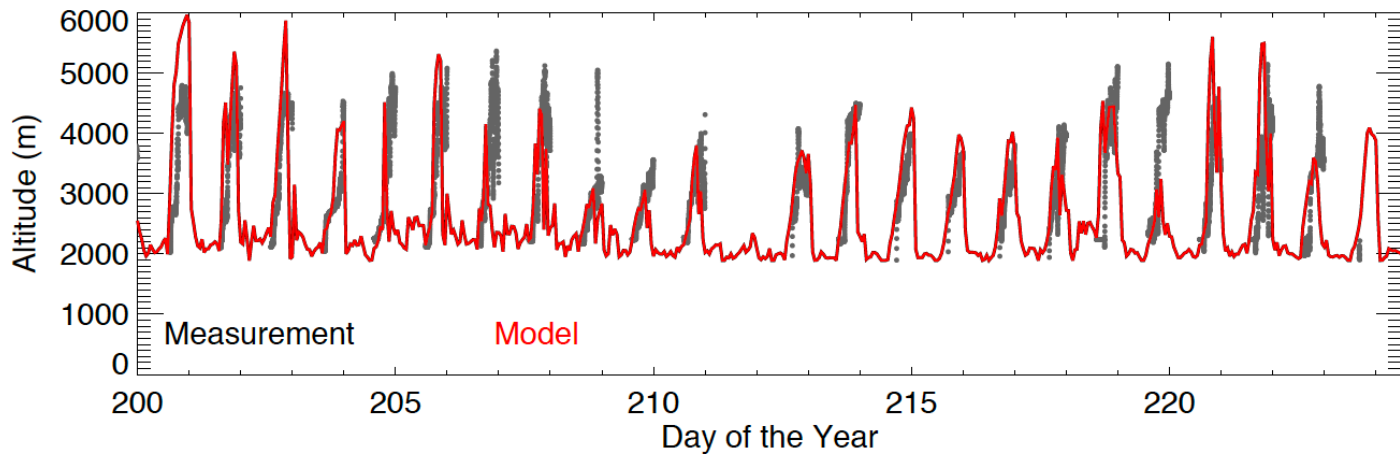
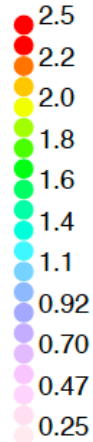
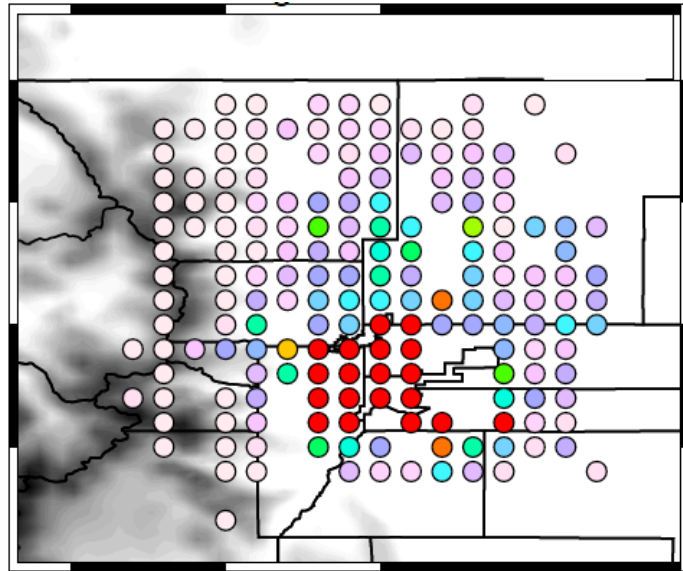
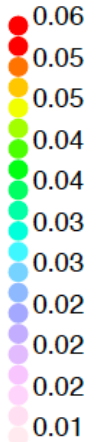
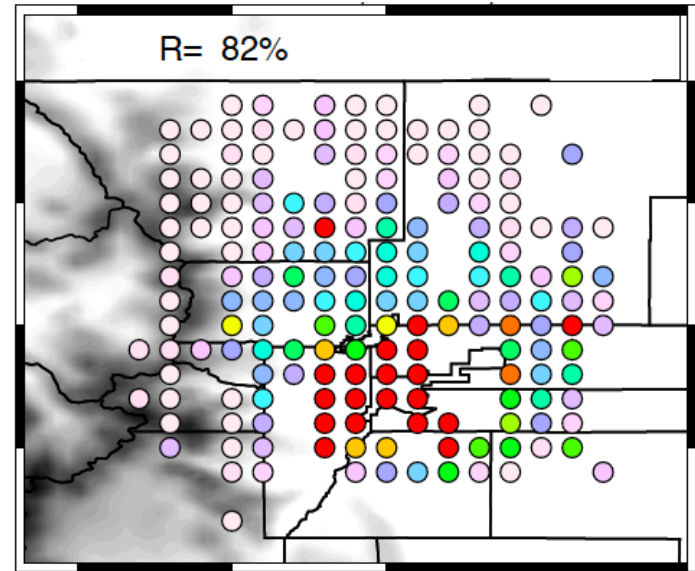


Figure 5.

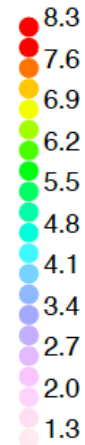
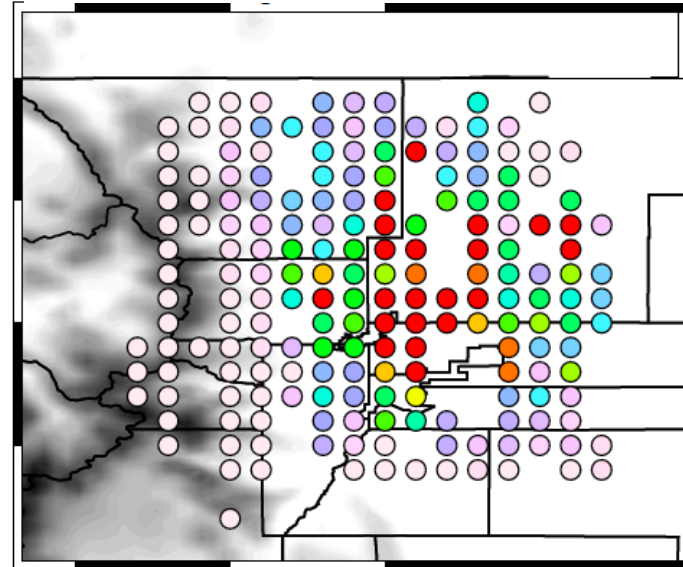
NCAR/NSF C-130 NO<sub>x</sub> (ppb)



TR<sup>AreaMobile</sup> (unitless)



NCAR/NSF C-130 Ethane (ppb)



TR<sup>OG</sup> (unitless)

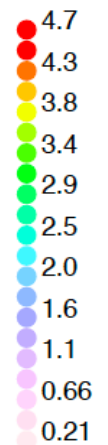
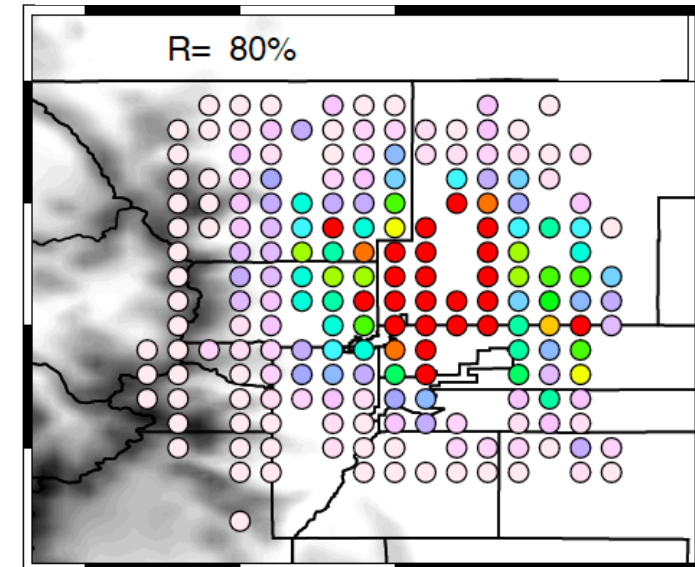
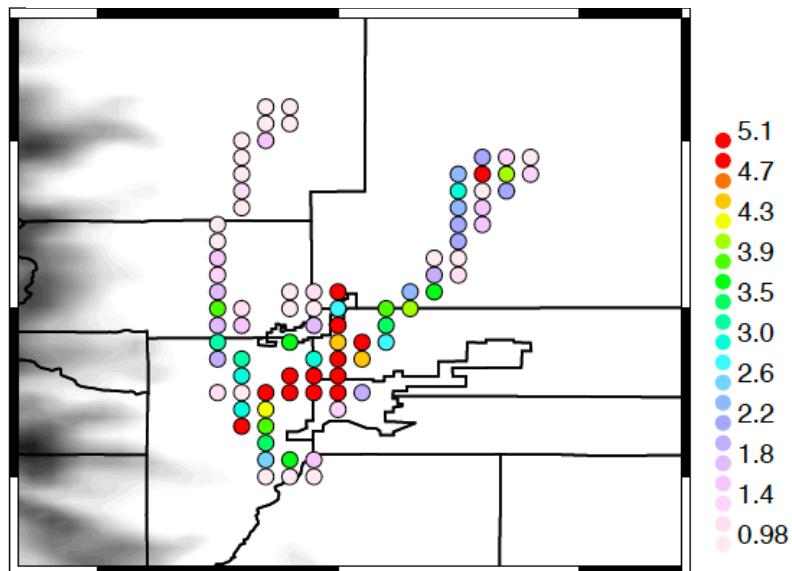
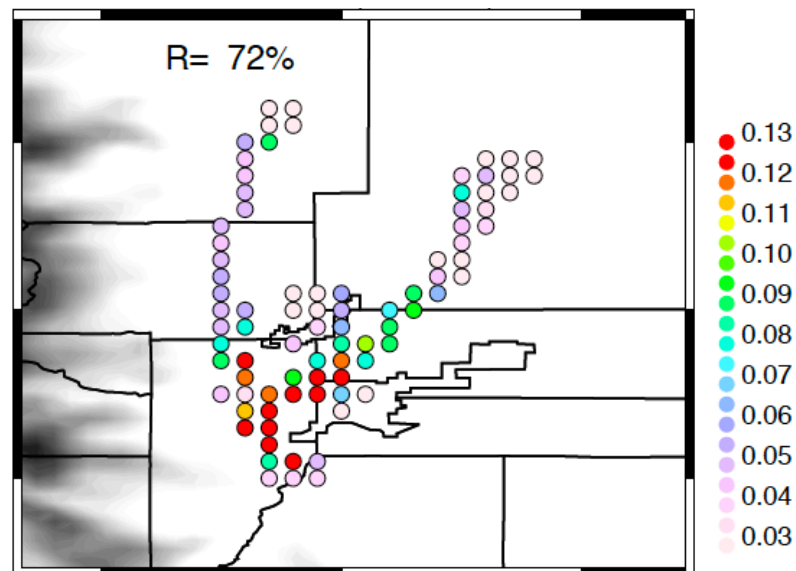


Figure 6.

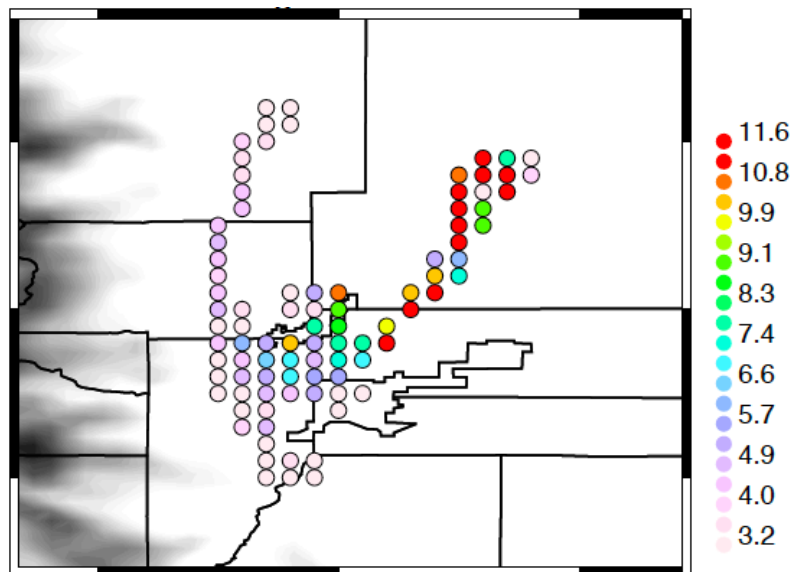
NASA P-3 NO<sub>x</sub> (ppb)



TR<sup>AreaMobile</sup> (unitless)



NASA P-3 Ethane (ppb)



TR<sup>OG</sup> (unitless)

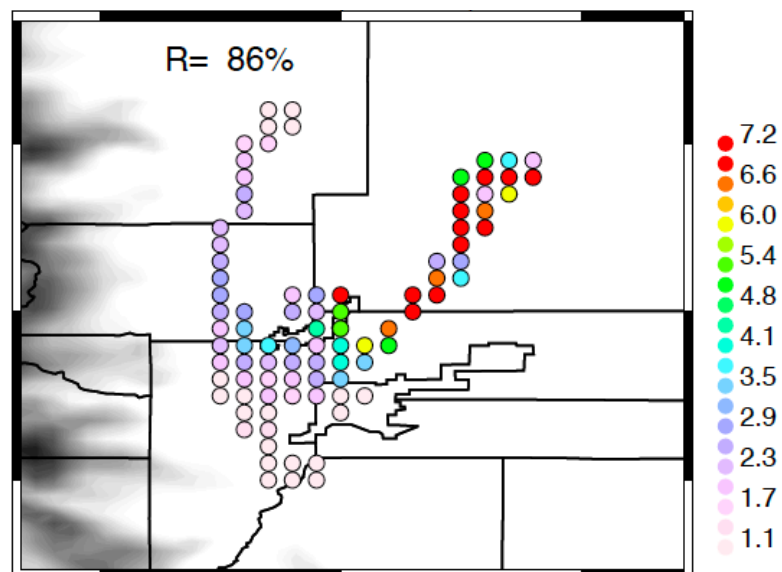
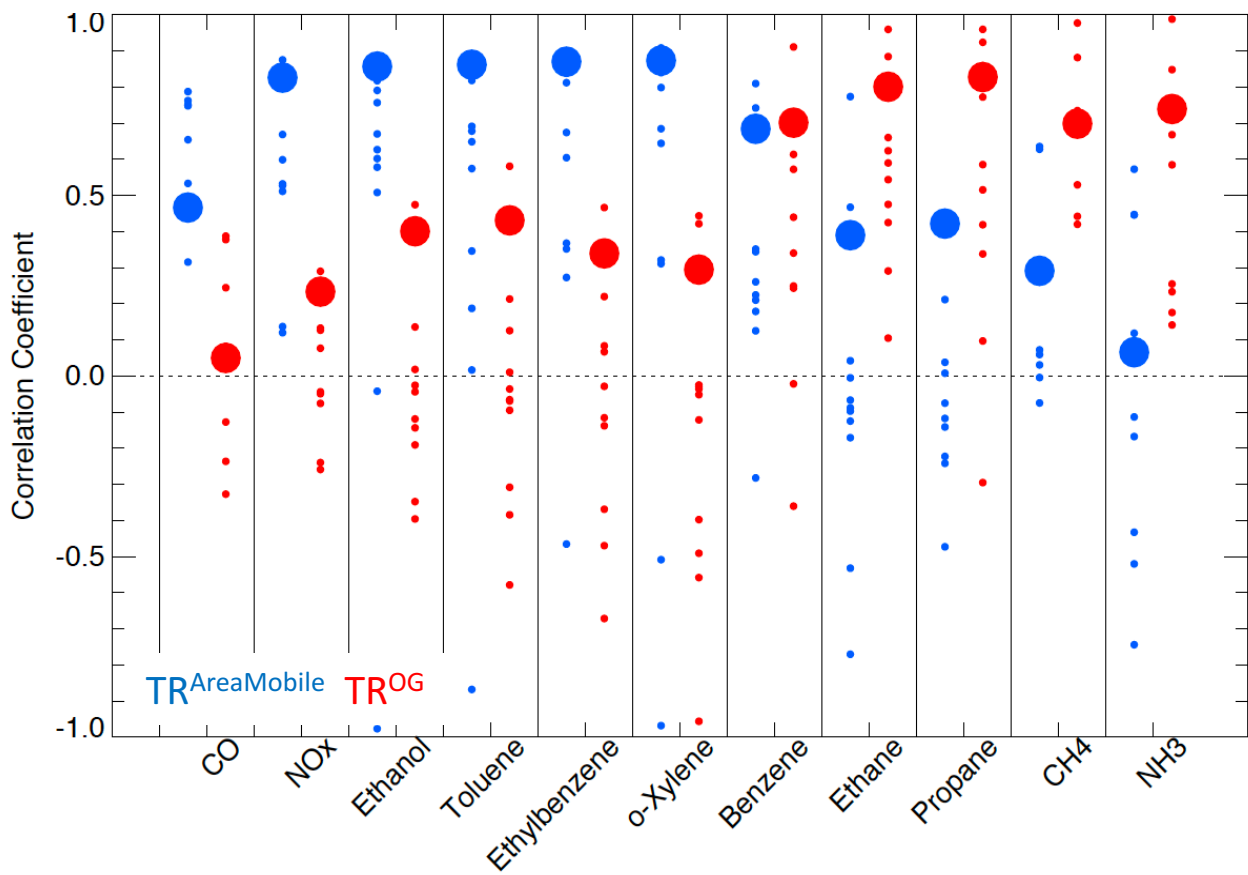


**Figure 7.**

# NCAR/NSF C-130



# NASA P-3

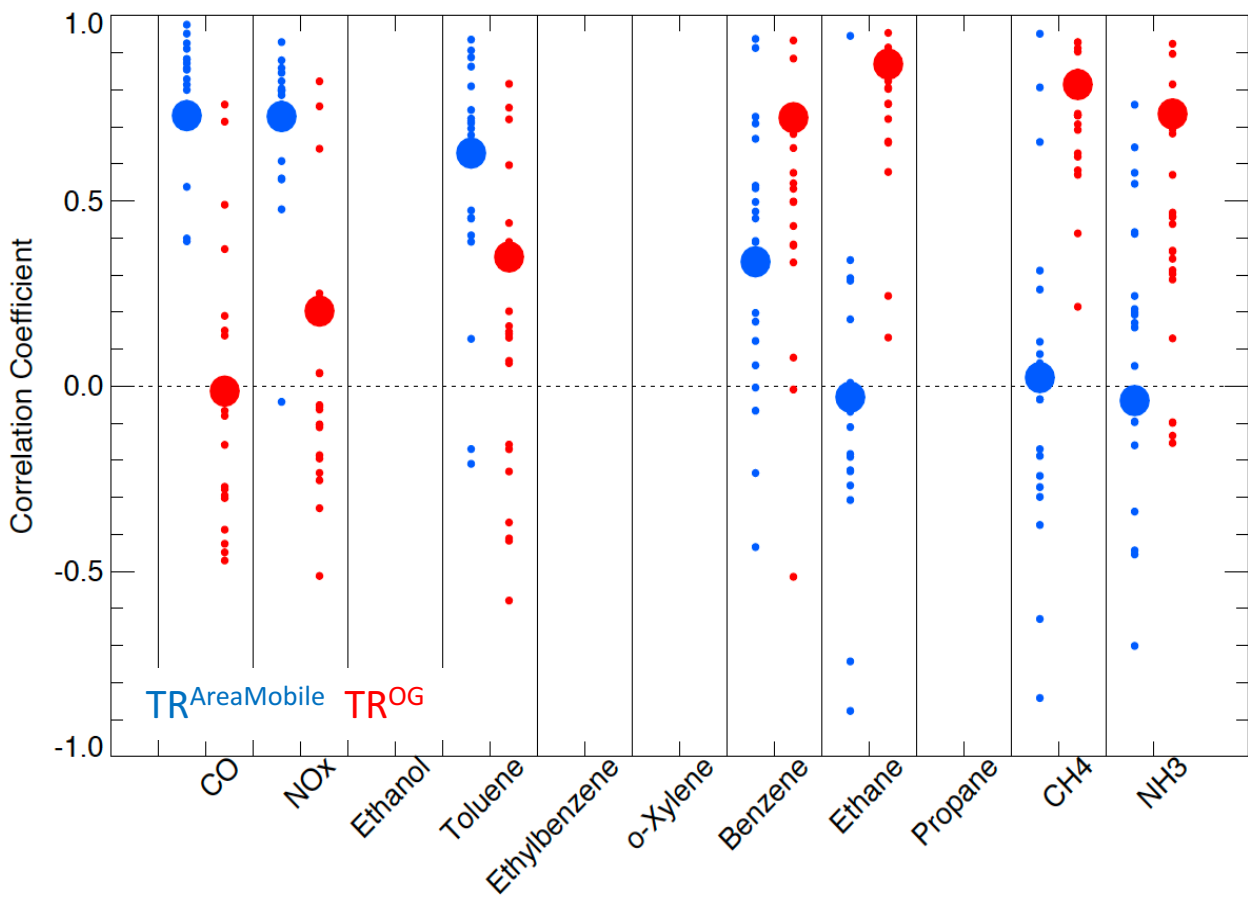
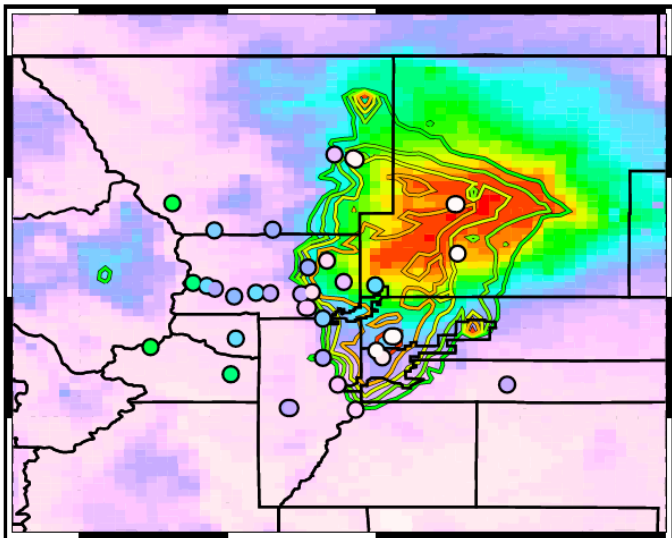


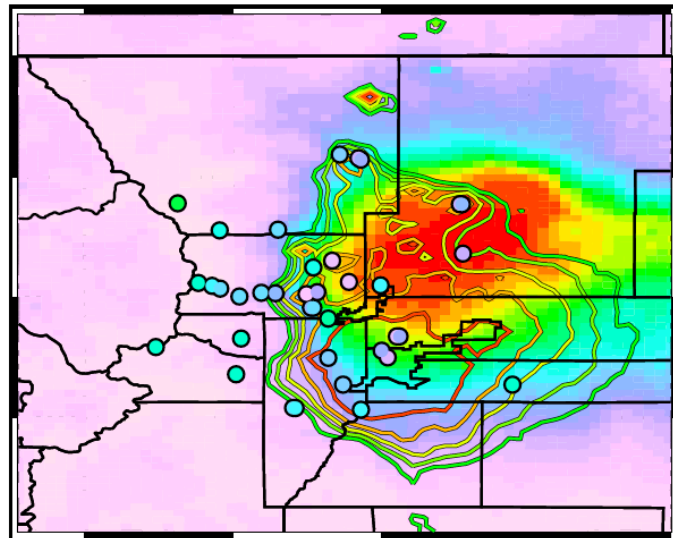
Figure 8.



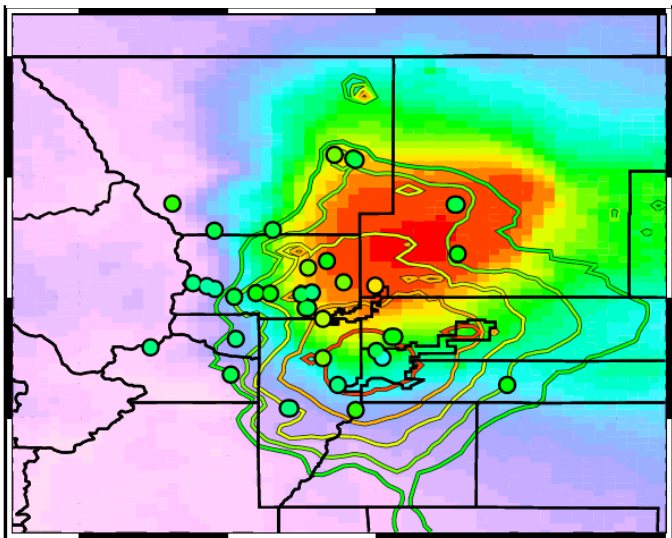
0-6 LT



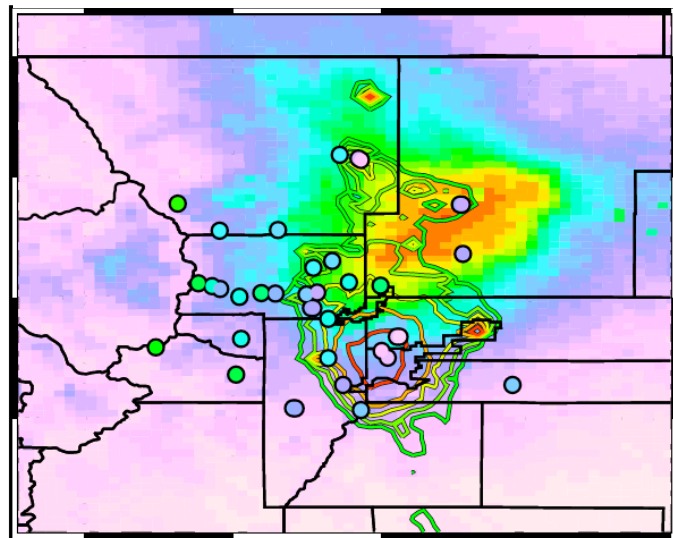
6-12 LT



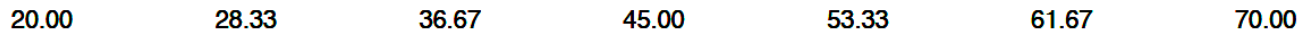
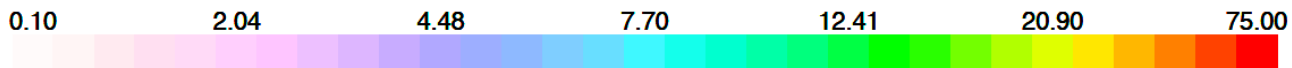
12-18 LT



18-24 LT



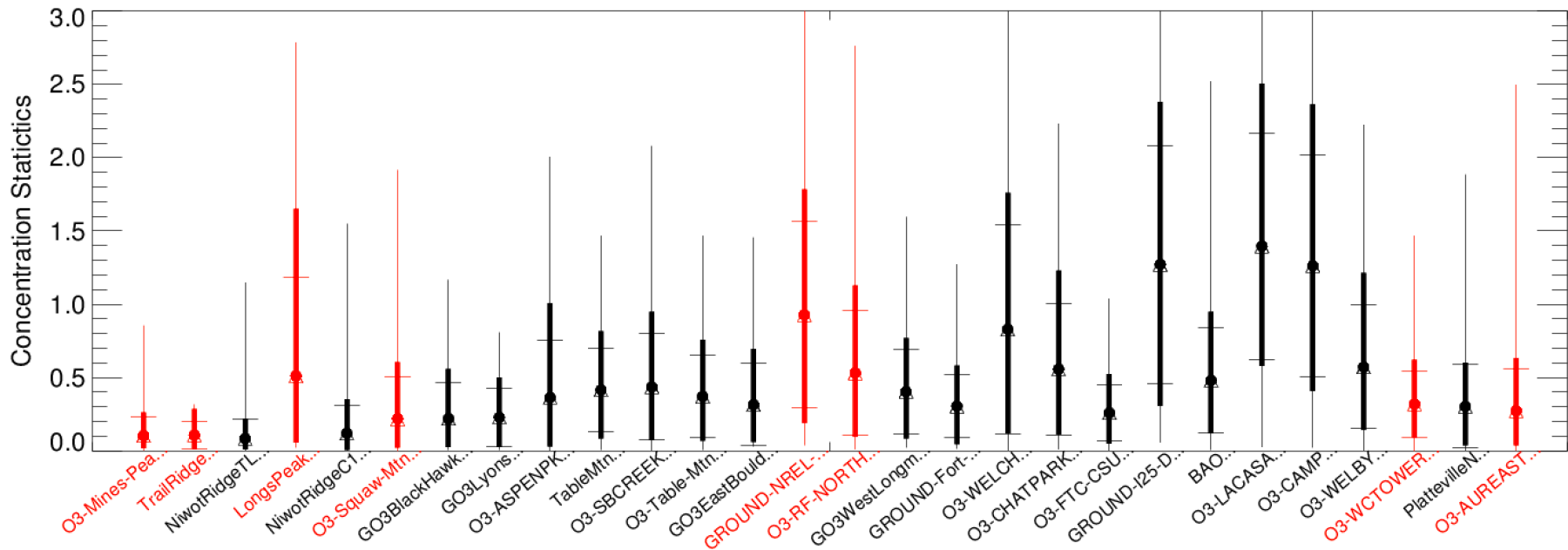
TR<sub>AreaMobile</sub>, TR<sup>OG</sup> (arbitrary units)



Ozone (ppb)

Figure 9.

### TR<sup>AreaMobile</sup> (PBL average concentration) 10-17 LT



### TR<sup>OG</sup> (PBL average concentration) 10-17 LT

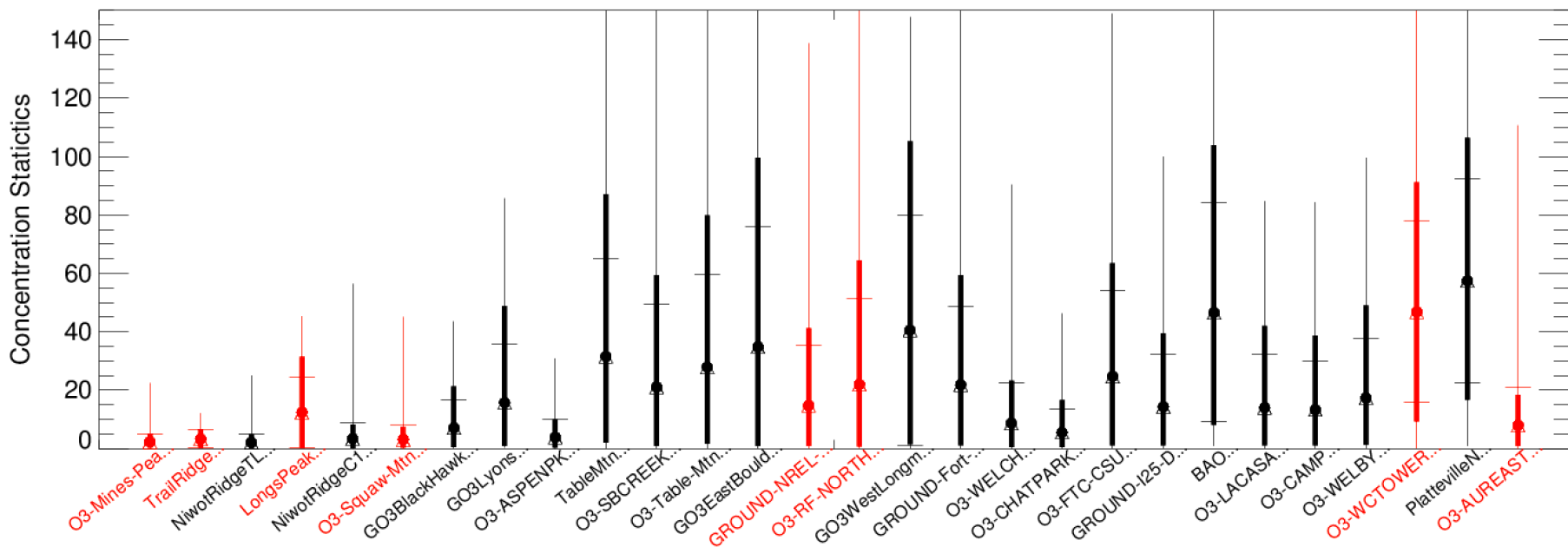
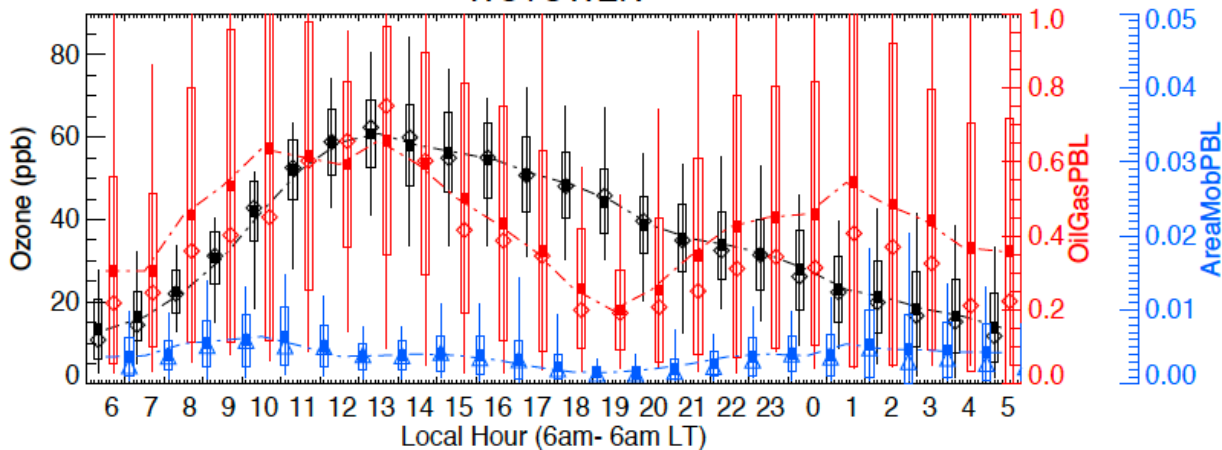
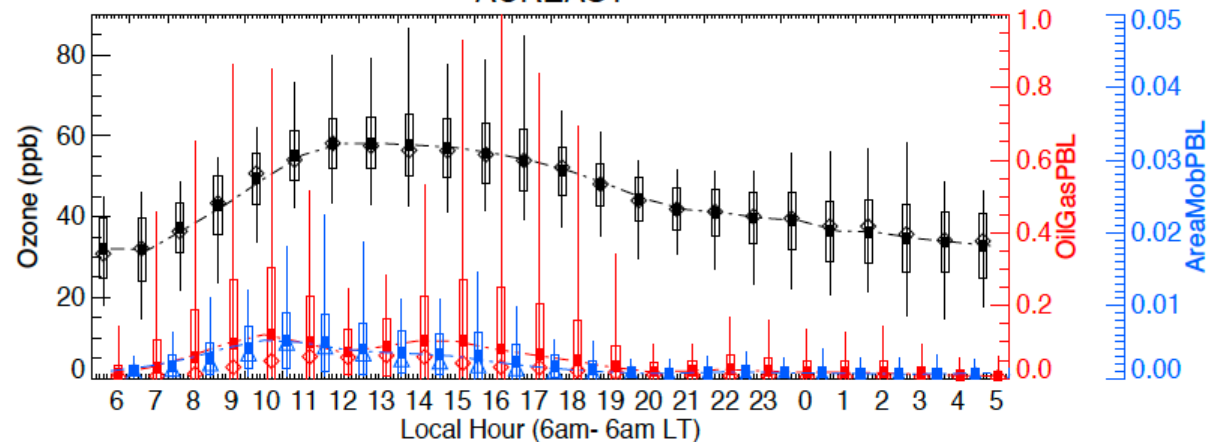


Figure 10.

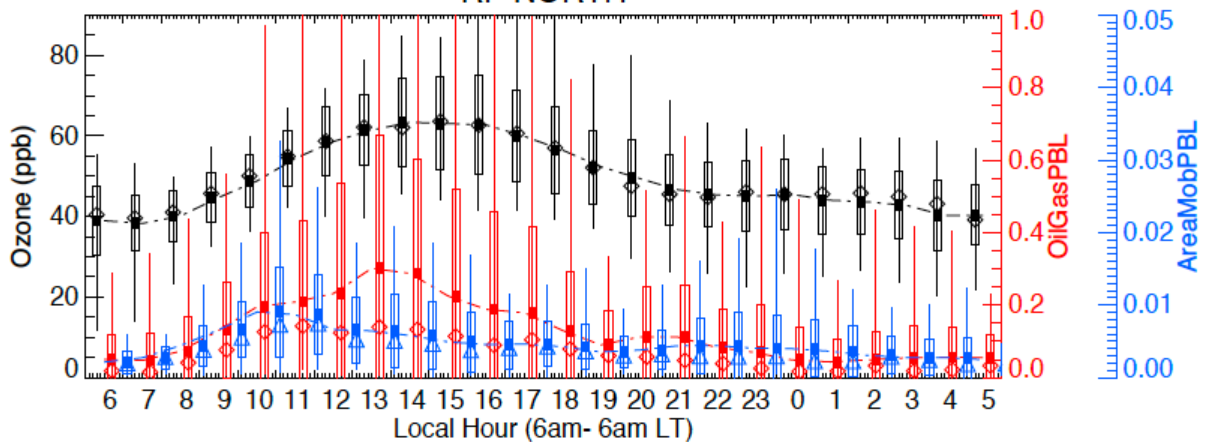
### WCTOWER



### AUREAST



### RF-NORTH



### NREL-GOLDEN

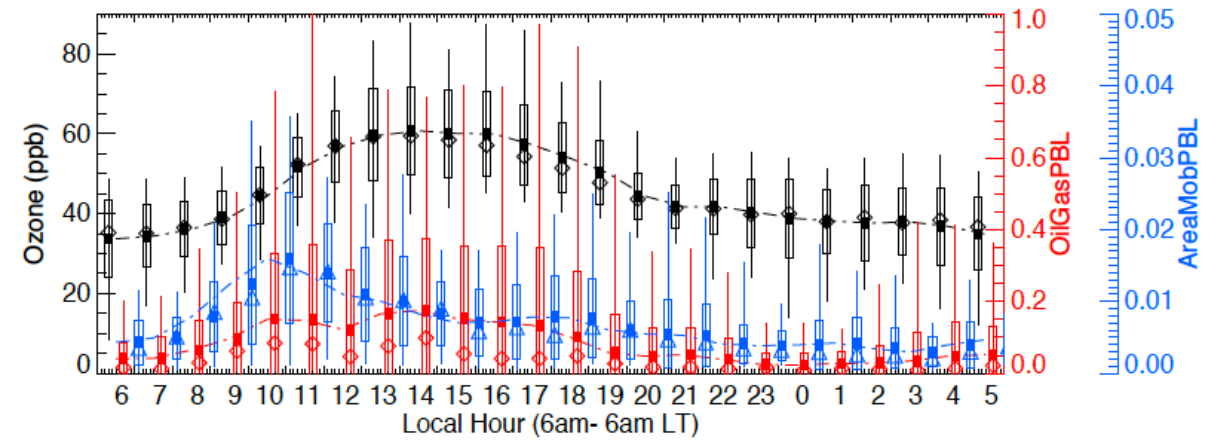
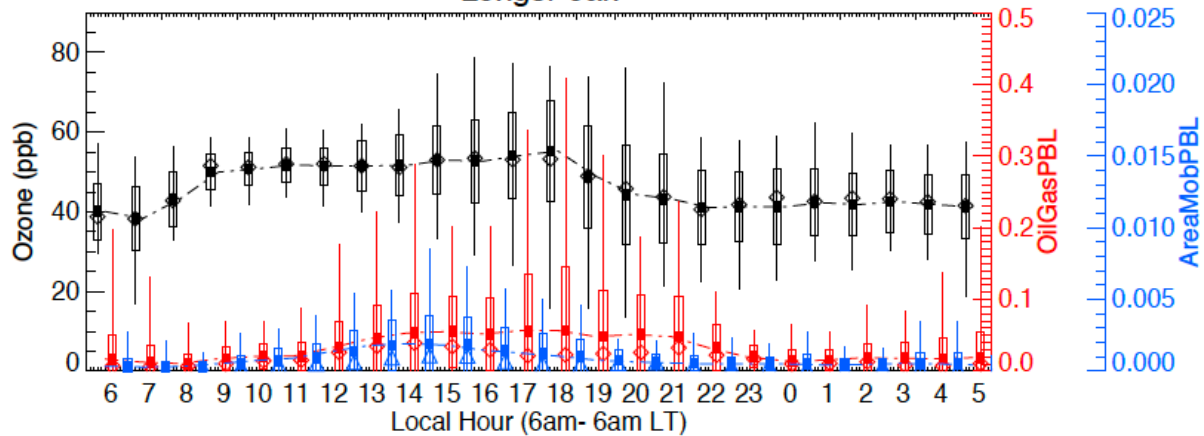
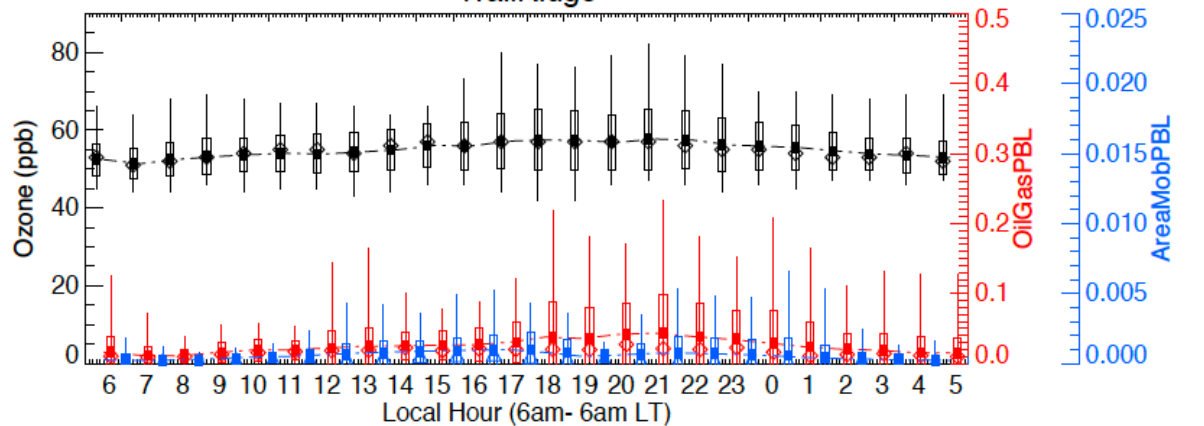


Figure 11.

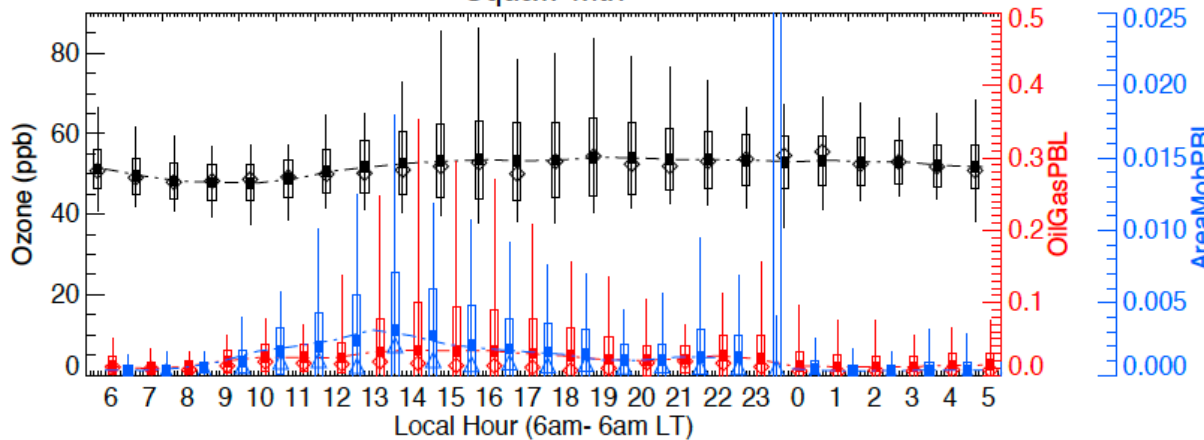
### LongsPeak



### TrailRidge



### Squaw-Mtn



### Mines-Peak

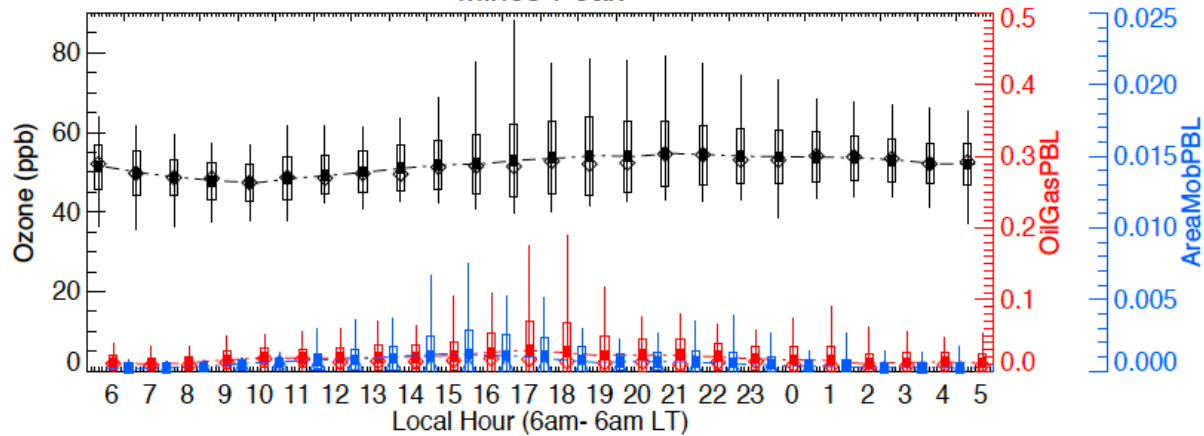
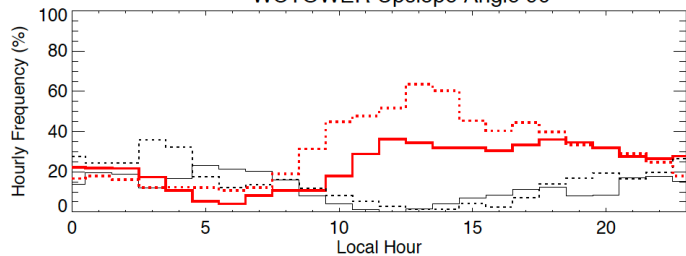


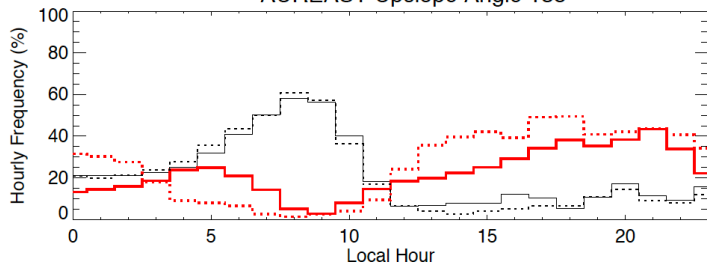
Figure 12.



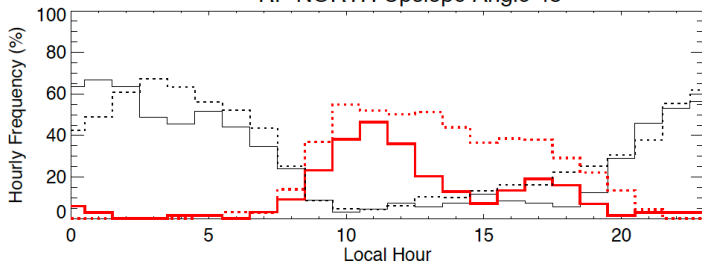
WCTOWER Upslope Angle 90



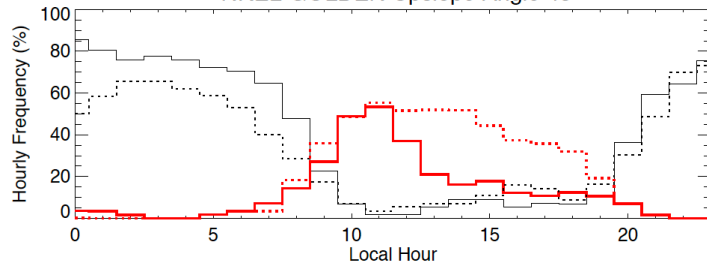
AUREAST Upslope Angle 135



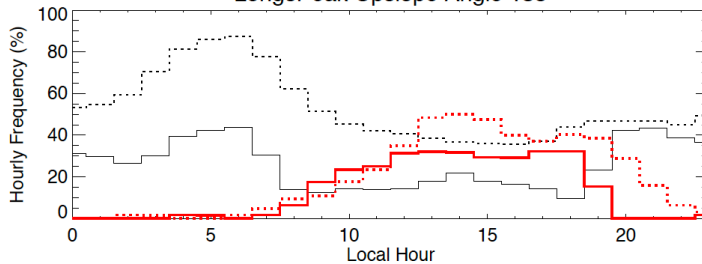
RF-NORTH Upslope Angle 45



NREL-GOLDEN Upslope Angle 45



LongsPeak Upslope Angle 135



TrailRidge Upslope Angle 90

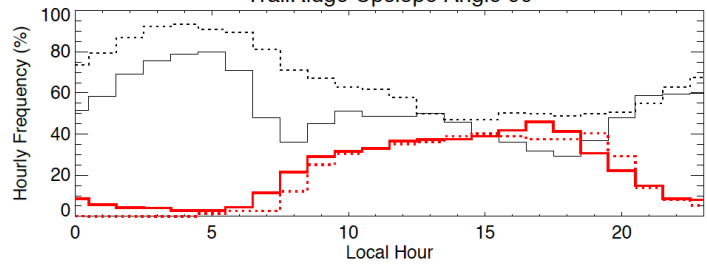


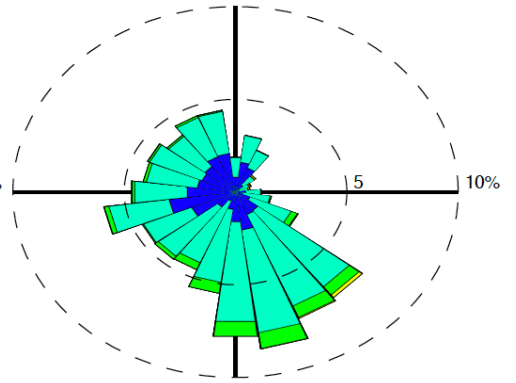
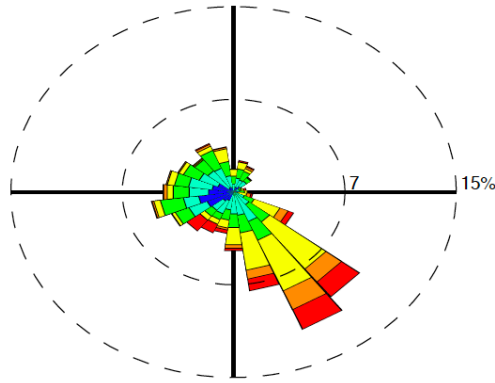
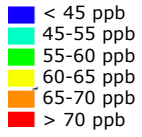
Figure 13.

(a)

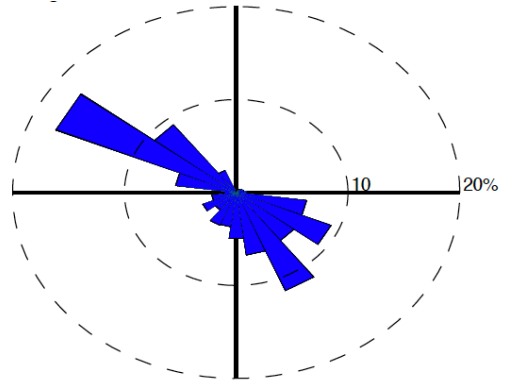
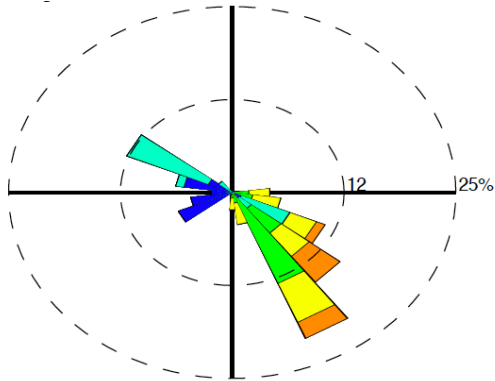
Longs Peak [RF North HIGH]

Longs Peak [RF North LOW]

Ozone



TROG (PBLavg)

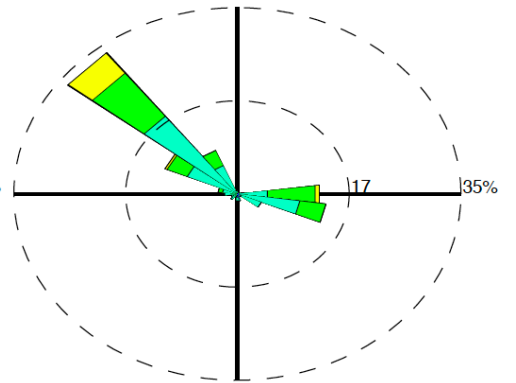
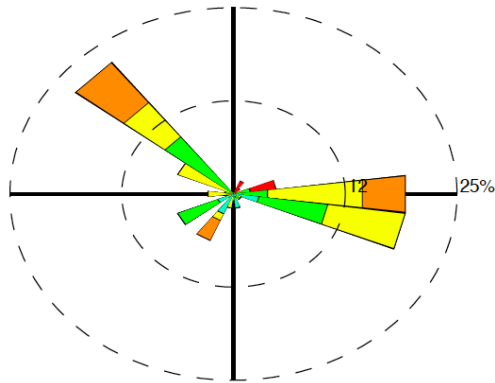
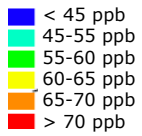


(b)

Trail Ridge [RF North HIGH]

Trail Ridge [RF North HIGH]

Ozone



TROG (PBLavg)

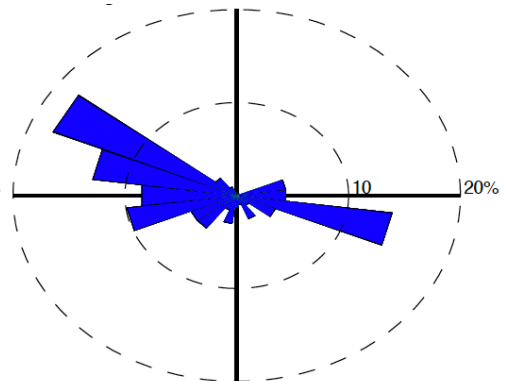
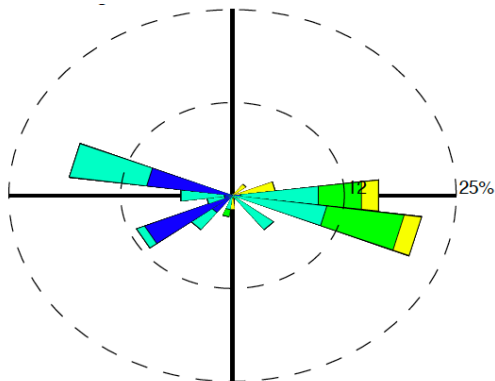
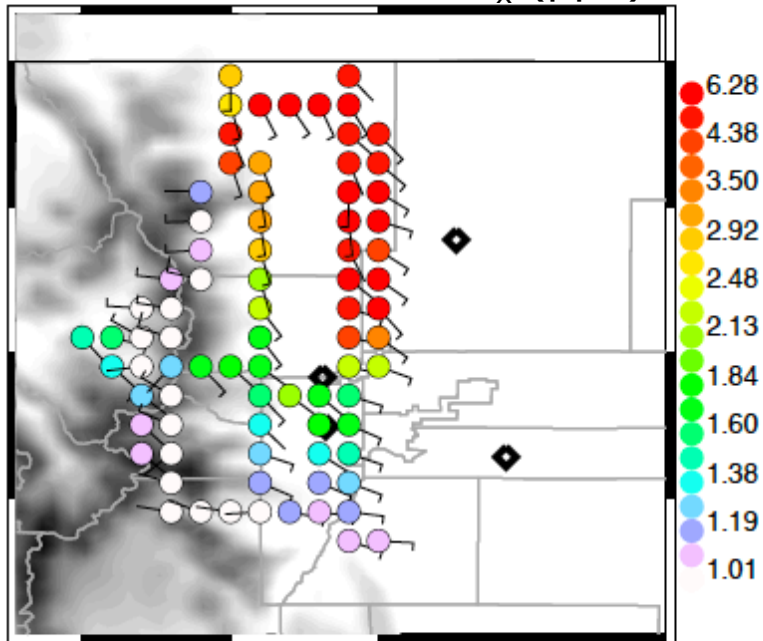
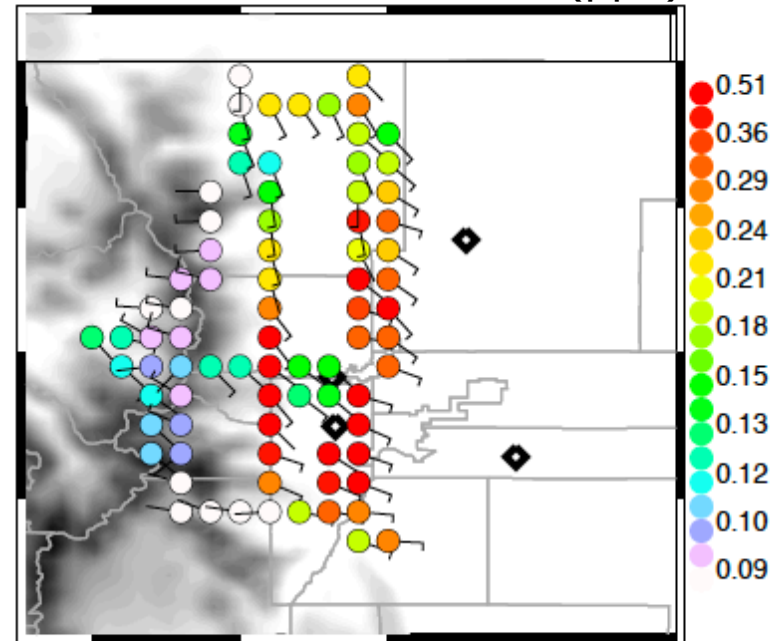


Figure 14.

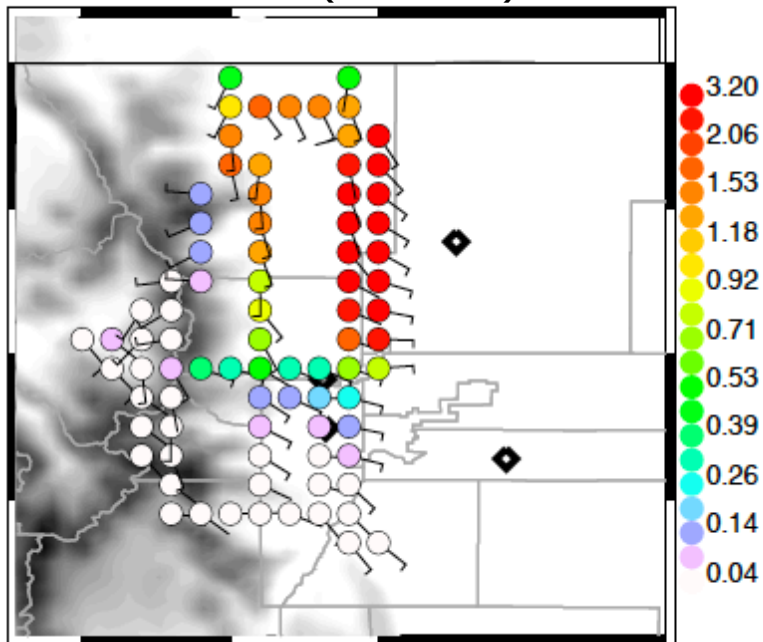
NCAR/NSF C-130 NO<sub>x</sub> (ppb)



NCAR/NSF C-130 Ethane (ppb)



TR<sup>OG</sup> (unitless)



TR<sup>AreaMobile</sup> (unitless)

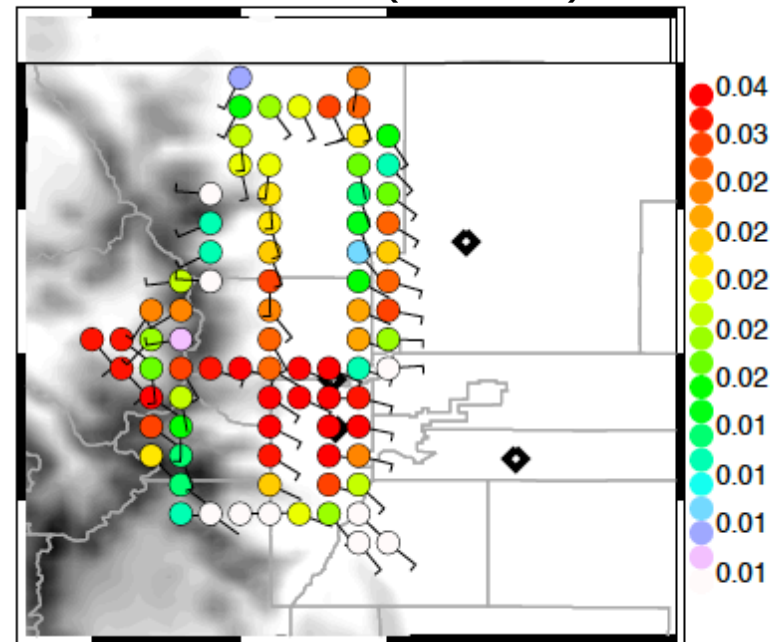
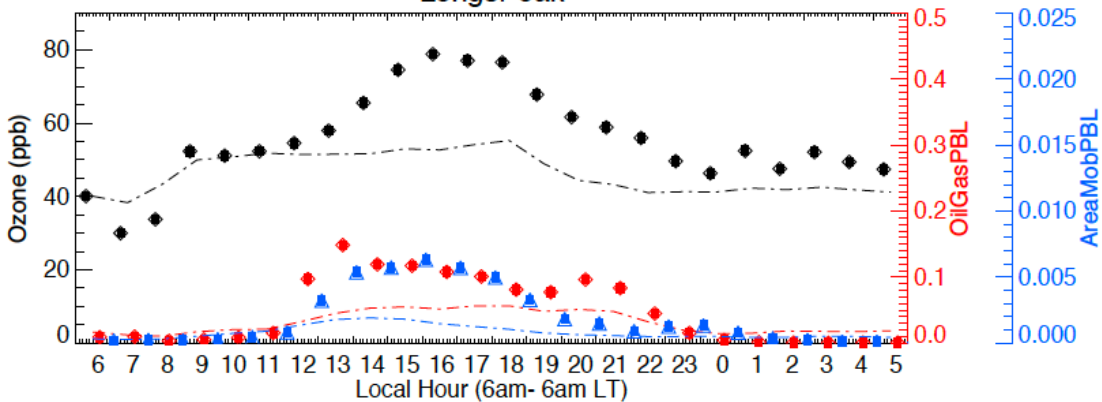
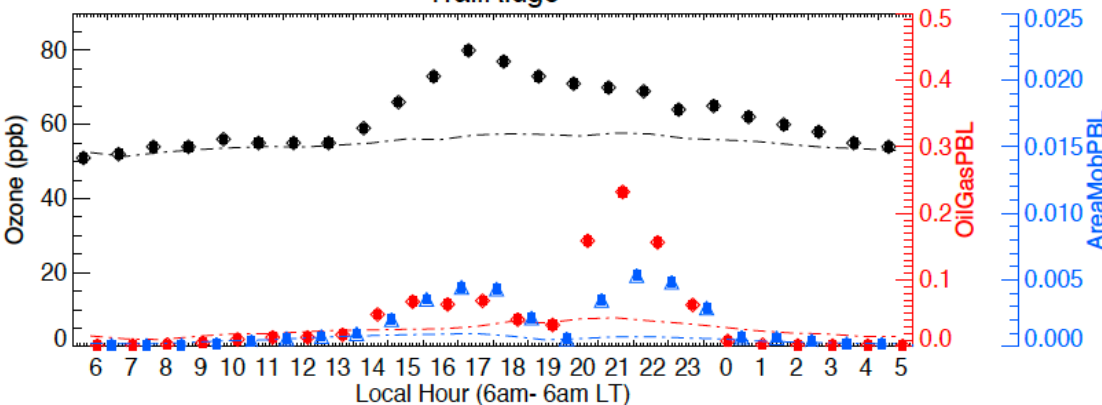


Figure 15.

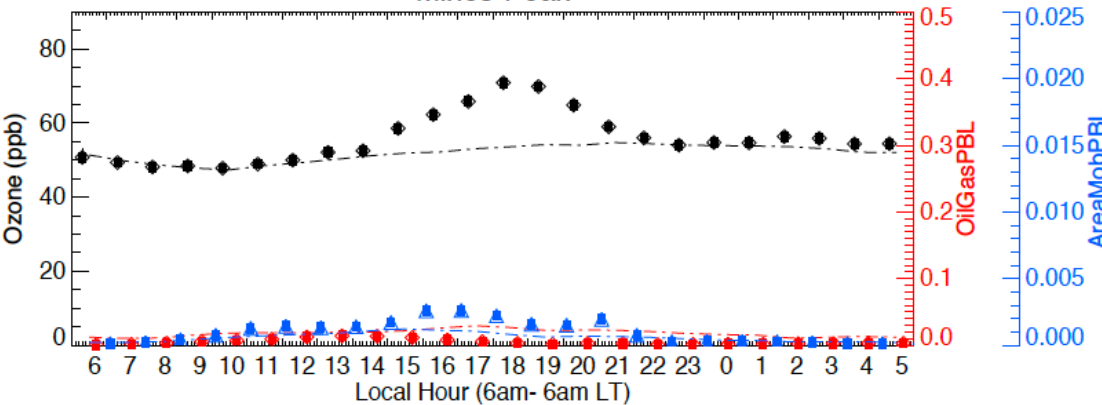
### LongsPeak



### TrailRidge



### Mines-Peak



### Squaw-Mtn

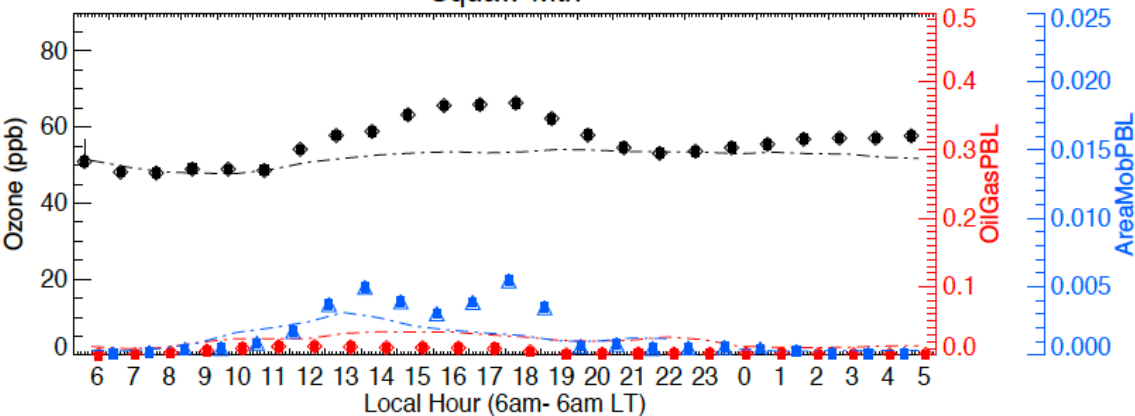
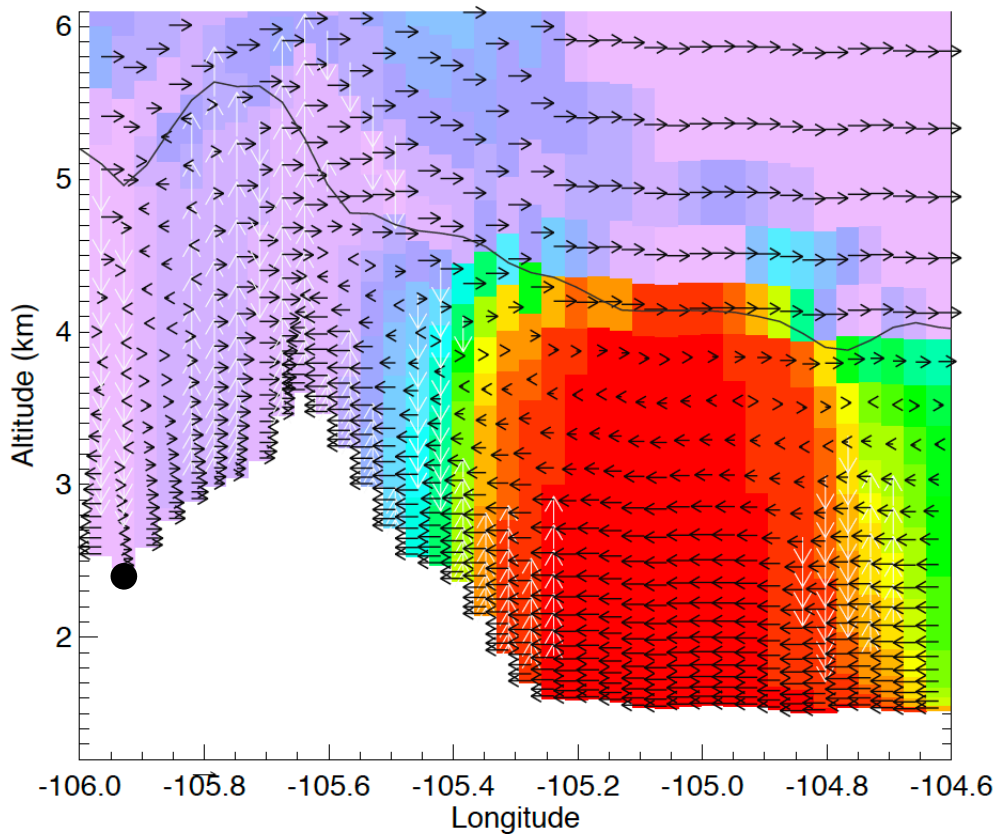


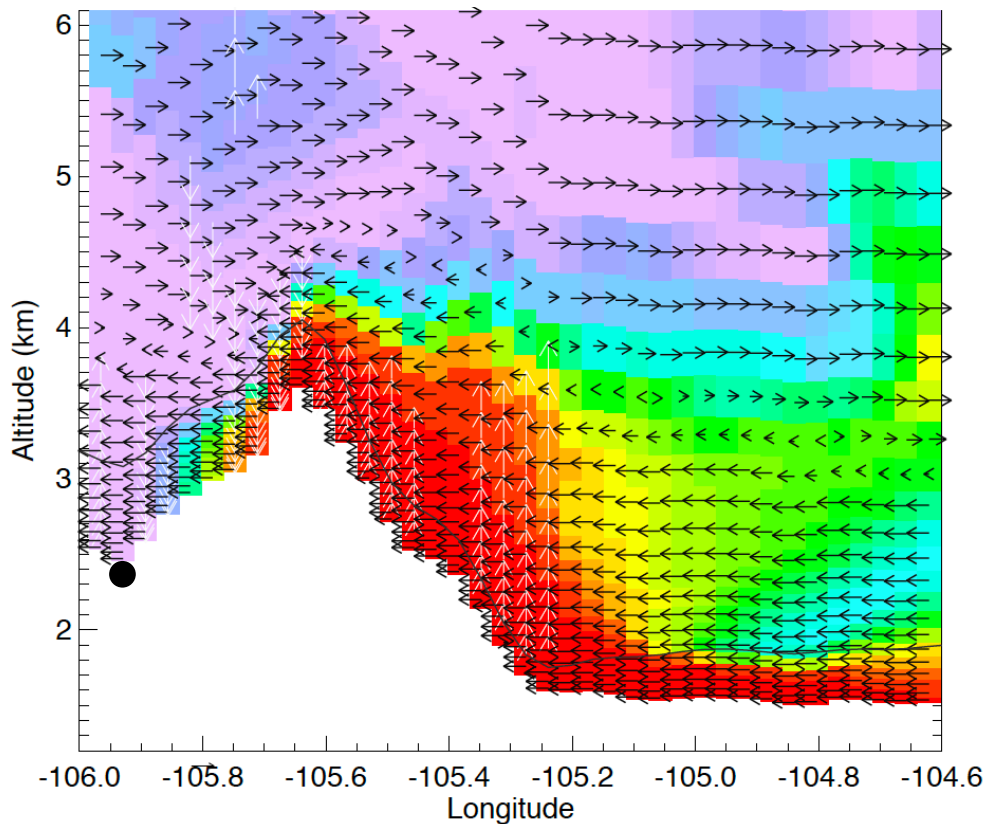
**Figure 16.**



2014-08-12 22 UTC Lat=40.07N



2014-08-13 02 UTC Lat=40.07N



TR<sup>OG</sup> Mixing Ratio (arbitrary units)

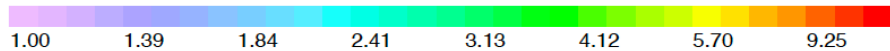
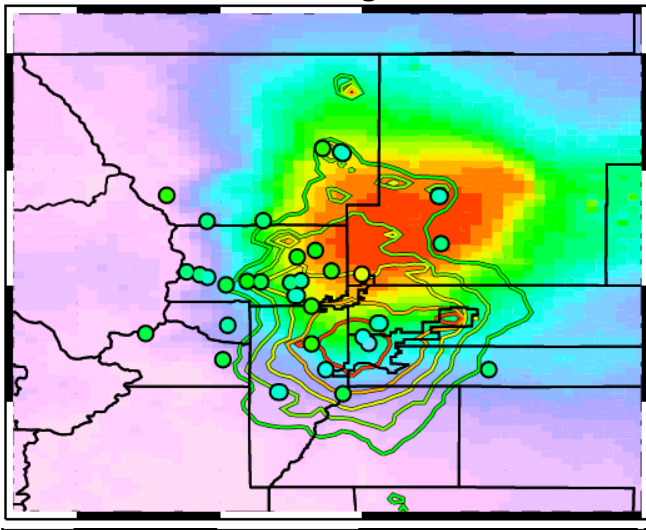
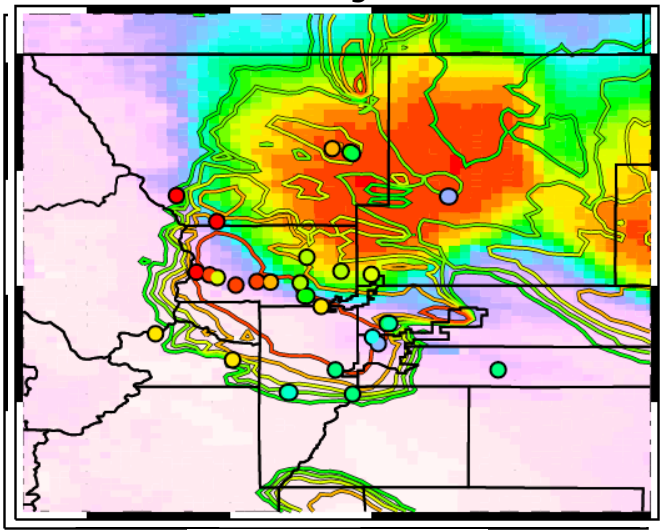


Figure 17.

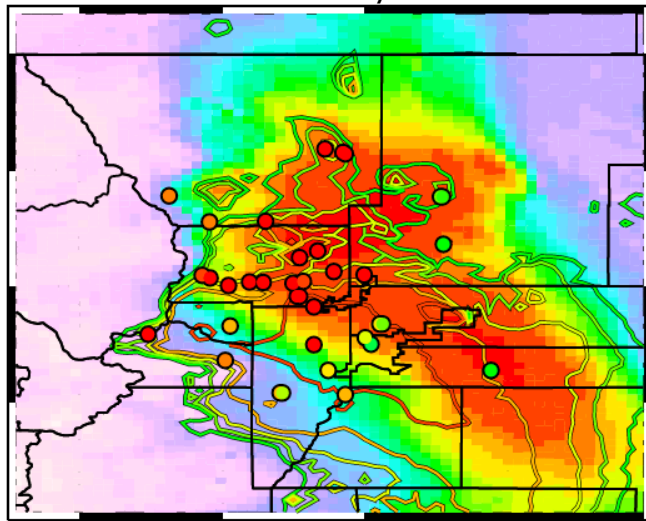
Average



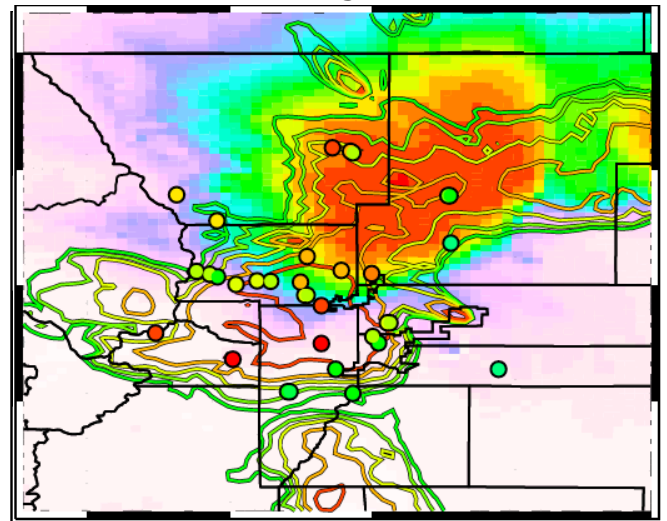
12 August



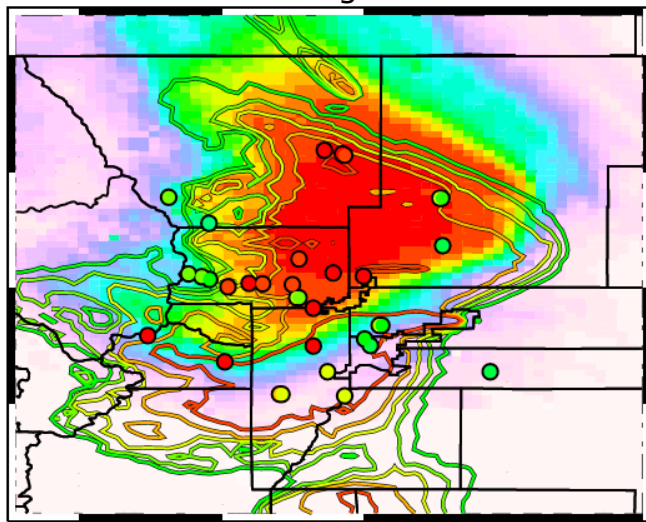
22 July



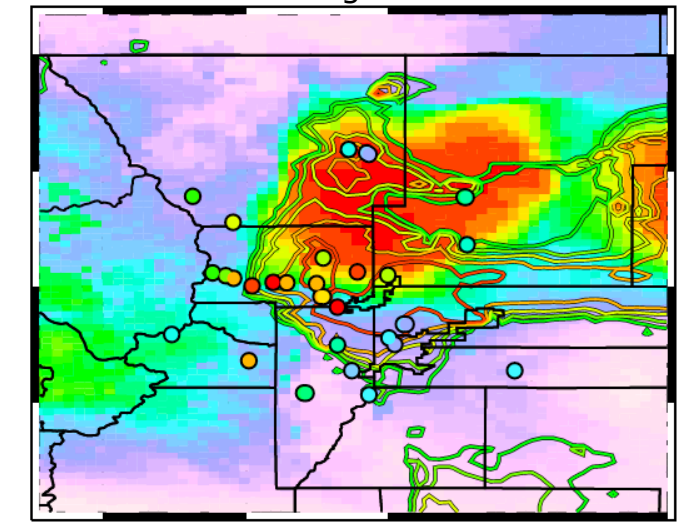
2 August



3 August



8 August



TR<sub>AreaMobile</sub>, TR<sub>OG</sub> (arbitrary units)

